High-Temperature Thermal Gradient Interaction Chromatography (HT-TGIC) of Polyolefins: Effect of Polymer Molecular Weight, Comonomer Fraction, and Comonomer Type

By

Amirreza Badri

A thesis submitted in partial fulfillment of the requirements for the degree of

Master of Science

in

Chemical Engineering

Department of Chemical and Materials Engineering

University of Alberta

Abstract

Polyolefins are the most important commodity polymers today. The demand for polyethylene and polypropylene, the two most important polyolefins, has been increasing steadily since their discovery in the late fifties.

The properties of polyolefins is defined by their distributions of molecular weight (MWD), chemical composition (CCD), and long chain branching (LCB). The MWD is measured by high-temperature gel permeation chromatography (GPC). Several crystallization-based techniques, such as temperature rising elution fractionation (TREF), crystallization analysis fractionation (CRYSTAF), and crystallization elution fractionation (CEF), are used to measure the CCD of polyolefins. They are time consuming, prone to co-crystallization artifacts, and limited to lower comonomer fractions (< 15 mol%). High-temperature solvent gradient interaction chromatography (HT-SGIC) can also be used to measure the CCD of polyolefins and does not suffer from the limitations of crystallization-based methods, but it unfortunately uses two solvents (good/bad solvent) and non-quantitative evaporative light scattering detectors. A newly introduced technique, high-temperature thermal gradient interaction chromatography (HT-TGIC), is an attractive alternative because of its short analysis time and wide range of comonomer fractions. In addition, HT-TGIC uses only one solvent and can be combined with regular chromatographic detectors such as infrared detectors, refractometers, viscometers, and light scattering detectors.

Previous HT-TGIC investigations were mostly limited to ethylene/1-octene copolymers with number average molecular weights (M_n) higher than 25 000. For these samples, M_n does not affect HT-TGIC fractionation, and peak temperatures display an inverse linear relation with comonomer fraction.

The main objective of this thesis was to determine empirical calibration curves relating peak temperature to polymer M_w, comonomer fraction, and comonomer type using a set of ethylene/α-olefin copolymers with $M_n < 25\,000$ and different comonomer types (1-hexene, 1-octene, and 1-decene). The complementary objective of this thesis was to develop a new packing material for HT-TGIC columns. Conventional HT-TGIC columns are filled with porous graphite particles, which may have lower resolution due to size exclusion effects. The proposed novel packing material consisted of non-porous silica particles covered with graphene (GNPSi) to reduce size exclusion effects.

Dedication

To

    My friend, Nassim Rahmanifar

    All the passengers in flight PS752

Acknowledgement

I would like to express my sincere gratitude to my supervisor Prof. João B.P. Soares for his consistent guidance, support, endless encouragement and giving me the opportunity to work under his supervision.

I would like to thank my best friend Vahid for being with me like a brother all the time and thank him for all his support. Thanks also to my colleagues Raunil, Anuar, Venu, and Ben for their support and inspiration. Special thanks to Dr. Saeid Mehdiabadi for his coaching and support throughout my project.

My deepest gratitude goes to my family. Mom and dad, I am very lucky to have you for your love, support, and motivation. Special thanks to my lovely sister for all your support during my studies. My brother, Sina, thank you for all your guidance and help while you were here in Edmonton next to me. Mom, dad, Samira and Sina, I love you.

Amirreza

Table of Contents

List of Figures

List of Tables

Nomenclature

Acronyms

AESL	Average ethylene sequence length
ALESL	Average longest ethylene sequence length
CCD	Chemical composition distribution
CEF	Crystallization elution fractionation
CGC	Constrained geometry catalyst
CR	Cooling rate
CRYSTAF	Crystallization analysis fractionation
^{13}C NMR	Carbon-13 nuclear magnetic resonance spectroscopy
ESLD	Evaporative light scattering detector
FTIR	Fourier-transform infrared
GNPSi	Graphene-coated non-porous silica
GPC	Gel permeation chromatography
HDPE	High-density polyethylene
HPLC	High-performance liquid chromatography
HR	Heating rate
HT-SGIC	High-temperature solvent gradient interaction chromatography
HT-TGIC	High temperature thermal gradient interaction chromatography
IR	Infrared
LCB	Long chain branch(ing)
LDPE	Low-density polyethylene
LLDPE	Linear low-density polyethylene
MAO	Methylaluminoxane
MW	Molecular weight
MWD	Molecular weight distribution
ODCB	o-Dichlorobenzene
PDI	Polydispersity index
QCM-D	Quartz crystal microbalance with dissipation/damping
RMSD	Root mean square deviation
SCB	Short chain branch

SEM	Scanning electron microscopy
TCB	Trichlorobenzene
TREF	Temperature rising elution fractionation

Symbols

d_p	Particle diameter
F_B	Comonomer molar fraction in the copolymer
F_c	Cooling flow rate
F_e	Elution flow rate
L	Length of the column
M_n	Number average molecular weight
M_w	Weight average molecular weight
SCB/1000 C	Number of short chain branches per 1000 carbon atoms
r_n	Number average chain length
T	Temperature
T_μ	Mean temperature
T_p	Peak elution temperature
n_c	Comonomer type

Greek Letters

σ	Standard deviation
φ	Comonomer molar percent

Chapter 1. Introduction

Polyethylene is an essential commodity polymer. High-density polyethylene (HDPE), linear low-density polyethylene (LLDPE), and low-density polyethylene (LDPE) are different types of polyethylenes. Versatile properties and low production costs allow them to be used in widely different applications such as plastic bags, food packaging, drums, detergent bottles, crates, dustbins, cable coatings, biomedical devices, automotive and aeronautical part, and water pipes among others. The mechanical properties of polyethylenes are defined by their molecular weight distribution (MWD), chemical composition distribution (CCD), and long chain branching (LCB). Copolymerizing ethylene with α-olefins (typically 1-butene, 1-hexene, or 1-octene) results in the production of copolymers of lower density.

The MWD of polyolefins is measured by high-temperature gel permeation chromatography (GPC). Their average chemical compositions are quantified with carbon-13 nuclear magnetic resonance (^{13}C NMR) or Fourier-transform infrared spectroscopy (FTIR). Since average compositions are often not enough to understand the properties of ethylene/α-olefin copolymers, several methods have been developed to measure their chemical composition distribution.[1] The traditional CCD analysis methods are based on differences in crystallizability caused by the copolymerization of ethylene with a α-olefin (the higher the α-olefin fraction, the lower the crystallizability of the copolymer). These methods, in order of their discoveries, are:[2] *i*) temperature rising elution fractionation (TREF), *ii*) crystallization analysis fractionation (CRYSTAF), and *iii*) crystallization elution fractionation (CEF). These methods have long analysis times, suffer from co-crystallization effects, and cannot analyze copolymers with high α-olefin fractions that do not crystallize from solution.

More recently, high-temperature interaction chromatography methods, which do not rely on crystallization as a fractionation mechanism, have been developed to analyze polyolefins. High-temperature solvent gradient interaction chromatography (HT-SGIC) fractionates polyolefin chains based on how they interact with the column support in the presence of a solvent mixture in which the good-to-bad solvent ratio changes as a function of time. Although this is a powerful method, it uses a non-quantitative evaporative light scattering detector because the composition of the solvent mixture changes during the analysis. High-temperature thermal gradient interaction chromatography (HT-TGIC), on the other hand, works with a single solvent and is compatible with conventional quantitative chromatographic detectors. In HT-TGIC, the temperature varies during the analysis to affect how the polyolefin chains interact with the column packing (porous graphite) *regardless* of their crystallizabilities. High-temperature thermal gradient interaction chromatography, therefore, is more practical than HT-SGIC. It is also the main subject of this thesis.

Chapter 2. Literature Review

2.1. Global Importance of Polyethylene

Polyethylene has many uses in modern life. Figure 2-1 shows how fast the production of plastics is increasing, while Figure 2-2 breaks down this demand among different polymer types in 2016. Polyethylene (HDPE, LLDPE, and HDPE) accounted for an impressive 38 % of the worldwide polymer demand in 2016.
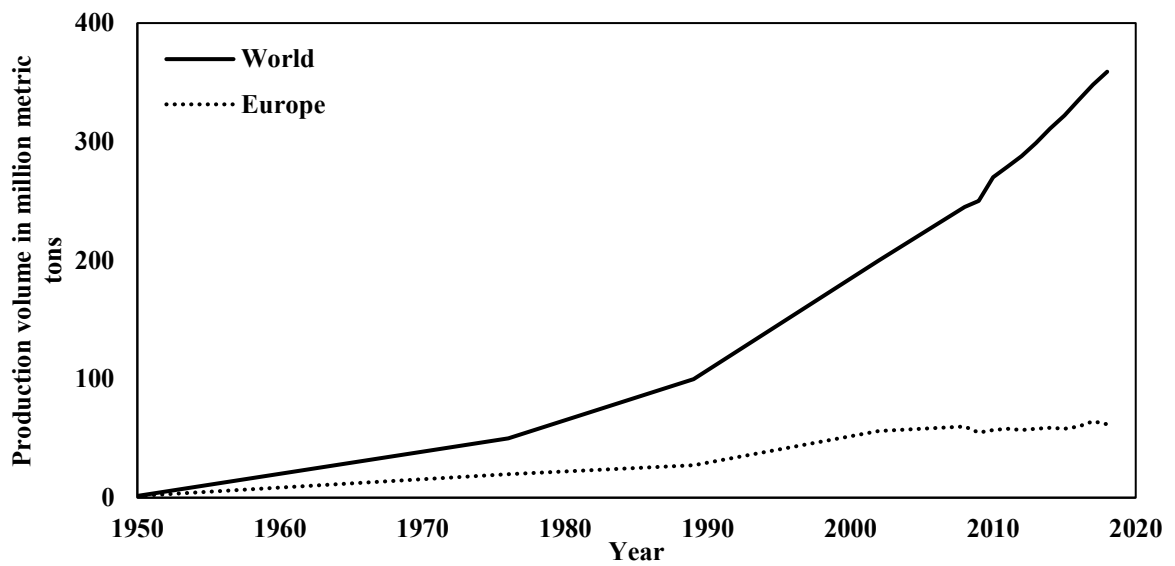
Figure 2-1. Increase in plastic production from 1950 to 2017.[3]
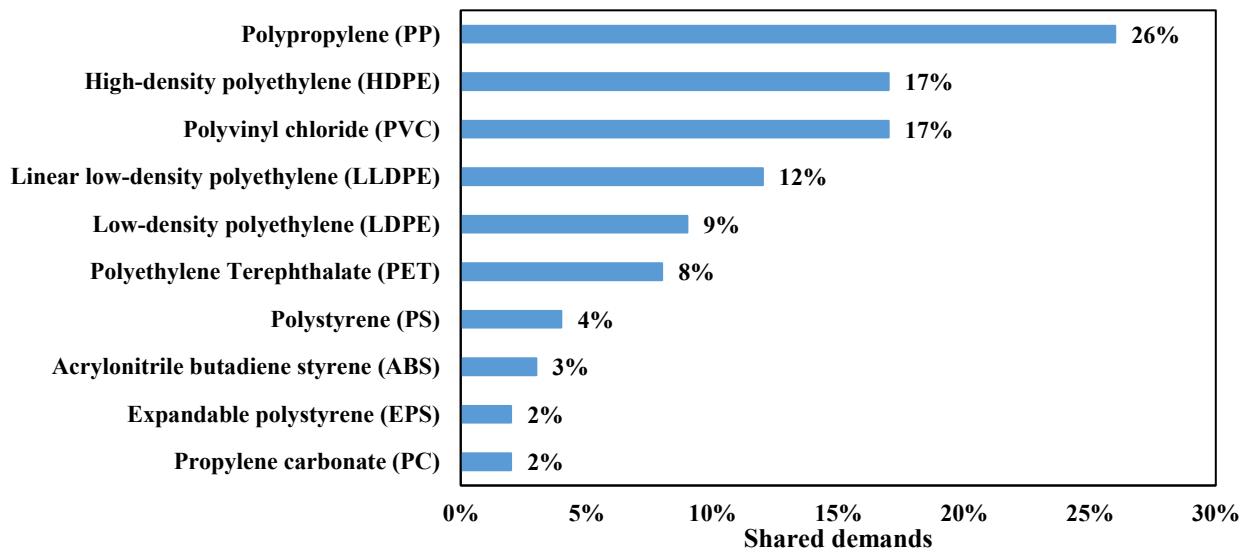
Figure 2-2. Distribution of polymer demand by type in 2016.[4]

The polymerization of ethylene with different α-olefins (1-butene, 1-hexene, and 1-octene in commercial products) using a coordination catalyst makes poly(ethylene-*co*-α-olefin) with different comonomer fractions and densities that are traditionally classified in two groups: high density polyethylene (HDPE, 0.941-0.970 g/cm^3), and linear low-density polyethylene (LLDPE, 0.915-0.940 g/cm^3). A third type of polyethylene, low density polyethylene (LDPE, 0.910-0.940 g/cm^3), having short and long chain branches (SCB and LCB), is made via free radical copolymerization. Figure 2-3 compares these three types of polyethylene.

Low density polyethylene was the first commercial polyolefin. It is made by the free radical polymerization of ethylene [5] at temperatures from 100 to 350 °C and ethylene pressures from 15 000 to 50 000 psi.[5-7] Short chain branches (SCB, typically 2 to 6 carbon-atom long) are generated by backbiting (40 to 150 SCB per 1000 ethylene units) while long chain branches

4

(LCB, generally longer than 270 C atoms) are formed by chain transfer to polymer (usually 1 LCB per 10 SCB).[8,9]
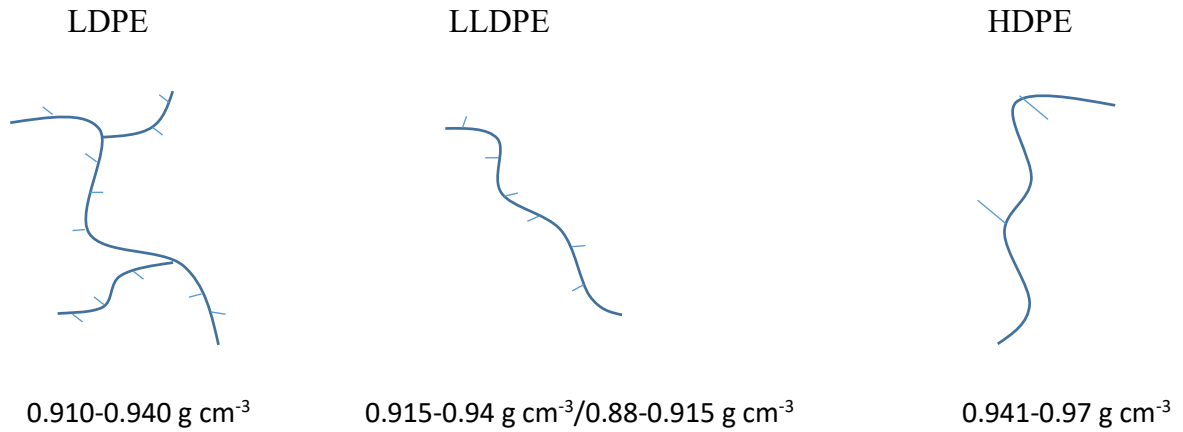
Figure 2-3. Different types of polyethylene.[5]

In contrast, LLDPE and HDPE are made by copolymerizing ethylene and α-olefins using a coordination catalyst. The incorporation of an α-olefin in the polyethylene backbone forms a SCB with length proportional to the α-olefin length. For instance, copolymerization with 1-hexene forms a 1-butene short chain branch. Increasing the fraction of α-olefin in the copolymer decreases its density.[7,9,10] Table 2-1 compares the properties of these three types of polyethylene.

Table 2-1. Molecular structure and properties of different polyethylene resins.[7]

Polyethylene type	Pros	Cons
HDPE	Stiff	
	Dense (good barrier)	Brittle
	High load carrying capability (HMW)	Hazy
	Higher temperature resistance	
LLDPE	Good optics	
	Toughness	Not stiff
	Relatively low barrier	Relatively low barrier
	Sealability	
LDPE	Good optics	
	Easy to process	Not very tough
	Enable TD shrinkage	

2.2. Catalysts for Olefin Polymerization

The catalyst is the most important factor when synthesizing ethylene/α-olefin copolymers because it determines the final microstructure and properties of the polyolefin. This section explains the most relevant differences among olefin polymerization catalysts.

Olefin polymerization with coordination catalysts started with the discovery of Ziegler-Natta and Philips catalysts in the early 1950s. These catalysts have more than one type of active site and make polyolefins with non-uniform microstructures (broad MWD and CCD). In the early 1980s, metallocene catalysts started being used to make commercial polyolefins. In contrast with the previous catalysts, metallocenes make polyolefins with more uniform microstructures because they are molecular catalysts with only one type of active site. The development of coordination catalyst continues to these days, with the development of late transition metal catalysts (post-metallocenes).[5] Figure 2-4 shows the timeline for discovery

and development of coordination catalysts for olefin polymerization. Low-density polyethylene, on the other hand, has been made since the mid-1950s by free radical polymerization. Table 2-2 summarizes the main characteristics of coordination catalysts for olefin polymerization.
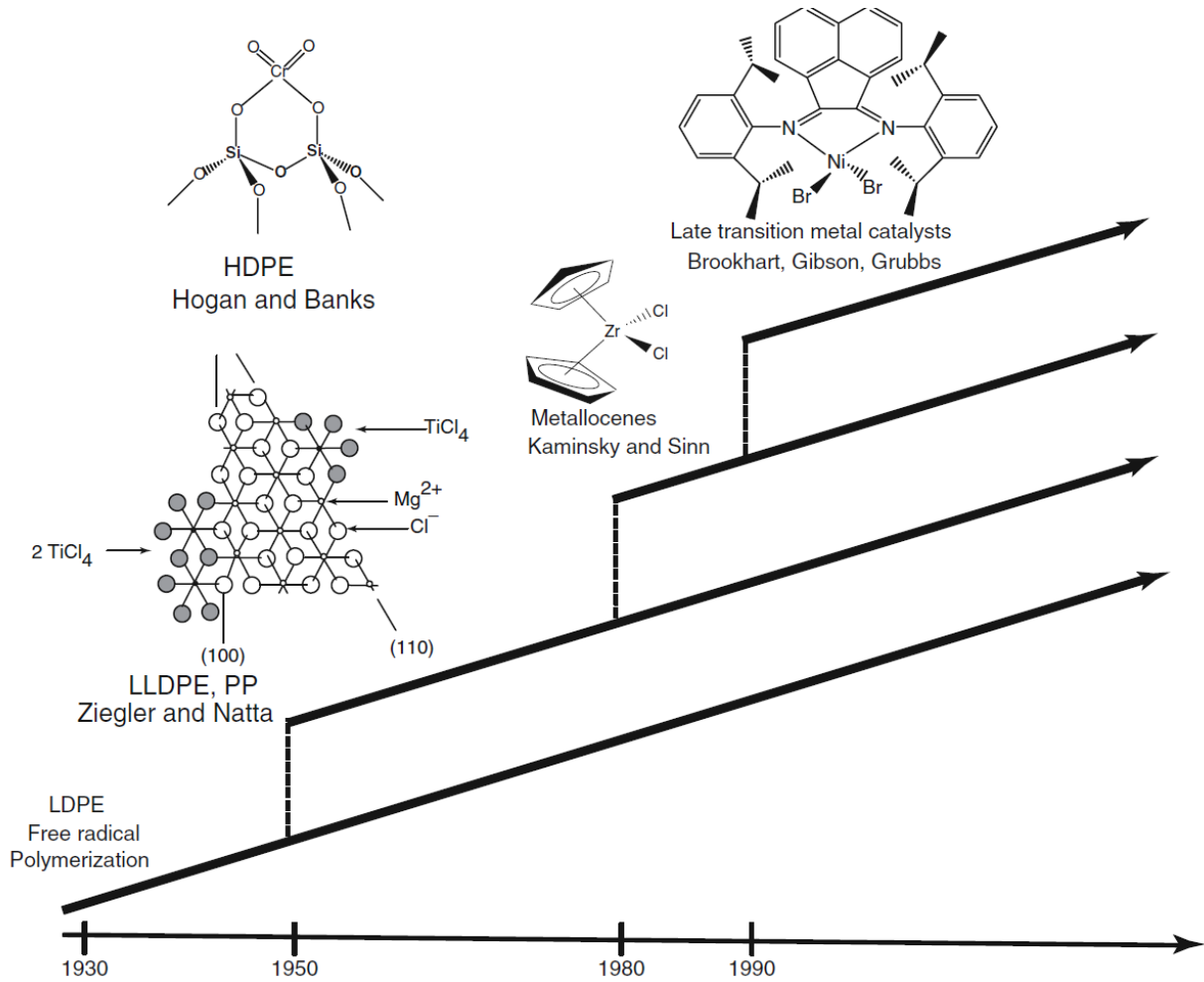
Figure 2-4. Evolution of coordination catalysts for olefin polymerization.[5]

Table 2-2. Main characteristics of coordination catalysts for polyolefin polymerization.[5]

Type	Physical state	Examples	Polymer type
Ziegler-Natta	Heterogeneous	$TiCl_3$, $TiCl_4/MgCl_2$	Non-uniform
	Homogeneous	VCl_4, $VOCl_3$	Uniform
Phillips	Heterogeneous	CrO_3/SiO_2	Non-uniform
Metallocene	Homogeneous	Cp_2ZrCl_2	Uniform
	Heterogeneous	Cp_2ZrCl_2/SiO_2	Uniform
Late transition metal	Homogeneous	Ni, Pd, Co, Fe with diamine and other ligands	Uniform

2.2.1. Multiple-Site-Type Catalysts

2.2.1.1. Ziegler-Natta Catalysts

Ziegler-Natta catalysts are composed of transition metals from the Periodic Table groups IV to VIII. Commercial Ziegler-Natta catalysts are based on titanium chloride or vanadium chloride ($TiCl_4$, $TiCl_3$, VCl_4, and $VOCl_3$).[11] The catalyst must be activated with an organometallic compound (activator or cocatalyst) such as trimethyl aluminum or triethyl aluminum.

Ziegler-Natta catalysts can polymerize ethylene, propylene, and higher α-olefins. Based on the polymerization medium, the catalysts may be homogeneous or heterogeneous. Most Ziegler-Natta catalysts are heterogeneous while most vanadium-based catalysts are homogeneous.

Most LLDPE resins are made with heterogeneous catalysts, such as $TiCl_4$ supported on $MgCl_2$ or SiO_2. The activity of $TiCl_4$-supported catalysts may be 100 times higher than that of unsupported $TiCl_3$ catalysts. The chemical structure of an $MgCl_2$-supported $TiCl_4$ catalysts is shown in Figure 2-5.[12,13]

Homogeneous vanadium-based Ziegler-Natta catalysts are mainly used to make ethylene-propylene-diene (EPDM) elastomers. Contrarily to heterogenous Ziegler-Natta catalysts, which have multiple site types and make polyolefins with broad MWD and CCD, these homogeneous catalysts make polymer with uniform microstructures.[5]
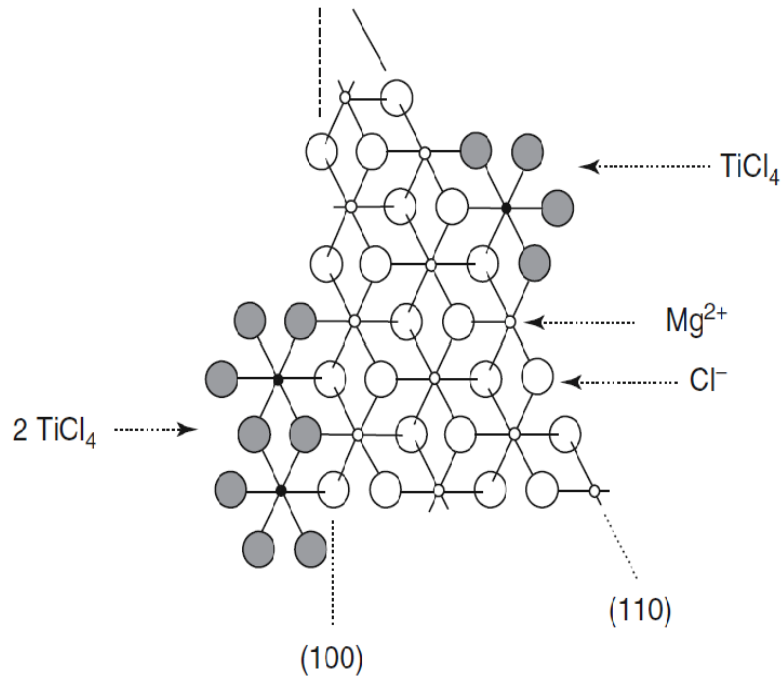
Figure 2-5. TiCl$_4$/MgCl$_2$ Ziegler-Natta catalyst.[5]

2.2.1.2. Phillips Catalysts

Phillips catalysts are based on chromium compounds such as CrO$_3$ supported on SiO$_2$. They are mainly used for the production of HDPE. They are activated using a high temperature process that also affects polymerization activity, MWD, and LCB. The MWD is also affected by the porosity of the support. Figure 2-6 shows the structure of a chromium oxide Phillips catalyst.[5]
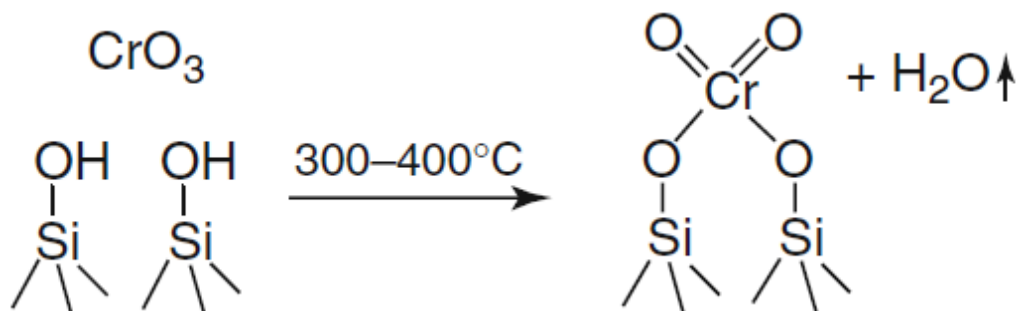
Figure 2-6. An example of Phillips catalyst.[5]

2.2.2. Single-Site Catalysts
2.2.2.1. Metallocene Catalysts

The discovery of single-site catalysts (metallocene and late transition metal catalysts) for olefin polymerization has opened a new chapter in polyolefin manufacturing. Metallocenes can be activated with an aluminum alkyl cocatalyst, such as the ones used to activate Ziegler-Natta catalysts, but their productivity is very low. In 1980, however, Kaminsky and Sinn found that when methylaluminoxane (MAO) was used as a cocatalyst, the activity of the resulting species could be 10 to 100 times higher than those of Ziegler-Natta catalysts.[14,15]

Metallocenes are sandwich or half-sandwich compounds in which the transition metal (Ti, Zr, HF) is located between two cyclopentadienyl (or cyclopentadienyl-substituted) rings. Figure 2-7 shows the structure of a half-sandwich metallocene, also called a *constrained geometry catalyst* (CGC-Ti). Figure 2-8 shows the structures of a few sandwich metallocene compounds.[5]
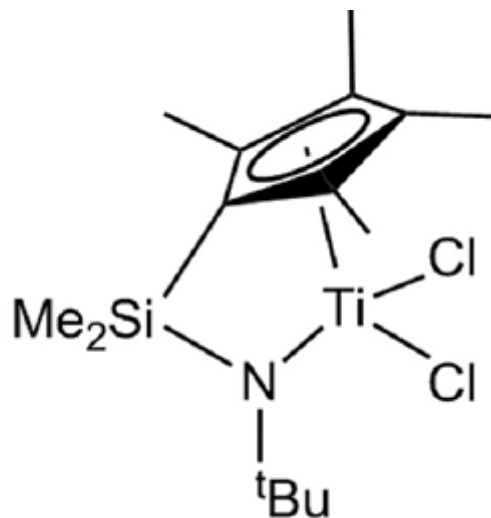
Figure 2-7. CGC-Ti catalyst structure.[16]

M = Zr, Hf X = C_2H_4, $(CH_3)_2Si$

X = C_2H_4, $(CH_3)_2Si$

X = $(CH_3)_2Si_4$, C_2H_4

X = C_2H_4, $R_1 = R_2 = CH_3$
X = $(CH_3)_2Si$, $R_1 = R_2 = CH_3$
X = $(CH_3)_2Si$, $R_1 = Ph$, $R_2 = H$
X = $(CH_3)_2Si$, $R_1 = Naph$, $R_2 = H$

M = Zr, X = $(CH_3)_2C$, R = H
M = Hf, X = $(CH_3)_2C$, R = H
M = Zr, X = Ph_2C, R = H
M = Zr, X = $(CH_3)_2C$, R = (CH_3)
M = Zr, X = $(CH_3)_2C$, R = tBu
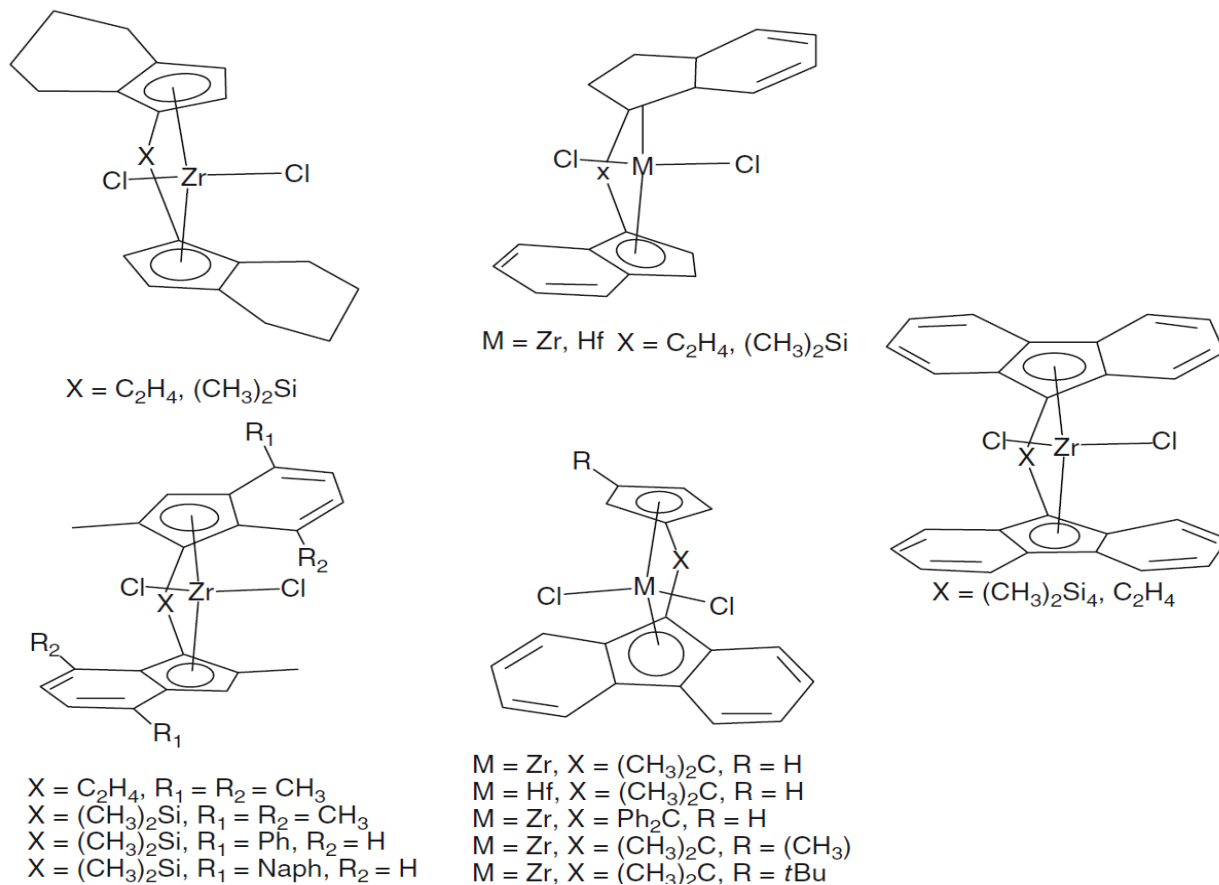
Figure 2-8. Different structures for metallocene catalysts.[5]

11

The metallocene catalyst used to make the polyolefins in this thesis is a constrained geometry catalyst. This type of metallocene contains only *one* cyclopentadienyl ring coordinated with the transition metal. In comparison with most other metallocenes, CGCs are more stable at the higher temperatures needed for solution polymerization. They are also excellent α-olefin incorporators. Thermal stability and high α-olefin reactivity were essential requirements for this thesis work.[17]

Figure 2-9 compares typical MWDs and average SCB frequencies (1-hexene fractions) across the MWD for ethylene/1-hexene copolymers made with metallocene and Ziegler-Natta catalysts. The MWD of the metallocene polyethylene is narrow and the average 1-hexene fraction does not depend on polymer molecular weight. In contrast, the MWD of the Ziegler-Natta polyethylene is broader and its average 1-hexene fraction depends inversely on polymer molecular weight.
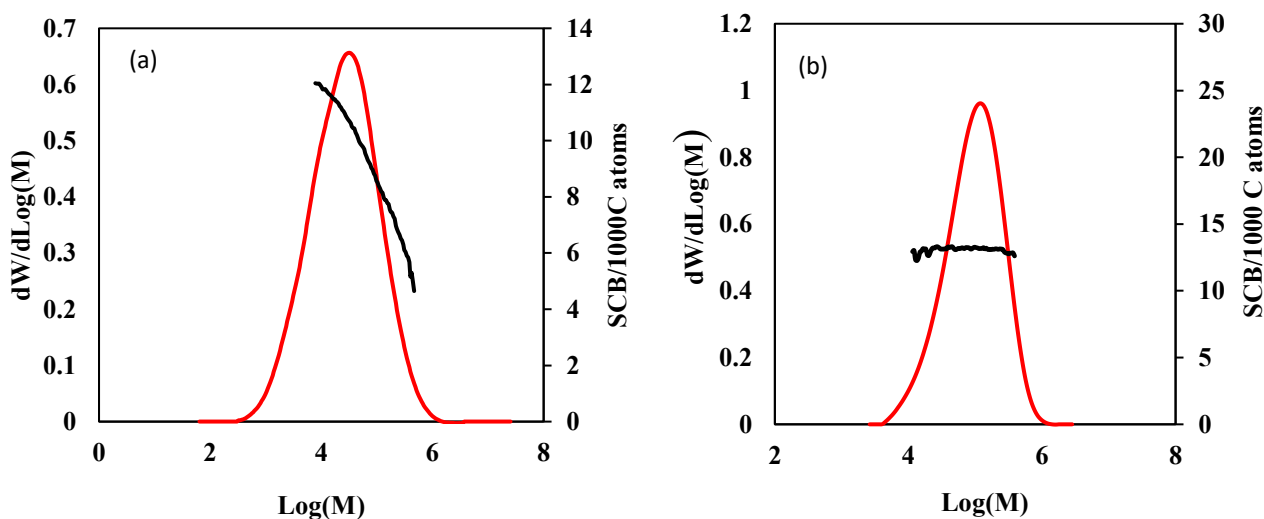
Figure 2-9. MWDs and SCB frequencies (1-hexene fractions) of ethylene/1-hexene copolymers made with: a) Ziegler-Natta, and b) metallocene catalysts (from Dr. S. Mehdiabadi).

In the early 1990s, Brookhart et al. showed how to use late transition metal catalysts to polymerize olefins. Since they are less oxyphilic than Ziegler-Natta, Phillips, and metallocene catalysts they can be used to copolymerize olefins with polar comonomers such as vinyl acetate or methyl metacrylate. Despite of their academic interest and promising potential, they have not yet reached the industrial importance of the other coordination catalysts for olefin polymerization.[18]

2.3. Polyethylene Microstructural Characterization

The microstructure of polyolefins is defined by three main distributions: molecular weight distribution (MWD), chemical composition distribution (CCD), and long chain branch distribution (LCBD). Three crystallization-based methods have been developed to measure the CCD of polyolefins: temperature rising elution fractionation (TREF), crystallization analysis fractionation (CRYSTAF), and crystallization elution fractionation (CEF). The recent high-temperature thermal gradient interaction chromatography (HT-TGIC) has attracted much attention because of its shorter analysis times and absence of co-crystallization effects.

Thermal gradient elution chromatography (TGIC) is an established analytical technique, first used by Lochmuller and Chang to fractionate poly(ethylene glycol) and polystyrene, respectively.[19-21] The fractionation mechanism relies on selectively adsorbing/desorbing polymer chains from the packing material in a chromatographic column by changing the temperature. The main challenge for polyolefins is to find the right support that has the right selectivity for their non-polar, non-functional chains at the high temperatures needed to keep them in solution.

2.3.1. Temperature Rising Elution Fractionation (TREF)

Temperature rising elution fractionation is a technique that fractionates polymers based on their crystallizability. Although Shirayama et al.[22] were the first researcher to use this method to fractionate LDPE, the actual technique was introduced earlier by Desreux and Spiegels.[23] During the analysis, the polymer is dissolved at high temperature in a good solvent, such as trichlorobenzene (TCB), and injected into a column packed with an inert material such as sand, glass beads, silica gel, or steel shots. The flow is stopped and the temperature is gradually reduced to allow the polymer chains to precipitate (crystallize) and coat the support particles (precipitation/crystallization step).[24] A slow cooling rate (typically 2 ºC/h) is essential to maximize resolution and minimize undesirable co-crystallization and polymer molecular weight effects.[25] Polymer chains with higher crystallizability (lower α-olefin fraction) precipitate first, followed by chains with lower crystallizability (higher α-olefin fraction). The process continues until the column temperature reaches room temperature.[26,27] The elution step starts when the solvent flow is turned back on and the temperature is increased slowly, allowing the copolymer chains with the highest fractions of α-olefin to dissolve in the solvent and elute from the column, followed by chains with decreasing fractions of α-olefin. Therefore, the polymer fractions leaving the column first have the lowest crystallizability and the fractions leaving the column last have the highest crystallizability. An on-line mass detector measures the concentration of polymer eluting from the TREF column as a function of temperature. Other detectors may also be installed to monitor intrinsic viscosity, radius of gyration, and α-olefin fraction of the polymer fractions. Figure 2-10 illustrates the separation mechanism in TREF.
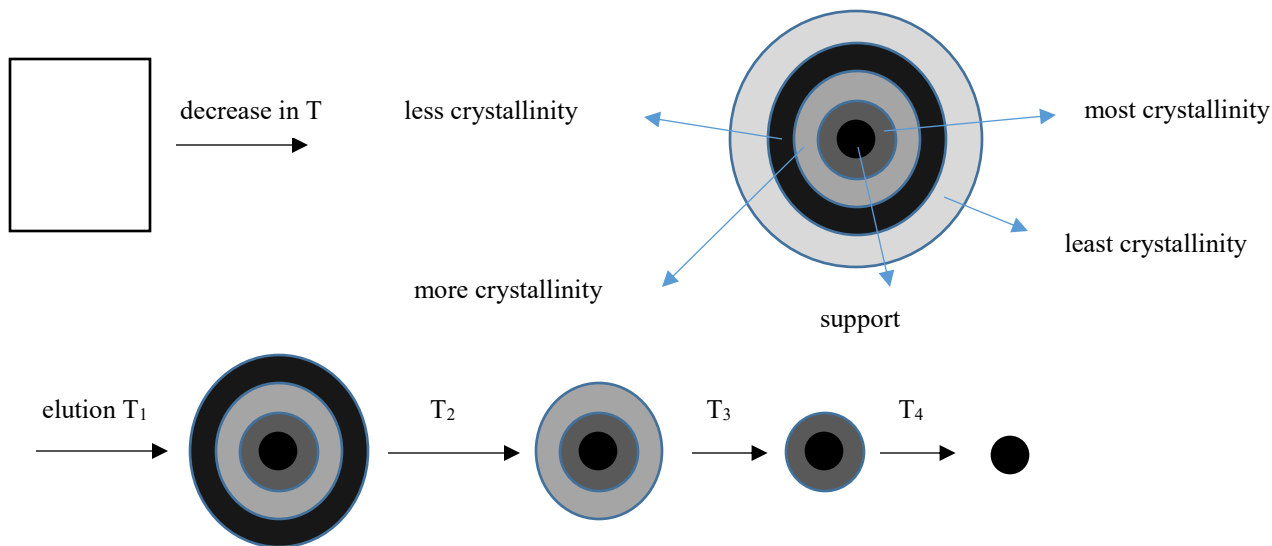
Figure 2-10. Schematic representation for the fractionation mechanism in TREF. The illustration shows the onion-skin model for TREF, in which polymer layers of decreasing crystallizabilities are envisioned to precipitate onto the TREF packing particles.[25,28]

Polymer molecular weight and comonomer fraction are the main factors affecting TREF peak temperatures, but molecular weight has little effect after $M_n = 10\ 000$.[29] Anantawarskul et al.[30,31] showed that higher peak temperatures are reached at low flow and heating rates.

2.3.2. Crystallization Analysis Fractionation (CRYSTAF)

Crystallization analysis fractionation[32] was developed as a faster alternative to TREF, since CRYSTAF does not need the elution step.[33] In CRYSTAF, the polymer is dissolved in a solvent at high temperature inside an empty crystallization vessel. The cooling process is similar to that used in TREF and a slow cooling rate is needed for better resolution. A mass detector (typically an infrared detector) monitors the concentration of polymer in solution as a function of temperature, measuring the cumulative polymer solution concentration versus the crystallization temperature. The first derivative of the cumulative distribution is comparable to the elution profile measured in TREF. Since CRYSTAF measures the crystallization profile while TREF measures the dissolution profile, CRYSTAF distributions are shifted to lower

temperatures.[34-37] Figure 2-11 compares CRYSTAF and TREF profiles for the same Ziegler-Natta ethylene/1-butene copolymer.

Anantawarskul et al.[30,31] found that the difference between the peak temperatures of profiles measured by TREF and CRYSTAF depended linearly on the cooling rate. Nieto et al.[37] showed that CRYSTAF peak temperatures were not a function of molecular weight for polymers with $M_n > 5000$. Further investigations by Anantawaraskul et al.[38] proved that polymer molecular weight and α-olefin molar fraction affected the broadness of the CCD in TREF and CRYSTAF, as theoretically expected.
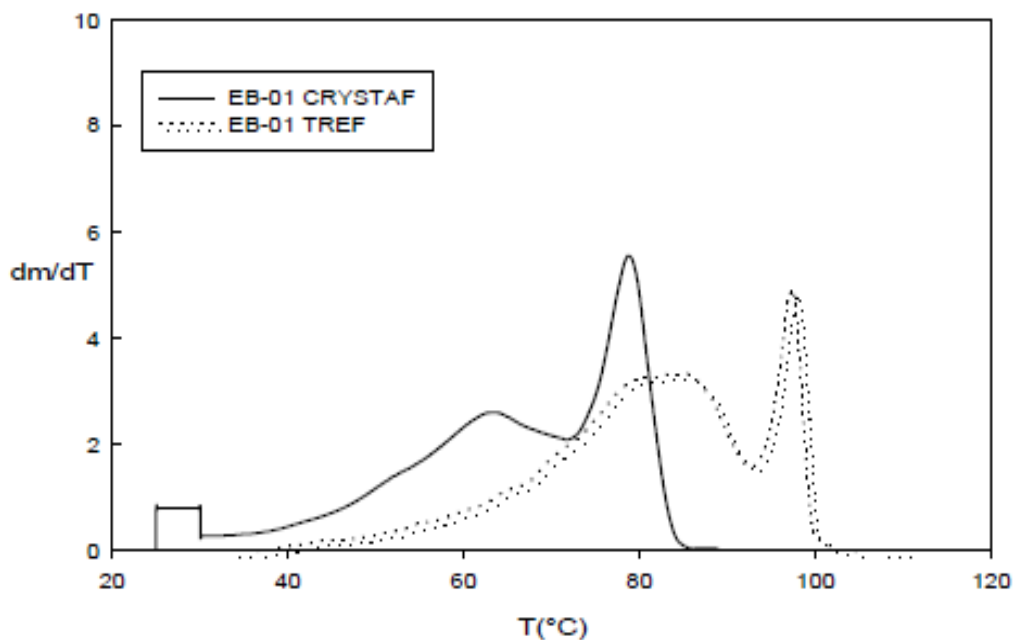
Figure 2-11. TREF and CRYSTAF profiles of the same Ziegler-Natta ethylene/1-butene copolymer.[39]

2.3.3. Crystallization Elution Fractionation (CEF)

Crystallization elution fractionation is a faster variant of TREF.[40] The main difference from TREF is that the solvent continues flowing during the precipitation/crystallization step, allowing the polymer chains to precipitate along the CEF column instead of precipitating in the same column location, as happens in TREF. This procedure reduces co-crystallization effects since polymer chains with different crystallizabilities precipitate on different locations along the column. As a consequence, higher cooling rates can be used in CEF without compromising peak resolution.[27,40,41] Figure 2-12 compares the fractionation steps in TREF and CEF, and Table 2-3 lists the main characteristics of TREF, CRYSTAF, and CEF.
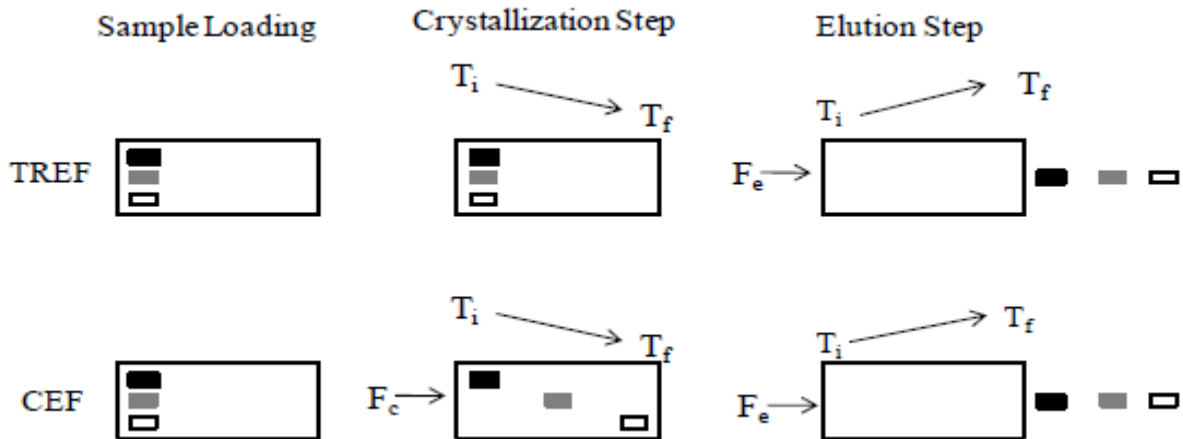
Figure 2-12. Fractionation steps in TREF and CEF. Rectangles with different shades represent polymer populations with different crystallizabilities: black = highest, grey = intermediate, white = lowest. (F_c = cooling flow rate, T_i = initial temperature, T_f = final temperature, F_e = elution flow rate).[40]

Table 2-3. The main Characteristics of TREF, CRYSTAF and CEF.

Technique	Characteristics
TREF	Column fractionation technique.
	No flow during the crystallization step.
	Detection during the elution step.
	Long analysis times.
CRYSTAF	Batch technique.
	Detection during the crystallization step.
	No elution step.
	Shorter analysis times than TREF.
CEF	Column fractionation technique.
	Flow during the crystallization step.
	Detection during the elution step.
	Short analysis times.

Calibration curves for these three methods can be determined using standards with varying α-olefin fractions and narrow CCDs. These standards may be made using a metallocene catalyst and the α-olefin fraction can be measured by ^{13}C NMR. The calibration curve is simply the relation–often linear–between the peak temperature for the standard and its α-olefin fraction. Figure 2-13 shows a calibration curve for CEF. Several TREF and CRYSTAF calibration curves have been reported in the literature.[28,33,42,43]

Sample	Comonomer Mole%
1	1.04
2	1.60
3	2.15
4	2.66
5	4.54
6	5.65
7	6.46

1) Comonomer fraction analysis using ^{13}C NMR
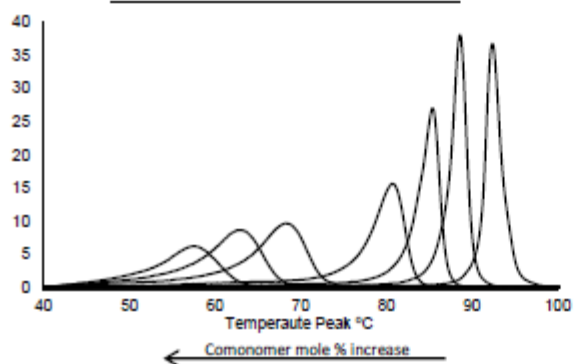
2) CEF peak temperature measurement
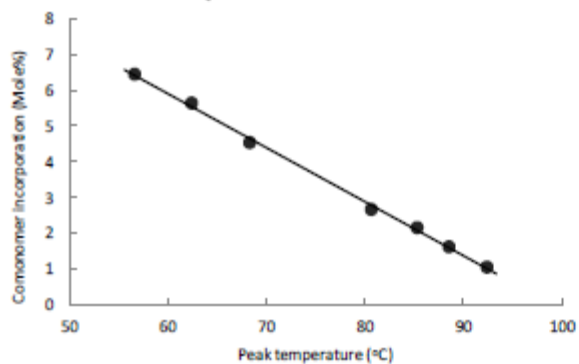
3) Plot of CEF peak temperature versus comonomer fraction (calibration curve)

Figure 2-13. CEF calibration curve for ethylene/1-octene copolymers.[44]

2.3.4. High-Temperature Solvent Gradient Interaction Chromatography (HT-SGIC)

High-temperature solvent gradient interaction chromatography is a fast technique because it is not limited by crystallization kinetics like CEF, TREF, and CRYSTAF. Instead, it depends on how polymer chains partition between a stationary support and a solvent mixture. This technique can fractionate ethylene/1-octene copolymers with 1-octene fractions varying from 0 to 100 mol %. Unfortunately, it needs[45] to be used with an evaporative light scattering detector (ELSD), which not only is hard to use, but also is not quantitative.[46,47] Macko and Pasch[48-52] fractionated a blend of polyethylene, atactic polypropylene, syndiotactic polypropylene, and isotactic polypropylene in a column filled with porous graphitic carbon using HT-SGIC. The polymer mixture was dissolved 1-decanol and transferred to the column, where it adsorbed on the packing at 160 °C. Increasing the trichlorobenze/decanol ratio in the eluent caused the different polymers to selectively desorb from the HT-SGIC column, as shown in Figure 2-14.
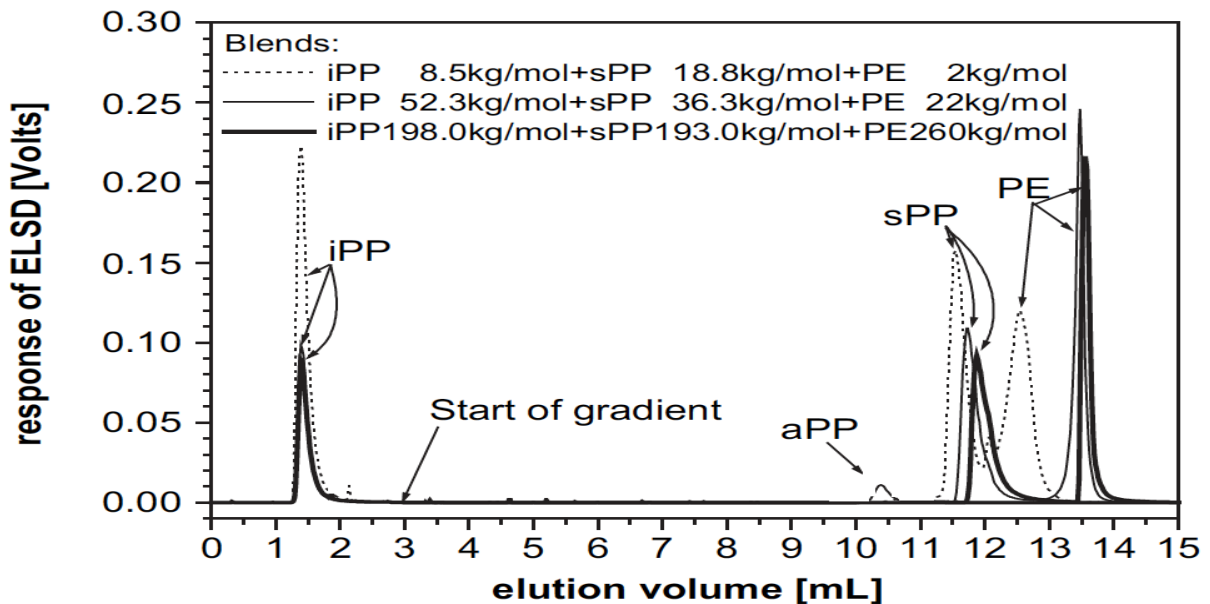
Figure 2-14. HT-SGIC profile of blends of isotactic polypropylene (iPP), atactic polypropylene (aPP), syndiotactic polypropylene (sPP) and linear polyethylene (PE).[49]

A similar procedure was followed by Macko et al.[49-51] to fractionate ethylene/4-methyl-1-pentene and ethylene/norbornene copolymers in a porous graphite Hypercarb column. The authors studied the effect of polymer molecular weight on the fractionation of isotactic polypropylene and polyethylene. The HT-SGIC profiles were not affected when $M_w > 15\text{-}20$ kg/mol.

Three different packing types (Hypercarb, Zirchrom-CARB, and activated carbon-TA95) and solvents (1-decanol, 2-ethyl-1-hexanol, and TCB) were used by Chitta et al.[48] to investigate the effect of packing type on the fractionation of linear polyethylene and polypropylene with different tacticities. All systems fractionated polyethylene. Polypropylene, however, could not be separated according to tacticity in the 2-ethyl-1-hexanol/TCB/ZirChrom-CARB system.

Ethylene-propylene copolymers were fractionated using a Hypercarb column and a mixture of 1-decanol and 1,2,4-trichlrobenzene by Cheruthazhekaat et al.[53]. Crystallization-based methods, such as CEF and TREF, can only analyze samples with a maximum fraction of propylene of 13 mol % because copolymers with higher propylene fractions do not crystalize in TCB.[45] Since HT-SGIC does not rely on crystallization, it could analyze ethylene/propylene copolymers ranging from pure polyethylene to pure polypropylene.

This versatile technique was also used by Ndiripo et al.[54] to separate isotactic, syndiotactic, and atactic polypropylene using a porous graphitic carbon packing and 1-decanol, decalin and decane as the adsorption solvents. The authors found that: *i*) tacticity, temperature, and adsorption solvent affect polypropylene retention in the column, *ii*) polypropylene could not be desorbed when decane was used.

2.3.5. High-Temperature Thermal Gradient Interaction Chromatography (HT-TGIC)

High-temperature thermal gradient interaction chromatography was invented by The Dow Chemical Company to quantify the CCD of polyolefins.[45,55] Most HT-TGIC experiments are done using Hypercarb columns (10 cm long and 4.6 mm internal diameter) and a CEF (Polymer Char, Valencia, Spain) or similar instrument. A typical Hypercarb column is packed with porous spherical graphite particles with surface area of 120 m^2/g and average pore size of 250 Å.[56-60] Figure 2-15 shows an HT-TGIC set up.
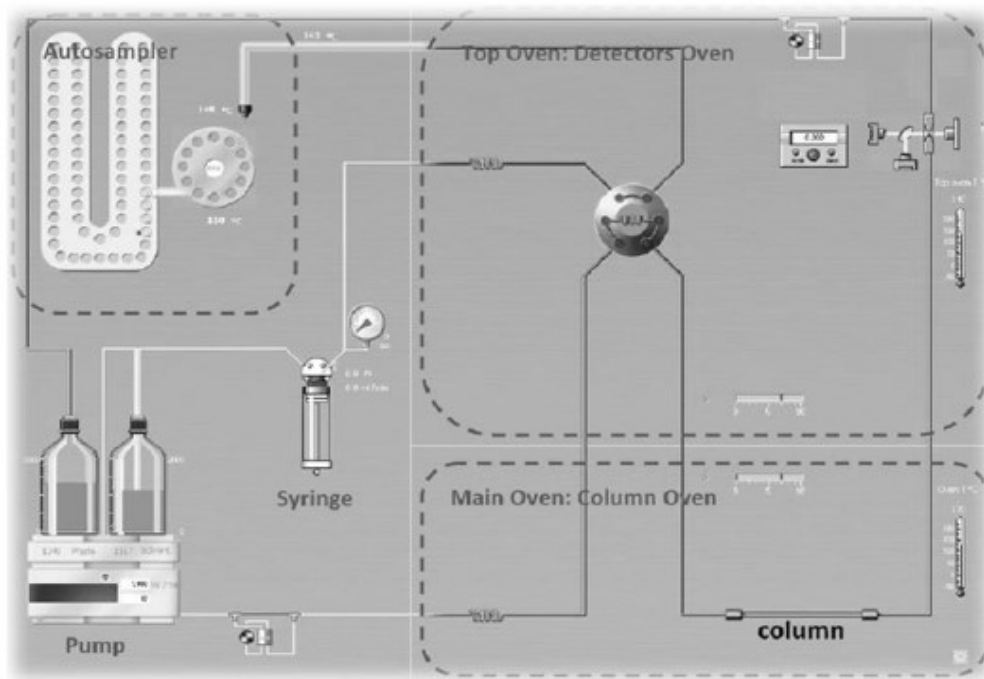
Figure 2-15. HT-TGIC experimental set up.[44]

The analysis procedure in HT-TGIC is similar to those in CEF or TREF: column loading/stabilization, cooling, and heating/elution (Figure 2-16). In the first step, 3 mg of polymer are dissolved in 8 ml of TCB (typically at 160 ºC), injected into the column through the autosampler, and allowed to stabilize for 10 minutes. In the cooling cycle, the temperature is decreased at a constant temperature rate (1 ºC/min), allowing the polymer chains to adsorb

onto the surface of the packing material. Eluent flow may continue (like in CEF) or be stopped (like in TREF) during this period. Copolymer chains with increasing α-olefin fractions adsorb on the column at lower temperatures. When the cooling process is finished (commonly at 30 ºC), the temperature is held constant for 10 minutes for stabilization. In the heating step, the temperature is increased slowly at a constant temperature rate (1 ºC/min), causing the polymer chains to desorb from the graphite surface and elute from the column: copolymers chains with higher α-olefin fractions desorb at lower temperatures, followed by chains with lower α-olefin fractions as the column temperature increases. The on-line IR detector installed at the end of the column measures the concentration (based on its CH_2 frequency signal) and chemical composition (using a ratio of CH_3/CH_2 frequency signals) of the chains flowing out of the column.
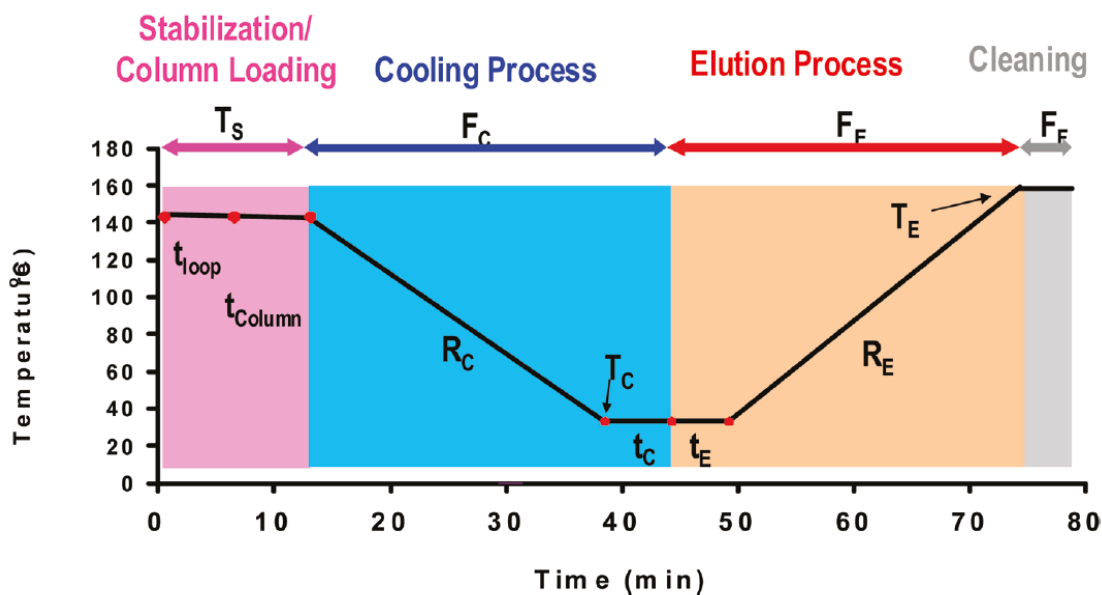
Figure 2-16. HT-TGIC experimental process (T_s = stabilization time, t_{loop} = time in the autosampler loop, F_c = cooling flow rate, R_c = cooling rate, t_{column} = column temperature, T_C = final cooling temperature, R_E = elution heating rate, T_E = final elution temperature, F_E = elution flow rate, F_F = cleaning flow rate, t_C and t_E = stabilization temperatures).[19]

High-temperature TGIC results may be affected by the fraction of α-olefin in the copolymer, polymer molecular weight, elution flow rate, heating rate, cooling rate, solvent type, column length, packing particle size and type.

Ethylene/ α-olefin copolymers with higher comonomer fractions have lower elution temperatures, as shown in Figure 2-17 for a series of ethylene/1-octene copolymers.
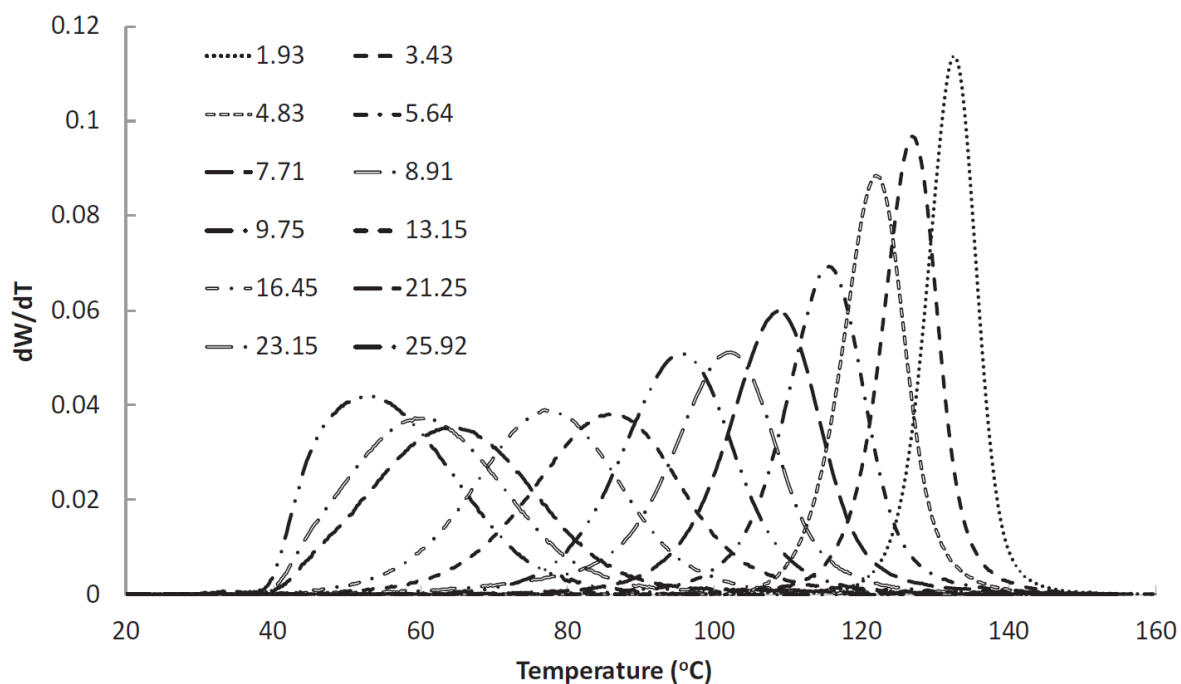
Figure 2-17. HT-TGIC profiles of ethylene/1-octene copolymers with different 1-octene molar percentages (indicated in the legends). Operation conditions: F_c = 0.02 mL/min, C_R = 5 °C /min, H_R = 3 °C/min, F_E = 0.5 mL/min, temperature range in both cycles = 160-35 °C.[61]

Polymer molecular weight affects the elution temperature when $M_n < 25\ 000$.[60] Figure 2-18 shows that the peak temperatures of polyolefins with $M_n > 25\ 000$ are not affected by polymer molecular weight. Detailed information on these samples is shown in Appendix B.
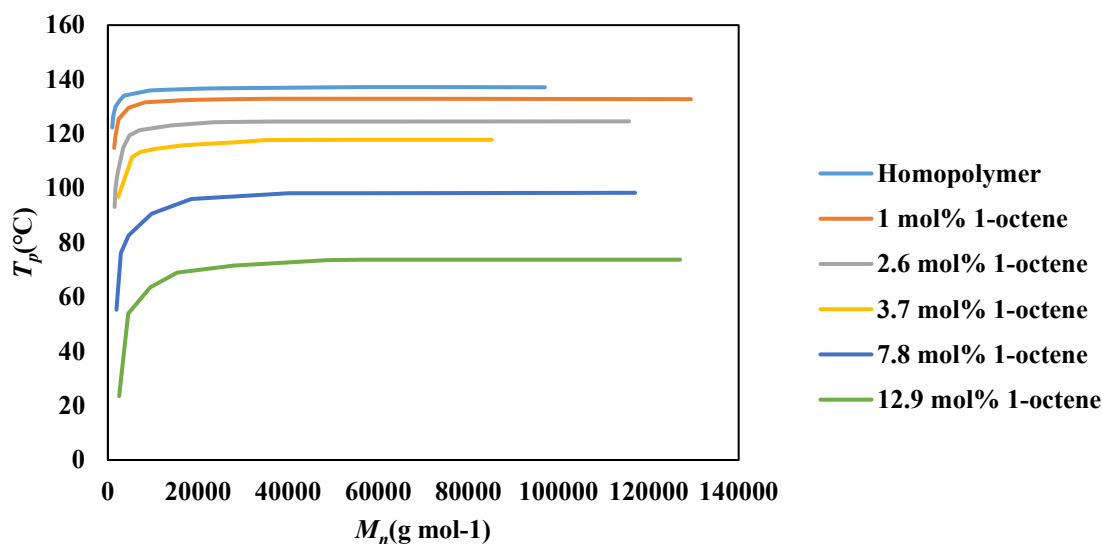
Figure 2-18. Relation between M_n and peak temperature for ethylene/1-octene copolymers with different 1-octene molar percentages.[60]

Al-Khazaal et al.[61] studied the effect of elution flow rate, heating rate, cooling rate, packing particle size, and column length on HT-TGIC profiles of ethylene/1-octene copolymers. The HT-TGIC peaks got narrower and shifted to lower temperatures when the elution flow rate increased, particularly at higher heating rates (Figure 2-19), while peak temperatures increased when the heating rate increased (Figure 2-20). The latter effect was more noticeable at higher elution flow rates. Finally, the cooling rate had a negligible effect on peak temperature and broadness (Figure 2-21).
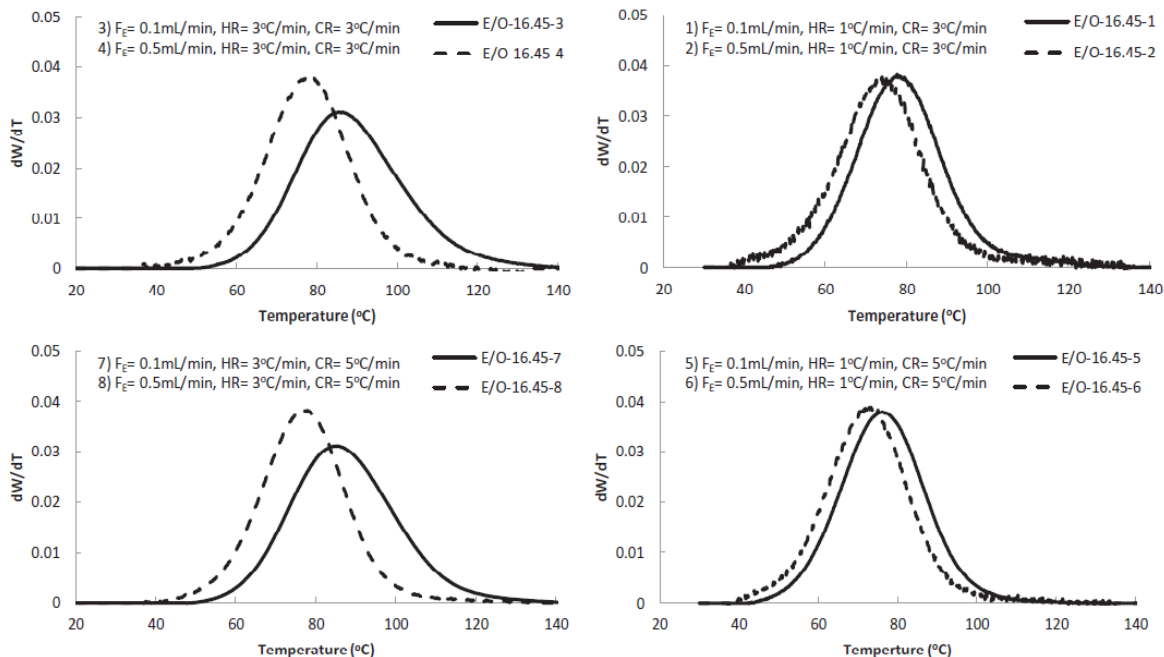
Figure 2-19. Effect of elution flow rate on HT-TGIC profile of an ethylene/1-octene copolymer with 16.45 mol % of 1-octene.[61]
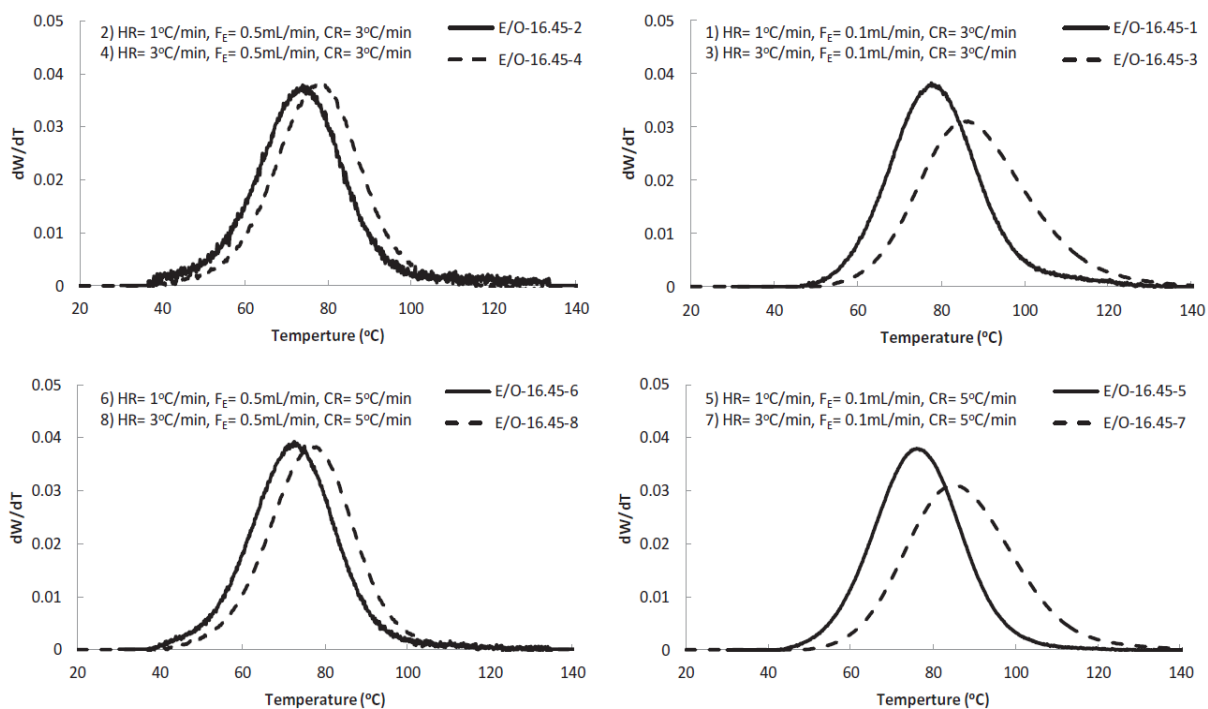
Figure 2-20. Effect of heating rate on HT-TGIC profile of an ethylene/1-octene copolymer with 16.45 mol % of 1-octene.[61]
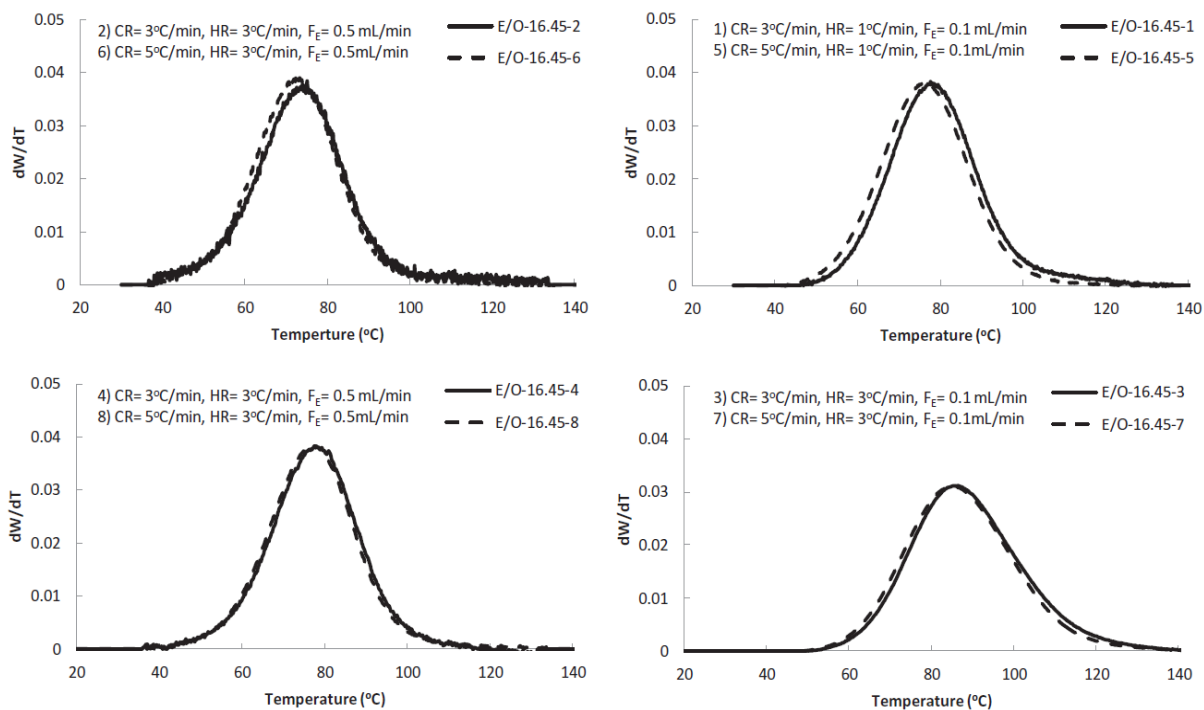
Figure 2-21. Effect of cooling rate on HT-TGIC profile of an ethylene/1-octene copolymer with 16.45 mol % of 1-octene.[61]

Al-Khazaal et al. [44] also studied the effect of packing particle size and column length on HT-TGIC fractionation. The size of the particle in the packing (d_p = 3, 5, 7 μm) had no significant effect on the fractionation of ethylene/1-olefin copolymers, likely because the polymer solutions were very dilute (0.75 mg/ml) and did not require the increased surface area of the smaller particles. Using longer columns (L = 100 and 250 mm) only moved the HT-TGIC peaks to higher temperatures because of the higher residence time in the column but did not affect peak resolution.

Alghyamah et al.[56] investigated the effect of solvent type (TCB and ODCB) on HT-TGIC profiles. Figure 2-22 shows that the slope of the calibration curves for ethylene/1-octene copolymers with either solvents is nearly the same, which indicates they have the same

27

resolution. Since TCB is a better solvent for polyolefins than ODCB, its calibration curve is shifted to lower temperatures by approximately 6 °C.

The chart shows two linear calibration curves. The blue line (TCB) is labeled $y = -0.2034x + 27.174$, $R^2 = 0.9962$. The orange line (ODCB) is labeled $y = -0.2379x + 33.884$, $R^2 = 0.9988$. The y-axis is "Comonomer fraction (mol%)" ranging from 0 to 4, and the x-axis is "Temperature (°C)" ranging from 110 to 150.
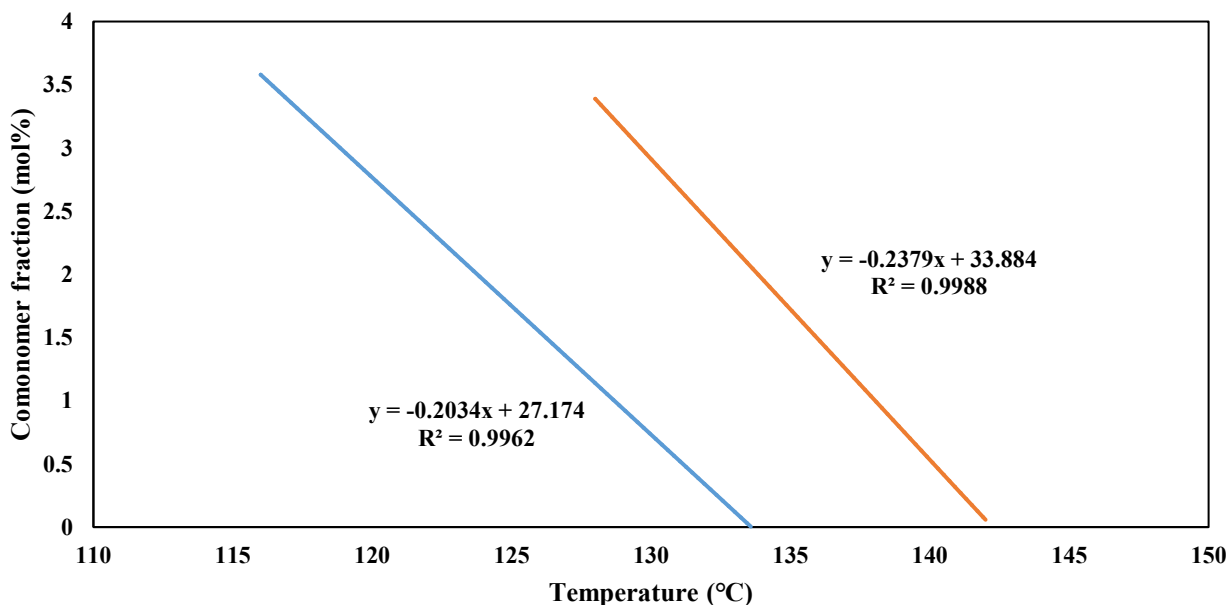
Figure 2-22. Effect of solvent type on HT-TGIC calibration curve of ethylene/1-octene copolymers (blue line = TCB, orange line = ODCB).[56]

Monrabal et al.[62] fractionated ethylene/1-octene copolymers using different HT-TGIC supports and compared these results with the equivalent TREF fractionations, as shown in Figure 2-23. The slopes of all calibration curves are almost the same, indicating they have approximately the same resolution. Among all supports, the copolymers interacted more strongly (higher peak temperatures) with porous graphite, which gives this solvent an advantage, since it can analyze ethylene/α-olefin copolymers with a wider range of α-olefin fractions.

All HT-TGIC supports reported in the open literature were porous solids. Dow Patent (WO 2019/090092)[63] proposed the use of non-porous particles (nickel, silica, glass, silicon carbide and glassy carbon) coated with graphene as chromatography packing materials for polymers. Non-porous supports are attractive because they may reduce or eliminate size exclusion effects

that may occur with porous supports. Ideally, HT-TGIC should fractionate polymer chains based only on how strongly they adsorb on a giving packing material. If the chains are also fractionated by size exclusion effects, it becomes much harder to interpret and quantify the results of these analyses. The results presented in Dow's patent show that the use of non-porous supports improved the polymer fractionation.[63]

In this thesis, I also propose the use of a non-porous support for HT-TGIC fractionation: non-porous silica coated with graphene (GNPSi). The difference of my work from Dow's patent was that I used the novel packing to fractionate the ethylene/α-olefin copolymers, while Dow's inventors used graphene-coated silica for the fractionation of maleic anhydride-modified LLDPE by HT-TGIC.
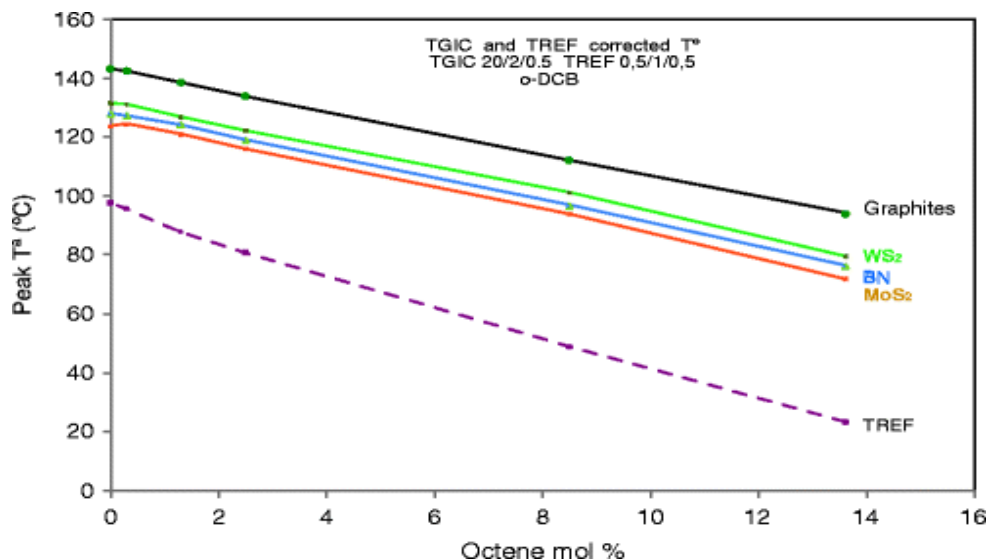
Figure 2-23. HT-TGIC analysis of a series of ethylene/1-octene copolymers using different adsorbents. TREF fractionation was used as a reference (WS$_2$ = tungsten disulfide, BN = boron nitride, MoS$_2$ = molybdenum disulfide).[62,64]

Calibration curves for HT-TGIC fractionation of ethylene/1-octene copolymers have been published in the literature for copolymers with $M_n > 25\ 000$, such as the one shown in Figure 2-24.[61]
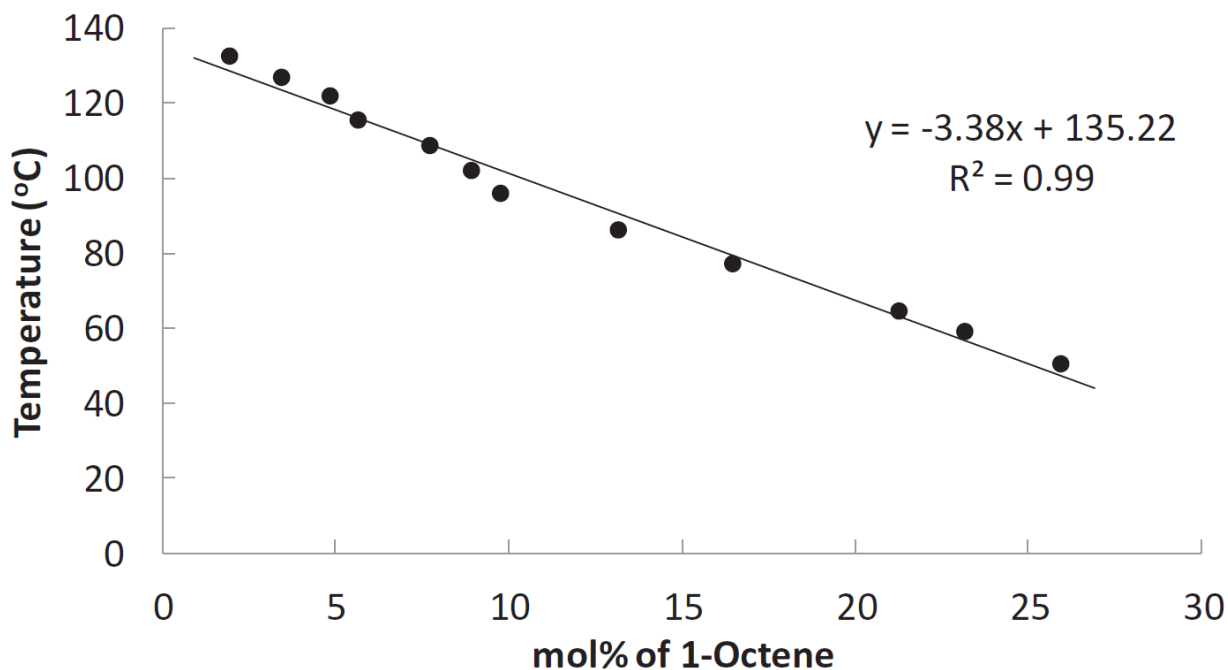
Figure 2-24. HT-TGIC calibration curve for ethylene/1-octene copolymers.[61]

Anantawaraskul et al.[65] developed a fundamental mathematical model for HT-TGIC fractionation to account for the effects of cooling rate, heating rate, and elution flow rate. Their model represented well their HT-TGIC experimental data, but could not be extrapolated to other systems without further experimental data. It is, therefore, a descriptive but not a predictive mathematical model.

An important question to answer in this area is: is there a unique calibration curve that can be used to quantify the HT-TGIC results for all kinds of polyolefins? The answer to this question would help widen the use of this technique to a variety of polyolefins. We expect the

calibration curves for different ethylene/α-olefin copolymers to follow the same behaviour: above a threshold M_n value, the HT-TGIC peak temperature is a linear function (with negative slope) of the α-olefin fraction in the copolymer. The accepted hypothesis is that the SCBs formed by α-olefin incorporation hinder the adsorption of the polymer chains on the surface of the packing material.[57] Figure 2-25 illustrates that the SCBs reduce the strength of the interactions between polymer chains and adsorbent surface. Because chains with higher SCB frequencies interact weaklier with the support, they adsorb at lower temperatures. According to this rationale, longer SCBs hinder adsorption more effectively than shorter SCBs. Finally, when the chains are too short (below a given M_n threshold), the weaker adsorption of their chain ends will start affecting the HT-TGIC elution temperatures.

Therefore, a general calibration curve for HT-TGIC must at least include three main factors: *i*) comonomer molar percent, φ, *ii*) SCB length, n_c, and *iii*) polymer molecular weight (M_n or M_w). Quantifying the effect of these factors is one of the main objectives of my thesis.

| Linear polyethylene (homopolymer), high molecular weight | Linear polyethylene (homopolymer), low molecular weight | Ethylene/1-olefin copolymers, short chain branches | Ethylene/1-olefin copolymers, longer chain branches |

Surface of packing material
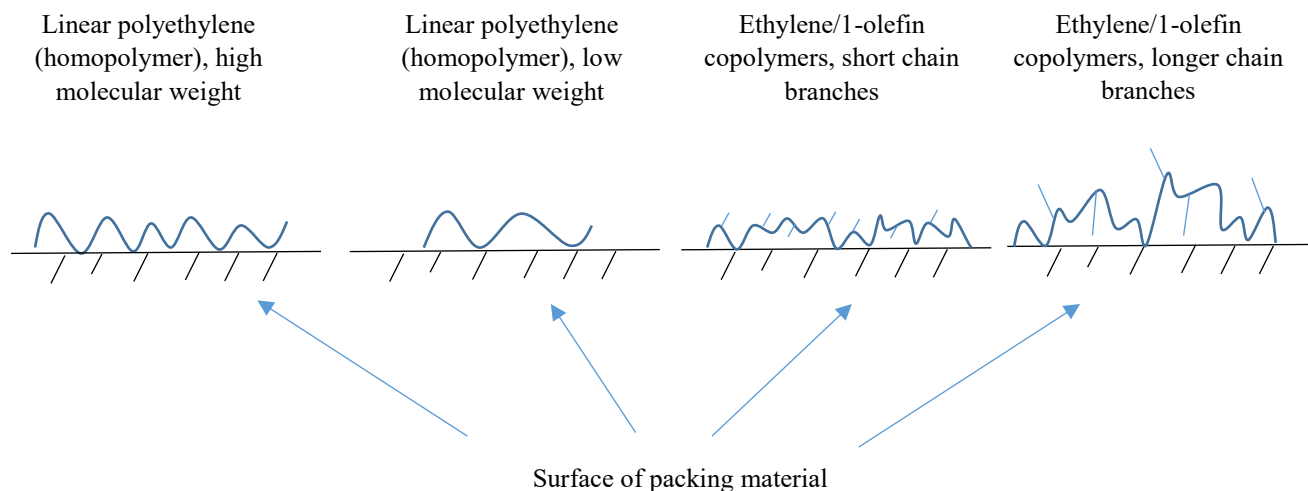
Figure 2-25. The presence of short chain branched hinders polymer chain adsorption on the surface of the packing material.[57]

Chapter 3. Polymer Synthesis and Characterization

3.1. Polyolefin Characterization

3.1.1. Gel Permeation Chromatography (GPC)

Gel permeation chromatography, also known as size exclusion chromatography (SEC), was used to measure the molecular weight distribution (MWD) of the polyolefins made in this thesis work. Our GPC unit (Polymer Char, Valencia, Spain) contained three linear columns filled with porous packing material (Agilent PLgel Olexis, 7.5×300 mm, 13 μm particles) and three detectors: infrared (IR), light scattering, and differential viscometer. Trichlorobenzene (TCB) was used as a solvent and continuous phase. All analyses were done at 145 °C at a TCB flow rate of 1.0 ml/min.

The GPC was calibrated (by Dr. S. Mehdiabadi) using narrow MWD polystyrene standards and the universal calibration curve. The online IR detector of the GPC unit was also used to measure the fraction of α-olefin across the MWD. This signal was calibrated using ethylene/α-olefin copolymer standards of known chemical composition.

The IR detector in the GPC unit acted as a mass and a composition detector by recording the CH_2 and CH_3 frequencies of the polymer chains eluting the column set. The CH_2 signal was proportional to the mass of polymer, while the CH_3/CH_2 signal ratio was used to measure the SCB frequency, which was converted to the α-olefin molar fraction in the copolymer, F_B, using the expression,

$$F_B = \frac{2*SCB}{1000+(2-n_c)*SCB} \tag{3.1}$$

where n_c is number of carbon atoms in the α-olefin (6 for 1-hexene, for instance) and SCB is the number of short chain branches per 1000 carbon atoms in the chain.

3.1.2. High-Temperature Thermal Gradient Interaction Chromatography (HT-SGIC)

High-temperature thermal gradient interaction chromatography was used (by Dr. S. Mehdiabadi help) to measure the CCD of the ethylene/α-olefin copolymers. Our unit included a Hypercarb column filled with porous graphite carbon (Hypercarb, 100×4.6 mm, $d_p = 5$ μm, 120 m²/g, 250 Å average pore size) installed in a CEF apparatus (Polymer Char, Valencia, Spain) and an online IR detector to measure the concentration of polymer eluting from the column as a function of temperature. Other operation conditions were: elution flow rate = 0.5 ml/min, heating rate = 2 ºC/min, and cooling rate = 3 ºC/min. The TGIC was calibrated for 1-hexene, 1-octene and 1-decene copolymers with the samples made previously in our group by Dr. S. Mehdiabadi.

The polymer samples were dissolved in TCB and transferred to the auto sampler at 160 ºC. A sample solution aliquot was injected into the column and the cooling step started by decreasing the temperature from 160 ºC to 30 ºC to adsorb the polymer on the packing material without TCB flow. The sample was then kept at 30 ºC for 10 min for stabilization, after which the heating step started by increasing the temperature gradually. The elution flow rate was 0.5 ml/min. During this step, the polymer desorbed, left the column, and its concentration was measured by the IR detector.

3.1.3. ^{13}C-NMR Analysis

Five ethylene/1-decene copolymers, made by Dr. Mehdiabadi, were analyzed by ^{13}C-NMR to determine a calibration curve for ethylene/1-decene copolymers. The calibration curves for ethylene/1-hexene and ethylene/1-octene had been previously determined in our group.

A mass of 100 mg of each sample was dissolved in 1,1,2,2-terachloroethane (TCE) in a 10 mL NMR tube and homogenized by heating the tube in a heating block at 120 ºC for about 4 hours. Quantitative ^{13}C NMR experiments were done at 100.5 MHz on a Varian INOVA 500 MHz at 120 ºC. The number of scans was 1712, with a delay time between scans of 10 s and an acquisition time of 2 s. The signal-to-noise ratio was 675.

The mole percent of 1-decene were obtained by integrating the spectra using Equation (3.2) to (3.7), according to ASTM-D5017-96. Table 3-1 shows the integration limits for the ethylene/1-decene copolymers.

$$O_1 = \frac{A+2C+2D}{2} \tag{3.2}$$

$$O_2 = \frac{1.5A+2B+(E+D)-D}{3} \tag{3.3}$$

$$O' = \frac{O_1+O_2}{2} \tag{3.4}$$

$$E' = \frac{(F+G+H)-(3A+3B+H+P+I)}{2} + O' \tag{3.5}$$

$$F_B = \frac{O'}{O'+E'} \tag{3.6}$$

$$\varphi = \frac{O'}{O'+E'} \times 100 \tag{3.7}$$

Table 3-1. Integration limits for ethylene/1-decene copolymers.

Area	Region (ppm)
A	40.5 to 41.5
B	39.5 to 40.5
C	37.0 to 39.5
D	Peak at 35.8
D+E	33.2 to 36.8
F+G+H	25.5 to 33.2
H	26.5 to 28.5
I	24.0 to 25.0
P	22.0 to 24.0

Appendix C contains ^{13}C NMR results of all ethylene/1-decene copolymers.

3.2. Materials

The materials used to make ethylene/α-olefin copolymers were toluene, ethanol, ethylene, 1-hexene, 1-octene, 1-decene, methylaluminoxane (MAO), nitrogen, triisobuylaluminum (TIBA), hydrogen, 1,2,4-trichlorobenzene (for characterization), and the metallocene catalyst (methyl (6-t-butoxyhexyl) silyl (η5-tetramethylcyclopentadienyl) (t-butylamido) titanium dichloride (CGC-Ti). Table 3-2 shows the detailed information for these materials.

Table 3-2. Materials used in the synthesis and characterization of ethylene/α-olefin copolymers.

Material	Supplier	Purity
Toluene	Sigma-Aldrich	99.9% for HPLC
Ethanol	Sigma-Aldrich	For HPLC
1-hexene	Sigma-Aldrich	97%
1-ocetene	Sigma-Aldrich	98%
1-decene	Sigma-Aldrich	94%
TIBA	Sigma-Aldrich	25 wt% in toluene
TCB	Sigma-Aldrich	For GPC and TGIC
MAO	Albemarle	10 wt% in toluene
Nitrogen	Praxair	99.998%
Ethylene	Praxair	99%
Hydrogen	Praxair	99.95%
CGC-Ti	LG Chem	0.428 M (dissolved in toluene)

3.3. Polymerization Procedure

All polymerizations were performed in a 300-ml autoclave reactor (Parr autoclave) under semi-batch operation. Before being injected in the reactor, ethylene was flown through molecular sieves (3A/4A mixture) and a copper (II) oxide bed to remove polar impurities. The catalyst, co-catalyst, and α-olefin comonomers were transferred to 20 ml vials and sealed with rubber caps and metal caps inside the glove box under N_2 pressure. The sealed vials were removed from the glove box and transferred to the reactor by using flexible needles to avoid contamination. Figure 3-1 shows the P&D diagram.

At the beginning of each polymerization, the reactor was washed with 150 ml toluene and 0.5 g of TIBA (used as a scavenger) and heated to 140 °C. After keeping the reactor at 140 ºC for 10 min, the toluene-TIBA mixture was removed under N_2 pressure. After washing with TCB solvent, the reactor was purged with N_2 six times to remove any impurities left in the system. Finally, the reactor was cooled to 40 °C.
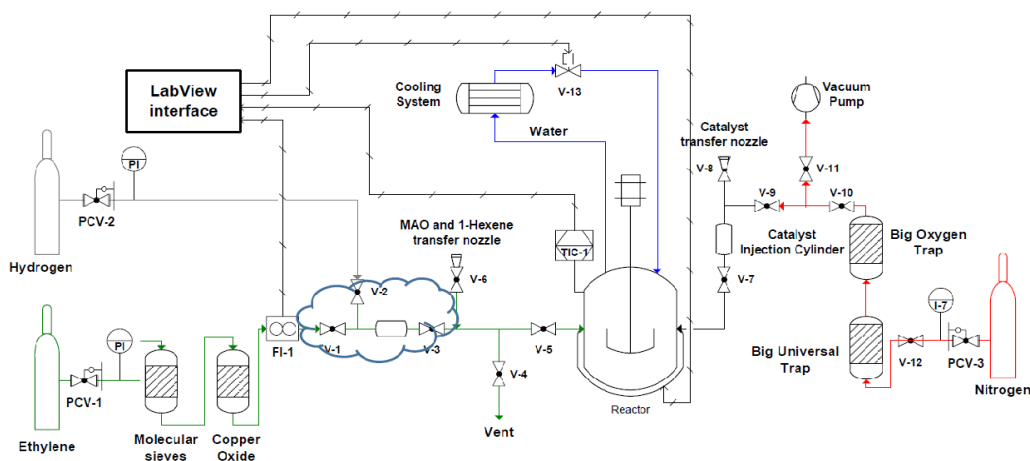
Figure 3-1. P&ID diagram of the reactor system.[66]

The Al/Ti ratio should be higher than 24 000 when using CGC-Ti to supress the formation of LCBs, which should not be added to the copolymers required in this investigation.[67] The desired amounts of cocatalyst, MAO, α-olefin comonomer, and 150 ml of toluene were transferred to the reactor (see Chapter 4). Then, desired volume of H_2 (10, 15, 20, 25 or 30 psi) was first transferred to a volumetric bomb. The H_2 pressure was controlled so that the mass of H_2 transferred to the reactor could be estimated. Finally, the ethylene line was connected to the H_2 bomb and the back pressure from the ethylene line forced the H_2 into the reactor. The ethylene pressure for all polymerizations was 110 psi. The catalyst, dissolved in 10 ml of toluene, was first injected into a bomb connected to the reactor, and then injected into the reactor using N_2 at 120 psi to start the polymerization. The polymerization solution was stirred at 1300 rpm.

A LabVIEW program was used to keep the reactor temperature at 120 °C using an external electrical heat mantle and a cooling coil connected to a water bath by varying the output to the mantle and water flow rate to the cooling coil.

After 15 min of polymerization, the reactor stirrer was stopped and the polymer solution was blown out of the reactor under N_2 pressure. The polymer was then precipitated in 150 to 200 ml of ethanol, filtered, and dried in an oven at 70 °C overnight.

Chapter 4.   A General Calibration Curve for a HT-TGIC Conventional Column

4.1. Introduction

The ethylene/ α-olefin copolymerizations were performed with different fractions of 1-hexene, 1-octene, and 1-decene in a 300-ml stainless steel autoclave reactor to make copolymers with different comonomer molar percent. Polymer molecular weight was regulated by varying H_2 partial pressure in the reactor. The ethylene pressure for all polymerizations was set to 110 psi, the toluene volume was 170 ml, and all polymerizations were performed at 120 °C. Table 4-1 summarizes these polymerization conditions.

The catalyst concentration was calculated based on the number of moles of catalyst divided by the volume of toluene in the reactor. The concentrations of 1-hexene, 1-octene, or 1-decene in the reactor were calculated in the same way.

Ethylene was polymerized alone under four H_2 partial pressures. These homopolymers were used as starting points in the calibration curves derived in this thesis. Copolymerizations were done under five H_2 partial pressures and six α-olefin concentrations. Since the polymer yield decreased when the concentrations of H_2 and comonomer increased, the catalyst concentration was adjusted to ensure that enough copolymer was produced for further analysis.

Table 4-1. Polymerization condition.

Comonomer	Catalyst (µmol/L)	H$_2$ (Psi)	α-olefin (mol/L)
Homopolymer	0.2-0.5	10, 15, 20, 25, 30	-
1-Hexene	0.2-0.5	10, 15, 20, 25, 30	0.140, 0.280, 0.489, 0.699, 0.987, 1.188
1-Octene	0.2-0.5	10, 15, 20, 25, 30	0.140, 0.280, 0.489, 0.699, 0.987, 1.188
1-Decene	0.2-0.5	10, 15, 20, 25, 30	0.140, 0.280, 0.489, 0.699, 0.987, 1.188

$P_E = 110$ psig, $T = 120$ °C, $V_S = 170$ mL

4.2. Anticipating the form of the Calibration curve

Alkhazaal et al.[60] made a series of ethylene homopolymers and ethylene/1-octene copolymers with different molecular weights and 1-octene molar percent (Appendix A).They showed that the relation between absolute peak temperature (T_p) and number average molecular weight (M_n) was exponential for ethylene homopolymers (Figure 4-1), while the relation between $1/T_p$ and $1/M_n$ was linear (Figure 4-2). They observed the same behaviour for ethylene/1-octene copolymers with the same 1-octene molar percent (Appendix A).
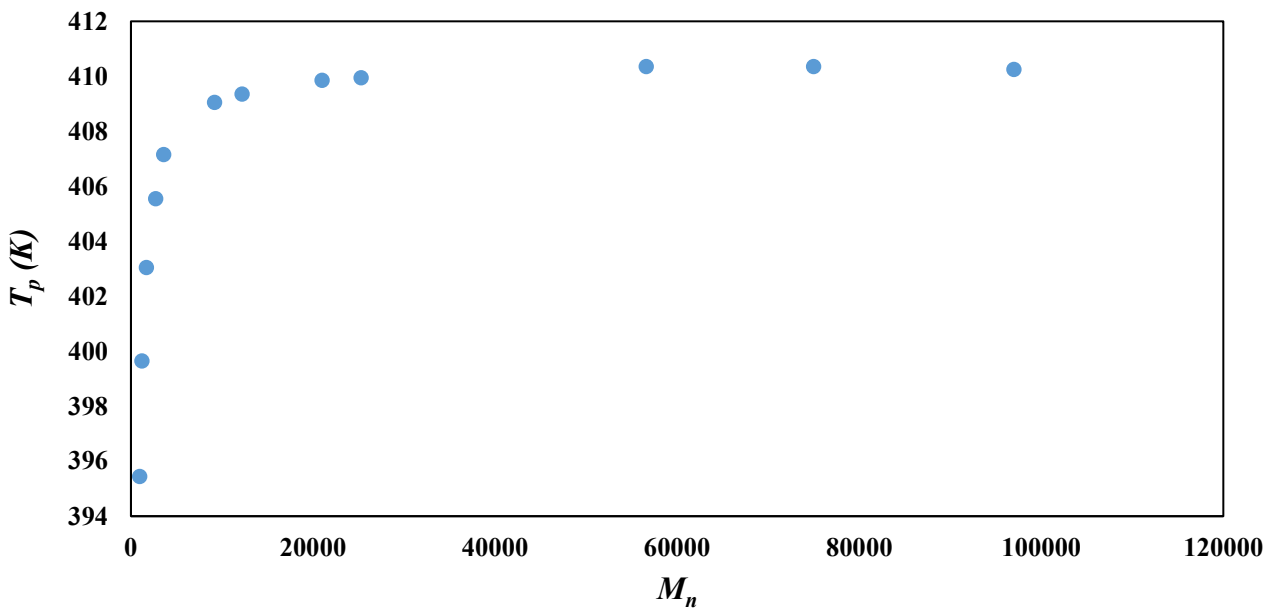
Figure 4-1. Relation between T_p (K) and M_n for homopolymers.[60]
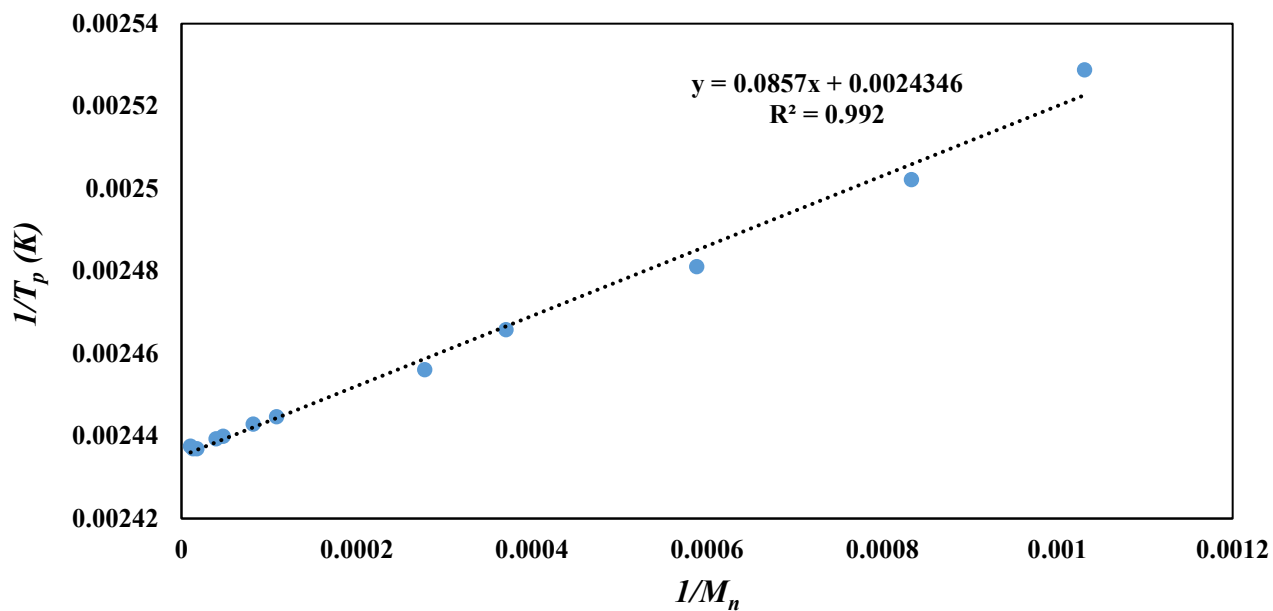
Figure 4-2. Relation between $1/T_p$ (K) and $1/M_n$ for homopolymers.[60]

The following equations relating $1/T_p$ to $1/M_n$ were found by us using Alkhazaal et al.[60] data for copolymers with the same 1-octene molar percent,

$$\frac{1}{T_p} = 0.0857\,\frac{1}{M_n} + 0.0024346 \quad \varphi = 0 \; (hompolymer) \tag{4.1}$$

$$\frac{1}{T_p} = 0.1662\,\frac{1}{M_n} + 0.0024513 \quad \varphi = 1\% \tag{4.2}$$

$$\frac{1}{T_p} = 0.3336\,\frac{1}{M_n} + 0.0024902 \quad \varphi = 2.6\% \tag{4.3}$$

$$\frac{1}{T_p} = 0.3606\,\frac{1}{M_n} + 0.0025425 \quad \varphi = 3.7\% \tag{4.4}$$

$$\frac{1}{T_p} = 0.6743\,\frac{1}{M_n} + 0.0022667 \quad \varphi = 7.8\% \tag{4.5}$$

$$\frac{1}{T_p} = 1.2678\,\frac{1}{M_n} + 0.0028346 \quad \varphi = 12.9\% \tag{4.6}$$

Equations (4.1) to (4.6) show that increasing the 1-octene fraction in the copolymer increases the slope and intercept of these linear relations. Moreover, these equations illustrate that the basic form of the calibration curve is,

$$\frac{1}{T_p} = a \times \frac{1}{M_w} + b \tag{4.7}$$

where M_n from Alkhazaal's work was replaced with M_w. Even though the form of Equation (4.7) should be valid for M_n or M_w (using different values for a), M_w is preferred because this value is less sensitive to experimental errors during GPC analysis than M_n.

Based on Equation (4.1) to (4.6), one may modify Equation (4.7) to quantify the effect of comonomer molar percent, φ, on the "constants" a and b,

$$\frac{1}{T_p} = f(\varphi)\,\frac{1}{M_w} + g(\varphi) \tag{4.8}$$

Different functional forms for $f(\varphi)$ and $g(\varphi)$ were attempted to fit of the widest range of HT-TGIC experimental data, as will be explained later in this chapter. The best functional forms were,

$$f(\varphi) = a_1 e^{a_2 \varphi} \tag{4.9}$$

$$g(\varphi) = b_1 \varphi + b_2 \tag{4.10}$$

Consequently, Equation (4.8) becomes,

$$\frac{1}{T_p} = a_1 e^{a_2 \varphi} \frac{1}{M_w} + b_1 \varphi + b_2 \tag{4.11}$$

4.3. Ethylene/1-Hexene Calibration Curve

Table 4-2 lists the number average molecular weights (M_n), weight average molecular weights (M_w), polydispersity indices (PDI), 1-hexene molar %, and the HT-TGIC peak temperatures of all ethylene/1-hexene copolymers. The following convention was adopted for the sample names: The first two letters indicate monomer (E = ethylene) and comonomer (H = 1-hexene) type, followed by M_w in kDa, and finally by the molar percent of comonomer, φ. For instance, sample E/H-18.0-0.71 is an ethylene/1-hexene copolymer with M_w = 18 000 and φ = 0.71 %. Samples H-11.8 and H-13.3 were made by my colleague, Mr. V. Hegde.

Table 4-2. Characterization data for ethylene/1-hexene copolymers.

Sample	SCB/1000C	M_w	M_n	PDI	1-hexene%	T_p (°C)
E/H-18.0-0.71	3.5	18 000	6 500	2.77	0.71	127.6
E/H-17.5-1.91	9.2	17 500	6 900	2.56	1.91	118.1
E/H-16.2-1.72	12.9	16 200	7 500	2.17	2.72	114.8
E/H-17.4-2.85	13.5	17 400	6 200	2.81	2.85	117.0
E/H-14.6-0.04	0.2	14 600	5 100	2.88	0.04	127.5
E/H-14.5-8.11	34.9	14 500	5 800	2.5	8.11	96.4
E/H-14.2-9.92	41.4	14 200	7 300	1.95	9.92	83.4
E/H-11.6-0.36	1.8	11 600	4 200	2.77	0.36	126.7
E/H-12.2-1.55	7.5	12 200	5 500	2.20	1.55	117.7
E/H-12.3-5.36	24.2	12 300	5 000	2.45	5.36	102.6
E/H-12.7-6.69	29.5	12 700	4 700	2.69	6.69	99.5
E/H-9.5-0.85	4.2	9 500	4 200	2.26	0.85	119.0
E/H-9.2-5.38	24.3	9 200	4 200	2.20	5.38	98.7
E/H-9.1-6.08	27.1	9 100	4 000	2.26	6.08	96.6
E/H-8.7-7.82	33.8	8 700	3 100	2.82	7.82	91.4
E/H-9.4-8.46	36.2	9 400	4 800	1.95	8.46	88.5

Table 4-2. Characterization data for ethylene/1-hexene copolymers (continued).

Sample	SCB/1000C	M_w	M_n	PDI	1-hexene%	T_p (°C)
E/H-8.9-9.04	38.3	8 900	5 000	2.08	9.04	86.2
E/H-23.0-1.93	9.3	23 000	7 900	2.93	1.93	117.2
E/H-27.7-23.23	79.3	27 700	14 000	1.98	23.23	46.2
E/H-19.3-1.52	7.4	19 300	6 800	2.85	1.52	124.1
E/H-19.5-12.50	50.0	19 500	7 700	2.54	12.50	79.9
H-23.0	0	23 000	9 300	2.48	0	129.0
H-15.3	0	15 300	6 900	2.23	0	128.6
H-11.8	0	11 800	5 800	2.04	0	127.0
H-13.3	0	13 300	6 500	2.03	0	127.3

Figure 4-3 compares the HT-TGIC profiles of all ethylene/1-hexene copolymers. Figure 4-4 shows the HT-TGIC profile of the homopolymers. The rectangular area indicated at the left-side of some profiles indicates the mass fraction of polymer that does not adsorb on the column at room temperature. This is not a chromatographic, but only an indication of how much polymer was not fractionated and eluted from the column at the beginning of the analysis. This area increases as the fraction of α-olefin in the copolymer increases, since highly branched (SCB) copolymers do not adsorb as easily on HT-TGIC supports as less branched chains.
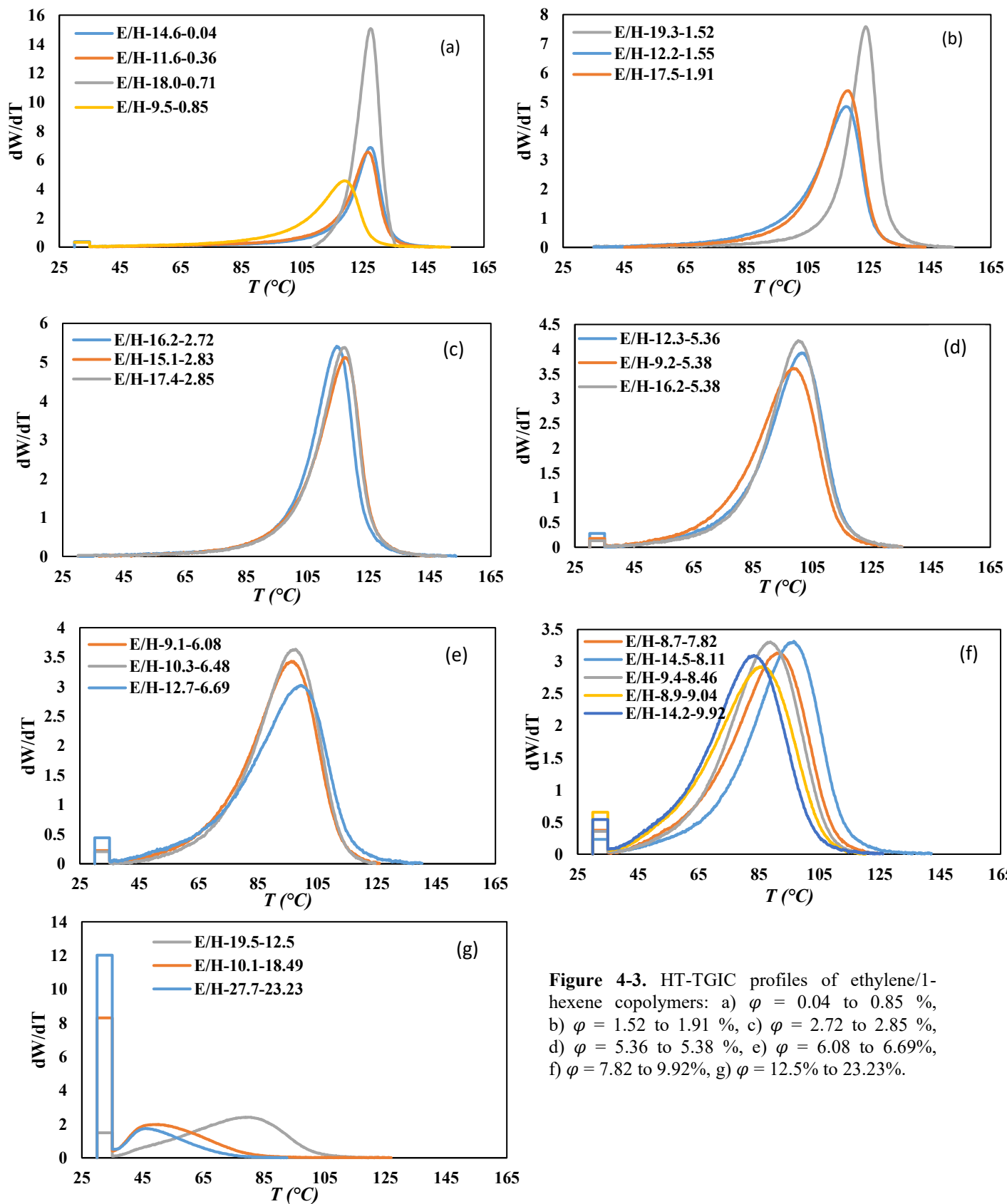
Figure 4-3. HT-TGIC profiles of ethylene/1-hexene copolymers: a) φ = 0.04 to 0.85 %, b) φ = 1.52 to 1.91 %, c) φ = 2.72 to 2.85 %, d) φ = 5.36 to 5.38 %, e) φ = 6.08 to 6.69%, f) φ = 7.82 to 9.92%, g) φ = 12.5% to 23.23%.
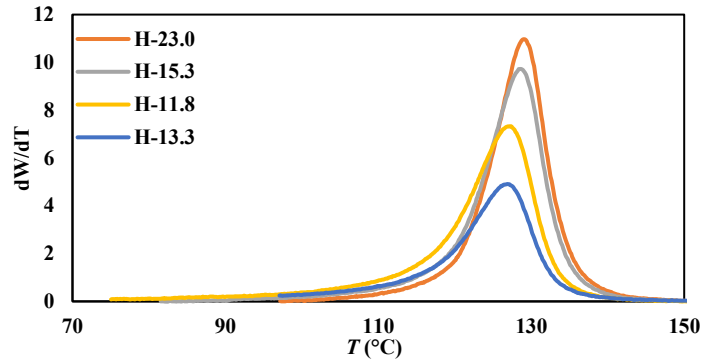
Figure 4-4. HT-TGIC profile of homopolymers.

The subroutine fitlnm available in MATLAB was used to estimate the coefficients of Equation (4.11) for the ethylene/1-hexene copolymers (Table 4-3).

Table 4-3. Calibration curve coefficients for ethylene/1-hexene copolymers.

	a_1	a_2	b_1	b_2	R^2	RMSD
Coefficients	0.50	0.050	2.7573×10^{-5}	0.002449	0.989	1.65×10^{-5}

Therefore, the peak temperature, in K, as a function of M_w and 1-hexene molar percent is given by,

$$\frac{1}{T_p} = 0.50e^{0.050\varphi}\frac{1}{M_w} + 2.7573 \times 10^{-5}\,\varphi + 0.002449 \tag{4.12}$$

Alkhazaal et al.[60] reported a peak temperature of approximately 135.2 °C for ethylene homopolymers with $M_n > 25\,000$. When $M_n \rightarrow \infty$ and $\varphi = 0$, the peak temperature according to Equation (4.12) is $1/T_p = 0.002449$ or $T_p = 408.33$ K $= 135.2$ °C, which agrees with this previous finding.

Figure 4-5 shows that the prediction errors were randomly distributed around zero and that all but 2 predictions deviated less than 1% of the experimental peak temperature.
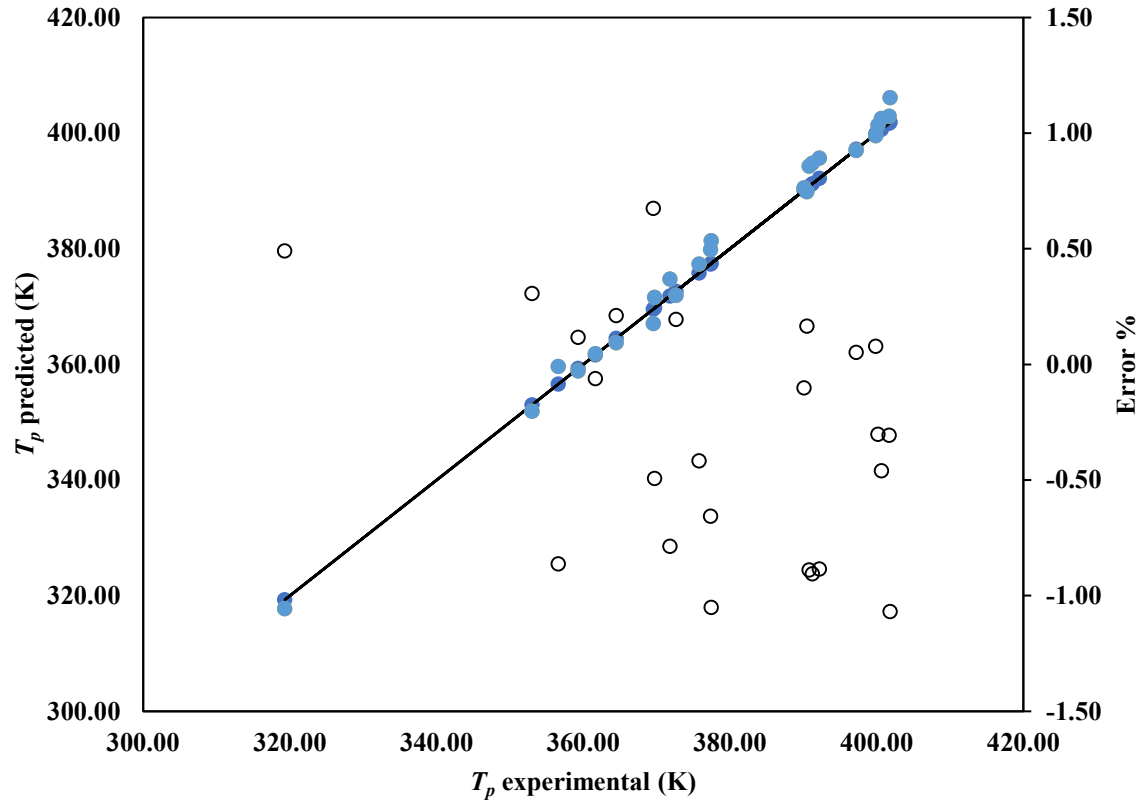
Figure 4-5. Predicted versus experimental HT-TGIC peak temperatures and prediction errors for ethylene/1-hexene copolymers.

4.4. Ethylene/1-Octene Calibration Curve

Table 4-4 summarizes the characterization data for the ethylene/1-octene copolymers made in this investigation.

Table 4-4. Characterization data for ethylene/1-octene copolymers.

Sample ID	SCB/1000C	M_w	M_n	PDI	1-octene%	T_p (°C)
E/O-31.3-10.01	38.5	31 300	10 800	2.89	10.01	90.9
E/O24.0-0.95	4.6	24 000	9 300	2.58	0.95	123.3
E/O25.3-1.01	4.9	25 300	9 400	2.69	1.01	122.7
E/O-24.6-3.01	13.8	24 600	11 000	2.23	3.01	116.3
E/O-26.4-5.28	22.8	26 400	11 500	2.29	5.28	104.0
E/O-25.1-6.85	28.4	25 100	10 000	2.52	6.85	99.4
E/O-19.5-2.87	13.2	19 500	8 400	2.31	2.87	112.3
E/O-20.0-3.39	15.4	20 000	6 800	2.94	3.39	108.5
E/O-19.8-7.14	29.4	19 800	6 900	2.93	7.14	100.7
E/O-21.3-10.49	39.9	21 300	8 900	2.38	10.49	87.4
E/O-16.0-2.77	12.8	16 000	6 100	2.64	2.77	110.2
E/O-16.7-2.94	13.5	16 700	7 500	2.23	2.94	109.8
E/O-15.0-4.26	18.9	15 000	6 400	2.34	4.26	109.0
E/O-16.5-5.47	23.5	16 500	5 800	2.83	5.47	103.7
E/O-16.9-10.55	40.1	16 900	7 700	2.19	10.55	81.1
E/O-13.8-1.24	6.0	13 800	5 400	2.56	1.24	119.3

Table 4-4. Characterization data for ethylene/1-octene copolymers (continued).

Sample ID	SCB/1000C	M_w	M_n	PDI	1-octene%	T_p (°C)
E/O-13.5-2.17	10.2	13 500	5 100	2.63	2.17	115.7
E/O-14.2-3.06	14.0	14 200	6 500	2.20	3.06	110.2
E/O-14.1-4.83	21.1	14 100	6 500	2.18	4.83	103.1
E/O-13.4-9.78	37.8	13 400	7 100	1.89	9.78	83.67
E/O-12.3-6.70	27.9	12 300	5 100	2.42	6.70	96.3
E/O-11.4-7.38	30.2	11 400	4 900	2.34	7.38	92.8
E/O-10.1-10.42	39.7	10 100	4 600	2.17	10.42	81.3
E/O-10.3-13.88	49.0	10 300	4 600	2.26	13.88	68.4
E/O-6.6-2.13	10.0	6 600	3 300	2.03	2.13	109.4
E/O-9.1-7.47	30.5	9 100	4 200	2.16	7.47	91.2
E/O-8.5-13.21	47.3	8 500	3 900	2.15	13.21	67.8
E/O-7.3-14.66	50.9	7 300	3 300	2.17	14.66	60.1
E/O-7.2-14.99	21.7	7 200	3 000	2.36	14.99	56.1
H-23.0	0	23000	9 300	2.48	0	129.0
H-15.3	0	15 300	6 900	2.23	0	128.6
H-11.8	0	11 800	5 800	2.04	0	127.0
H-13.3	0	13 300	6 500	2.03	0	127.3

Figure 4-6 compares the HT-TGIC profiles of all ethylene/1-octene copolymers.
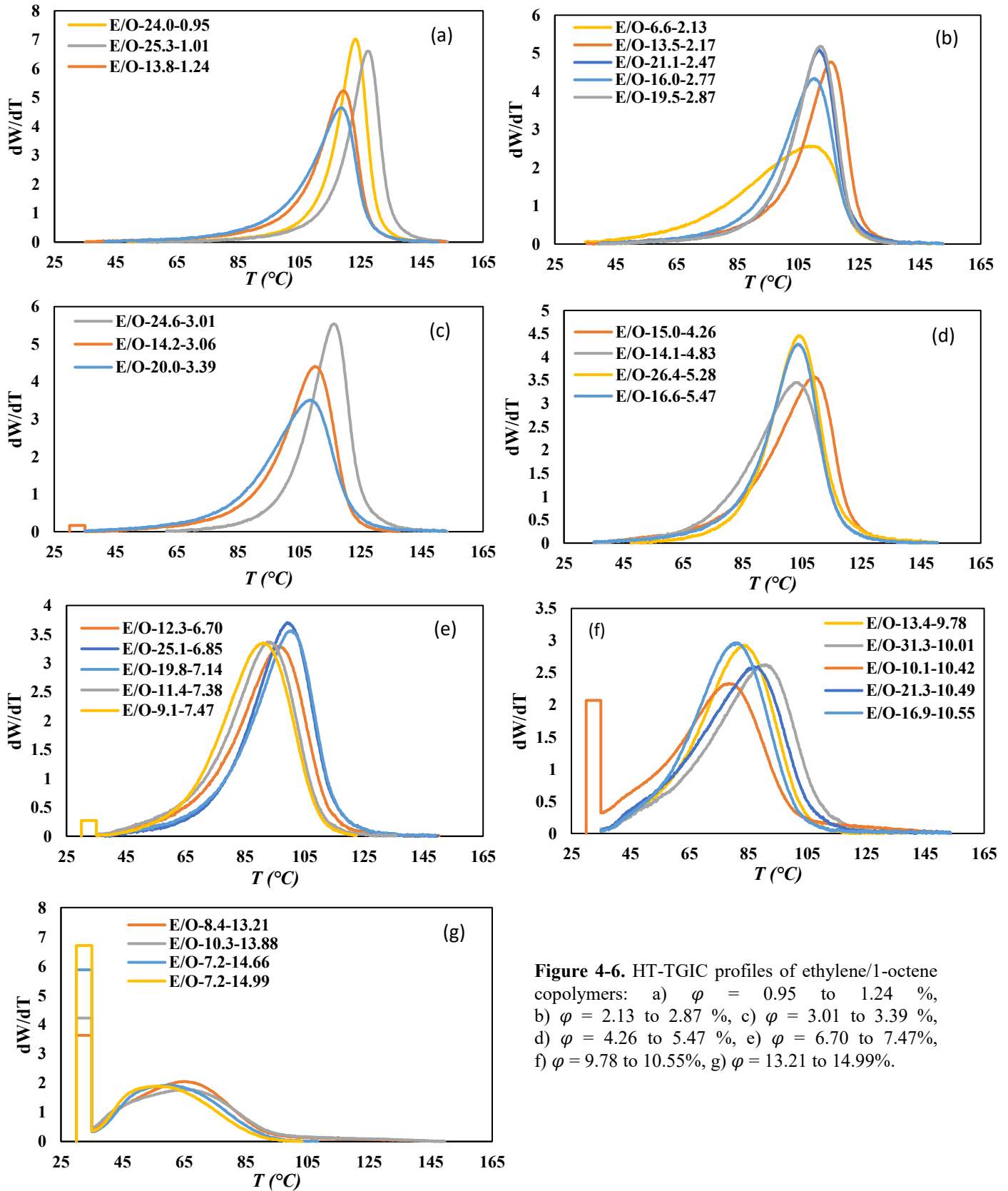
Figure 4-6. HT-TGIC profiles of ethylene/1-octene copolymers: a) φ = 0.95 to 1.24 %, b) φ = 2.13 to 2.87 %, c) φ = 3.01 to 3.39 %, d) φ = 4.26 to 5.47 %, e) φ = 6.70 to 7.47%, f) φ = 9.78 to 10.55%, g) φ = 13.21 to 14.99%.

The model parameters for the ethylene/1-octene copolymers were estimated using the same MATLAB algorithm used for the ethylene/1-hexene samples (Table 4-5).

Table 4-5. Calibration curve coefficients for ethylene/1-octene copolymers.

	a_1	a_2	b_1	b_2	R^2	RMSD
Coefficients	0.50	0.030	3.0616×10^{-5}	0.002449	0.980	2.09×10^{-5}

The calibration curve for these copolymers is,

$$\frac{1}{T_p} = 0.50e^{0.030\varphi}\frac{1}{M_w} + 3.0616 \times 10^{-5}\varphi + 0.002449 \qquad (4.13)$$

The coefficient b_1 in Equation (4.13) is larger than the equivalent one in Equation (4.12) for ethylene/1-hexene copolymers. This implies that the presence of 1-octene in the copolymer (longer SCBs) affects the value of T_p more than 1-hexene. In other words, ethylene/1-octene copolymers have lower T_p values than ethylene/1-hexene copolymers with the same φ and M_w. Figure 4-7 shows that the prediction errors of Equation (4.13) are randomly distributed around zero for ethylene/1-octene copolymers.
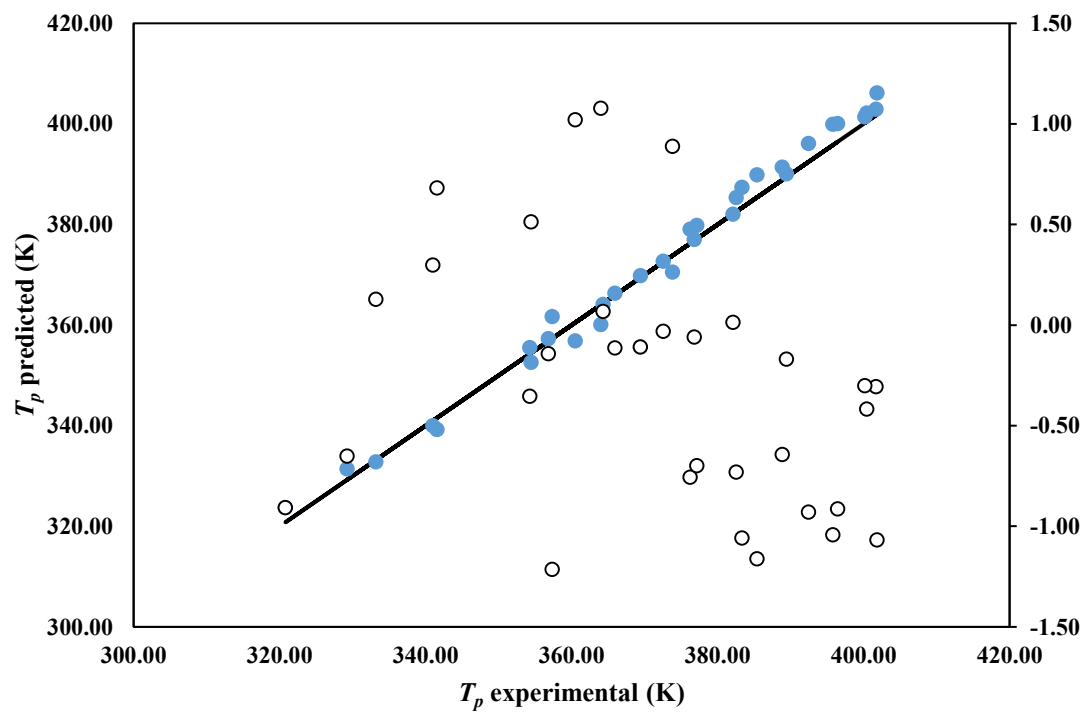
Figure 4-7. Predicted versus experimental HT-TGIC peak temperatures and prediction errors for ethylene/1-octene copolymers.

4.5. Ethylene/1-Decene Calibration Curve

Table 4-6 summarizes the characterization data for the ethylene/1-octene copolymers.

Table 4-6. Characterization data for ethylene/1-decene copolymers.

Sample ID	SCB/1000C	M_w	M_n	PDI	1-decene%	T_p (°C)
E/D-38.9-6.50	25.8	38,900	15,900	2.44	6.50	100.60
E/D-35.9-7.12	27.7	35,900	14,600	2.47	7.12	99.71
E/D-29.2-2.06	9.5	29,200	12,200	2.40	2.06	121.63
E/D-25.7-1.02	4.9	25,700	9,700	2.64	1.02	126.18
E/D-24.5-3.41	15.0	24,500	11,900	2.07	3.41	112.02
E/D-24.2-4.42	18.8	24,200	9,200	2.62	4.42	106.35
E/D-23.9-4.48	19.0	23,900	9,500	2.51	4.48	107.20
E/D-22.7-5.16	21.4	22,700	11,200	2.03	5.16	102.68
E/D-26.4-6.34	25.3	26,400	10,600	2.49	6.34	100.33
E/D-23.0-6.92	27.1	23,000	9,000	2.55	6.92	98.83
E/D-21.6-7.96	30.2	21,600	10,100	2.15	7.96	93.04
E/D-17.6-0.83	4.0	17,600	6,400	2.75	0.83	125.00
E/D-18.0-3.51	15.4	18,000	9,000	2.00	3.51	109.44
E/D-14.2-2.39	10.9	14,200	6,500	2.17	2.39	116.29
E/D-14.4-3.94	17.0	14,400	6,900	2.09	3.94	106.70
E/D-16.0-4.42	18.8	16,000	7,000	2.30	4.42	102.09

Table 4-6. Characterization data for ethylene/1-decene copolymers (continued).

Sample ID	SCB/1000C	M_w	M_n	PDI	1-decene%	T_p (°C)
E/D-15.1-5.11	21.2	15,100	7,000	2.14	5.11	100.92
E/D-12.4-0.80	3.6	12,400	6,700	1.84	0.80	123.50
E/D-12.4-1.22	5.8	12,400	6,200	2.02	1.22	123.32
E/D-13.2-1.33	6.3	13,200	6,400	2.08	1.33	122.52
E/D-13.7-2.22	10.2	13,700	7,200	1.89	2.22	118.20
E/D-12.4-2.68	12.1	12,400	5,700	2.16	2.68	110.28
E/D-13.8-6.79	26.7	13,800	6,300	2.18	6.79	90.93
E/D-9.8-1.35	6.4	9,800	4,200	2.35	1.35	118.88
H-23.0	0	23,000	9,300	2.48	0	129.02
H-15.3	0	15,300	6,900	2.23	0	128.57
H-11.8	0	11,800	5,800	2.04	0	127.05
H-13.3	0	13,300	6,500	2.03	0	127.32

Figure 4-8 compares the HT-TGIC profiles of all ethylene/1-decene copolymers, subdivided according to their φ ranges.
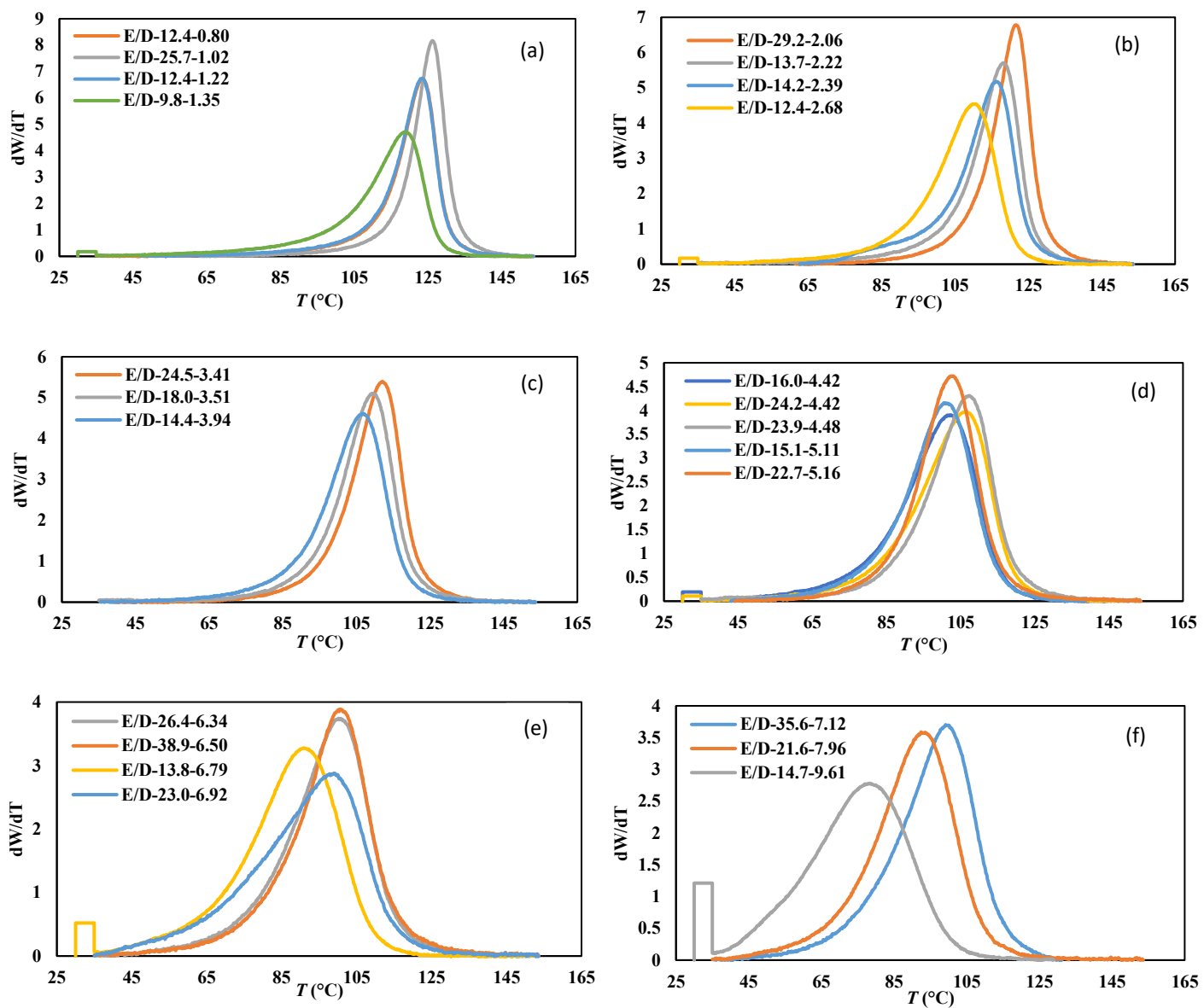
Figure 4-8. HT-TGIC profiles of ethylene/1-decene copolymers: a) φ = 0.80 to 1.33 %, b) φ = 2.06 to 2.68 %, c) φ = 3.41 to 3.94 %, d) φ = 4.42 to 5.16 %, e) φ = 6.34 to 6.92%, f) φ = 7.12 to 9.61%.

The model parameters for the ethylene/1-decene copolymers were estimated using the same MATLAB algorithm used for the ethylene/1-hexene and ethylene/1-octene samples. Table 4-7 lists these values.

Table 4-7. Calibration curve coefficients for ethylene/1-decene copolymers.

	a_1	a_2	b_1	b_2	R^2	RMSD
Coefficients	0.50	0.025	3.4148×10^{-5}	0.002449	0.966	1.47×10^{-5}

The calibration curve is given as,

$$\frac{1}{T_p} = 0.50e^{0.025\varphi}\frac{1}{M_w} + 3.4148 \times 10^{-5}\varphi + 0.002449 \tag{4.14}$$

The coefficients b_1 in Equation (4.14) is larger than the equivalent ones in Equation (4.12) and (4.13) for ethylene/1-hexene and ethylene/1-octene copolymers. This implies that the longer SCBs formed by 1-decene affects the value of T_p more than 1-hexene and 1-octene. In other words, ethylene/1-decene copolymers have lower T_p values than ethylene/1-hexene and ethylene/1-octene copolymers with the same φ and M_w. Figure 4-9 shows that the prediction errors for Equation (4.14) are randomly distributed around zero for ethylene/1-decene.
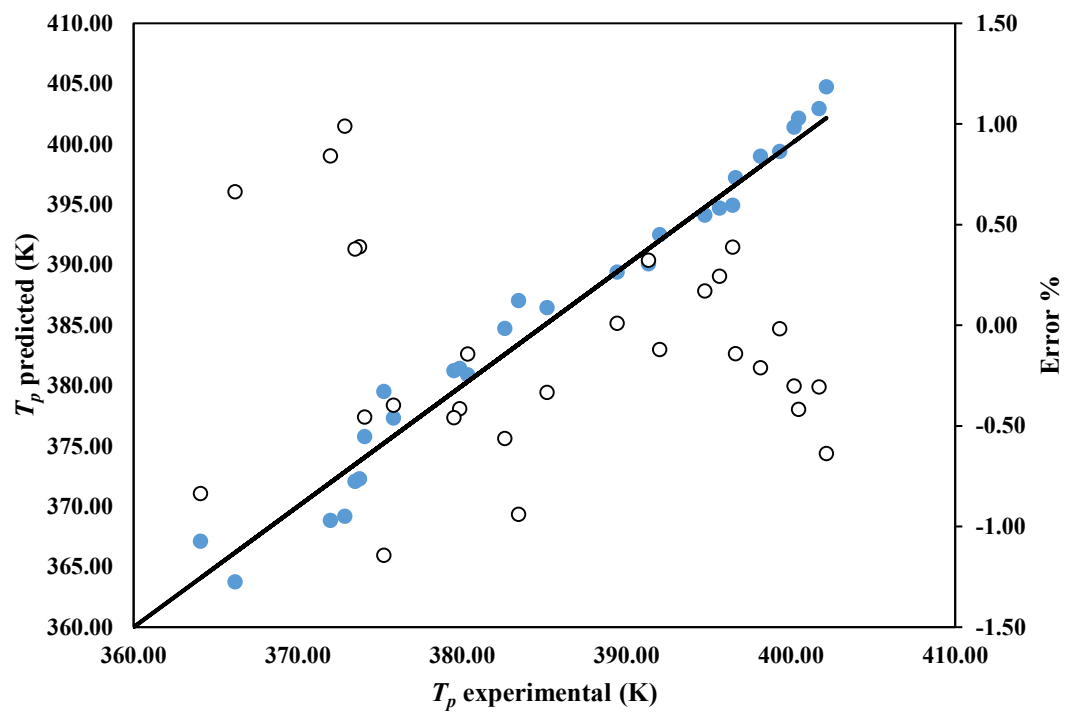
Figure 4-9. Predicted versus experimental HT-TGIC peak temperatures and prediction errors for ethylene/1-decene copolymers.

4.6. General Calibration Curve: Simultaneous Effect of Molecular Weight, Comonomer Fraction, and Comonomer Type

In the preceding sections, individual calibration curves were derived for ethylene/1-hexene, ethylene/1-octene, and ethylene/1-decene copolymers. All calibration curves assumed the same form,

$$\frac{1}{T_p} = a_1 e^{a_2\varphi} \frac{1}{M_w} + b_1\varphi + b_2 \tag{4.11}$$

Table 4-8 summarizes the estimated coefficients, R-squared and root mean squared deviation for each copolymer.

Table 4-8. Parameters of all calibration curves.

	a_1	a_2	b_1	b_2	R^2	RMSD
1-Hexene	0.50	0.050	2.7573×10^{-5}	0.002449	0.989	1.65×10^{-5}
1-Octene	0.50	0.030	3.0616×10^{-5}	0.002449	0.980	2.09×10^{-5}
1-Decene	0.50	0.025	3.4148×10^{-5}	0.002449	0.966	1.47×10^{-5}

It is possible to collapse these three equations in one master calibration curve by relating a_2 and b_1 to the number of carbons (n_c) in the α-olefin using the expressions,

$$a_2 = a_{21} e^{a_{22}n_C} \tag{4.15}$$

$$b_1 = b_{11}n_C + b_{12} \tag{4.16}$$

The functional forms shown in Equations (4.15) and (4.16) were found by trial-and-error. Substituting these equations into Equation (4.11), one gets,

$$\frac{1}{T_p} = \left[a_1 \exp(a_{21} e^{a_{22}n_C}\varphi)\right] \frac{1}{M_w} + (b_{11}n_C + b_{12})\varphi + b_2 \tag{4.17}$$

Figure 4-10 and Figure 4-11 illustrate these empirical correlations.
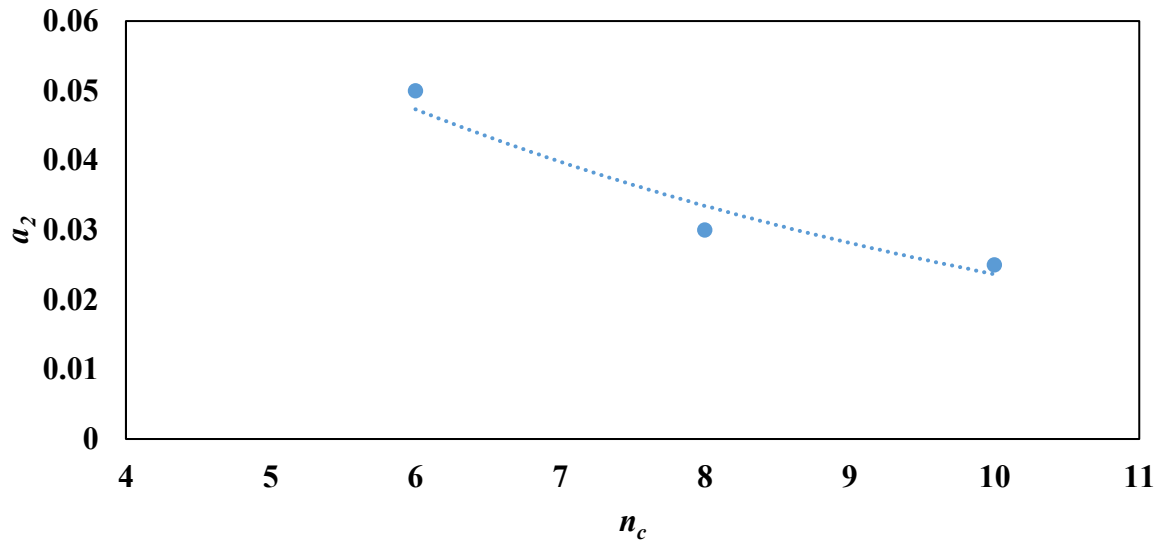
Figure 4-10. Correlation for a_2 as a function of n_c.
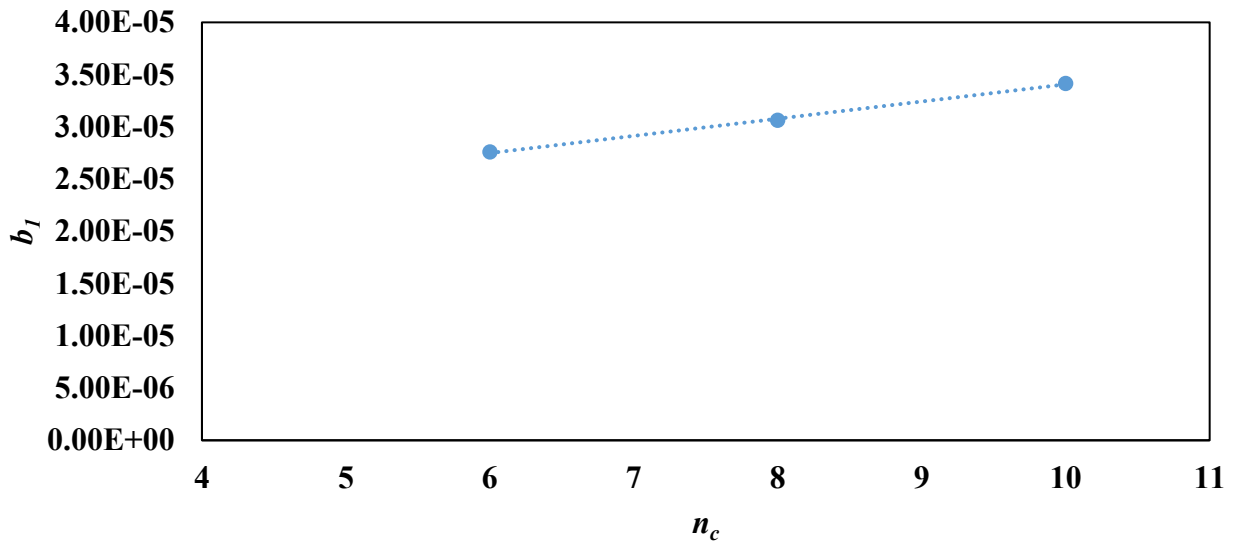
Figure 4-11. Correlation for b_1 as a function of n_c.

Table 4-9. Predicted constants for Equations (4.15) and (4.16).

a_{21}	a_{22}	b_{11}	b_{12}
0.1339	-0.173	1.4×10^{-6}	2×10^{-5}

The final calibration curve becomes,

$$\frac{1}{T_p} = 0.50 \frac{e^{\left(0.1339e^{-0.173n_c}\right)}\varphi}{M_w} + (1.4 \times 10^{-6}n_c + 2 \times 10^{-5})\varphi + 0.002449 \qquad (4.18)$$

Figure 4-12 and Figure 4-13 compare predicted and experimental peak temperatures and the error distribution. Equation (4.18) fits the peak temperatures for all copolymers adequately, but the prediction errors are slightly correlated with the peak temperatures.

The detailed information on the errors calculated between experimental and predicted peak temperature was presented in Appendix B.
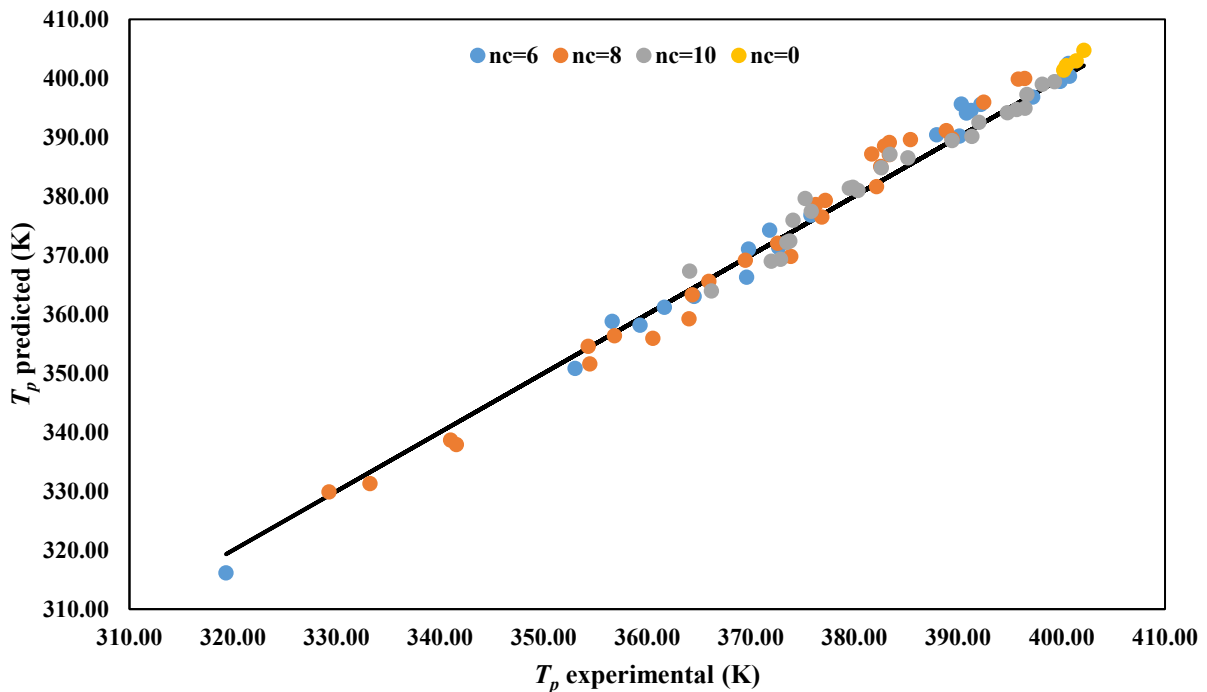
Figure 4-12. Predicted versus experimental HT-TGIC peak temperatures for all copolymers.
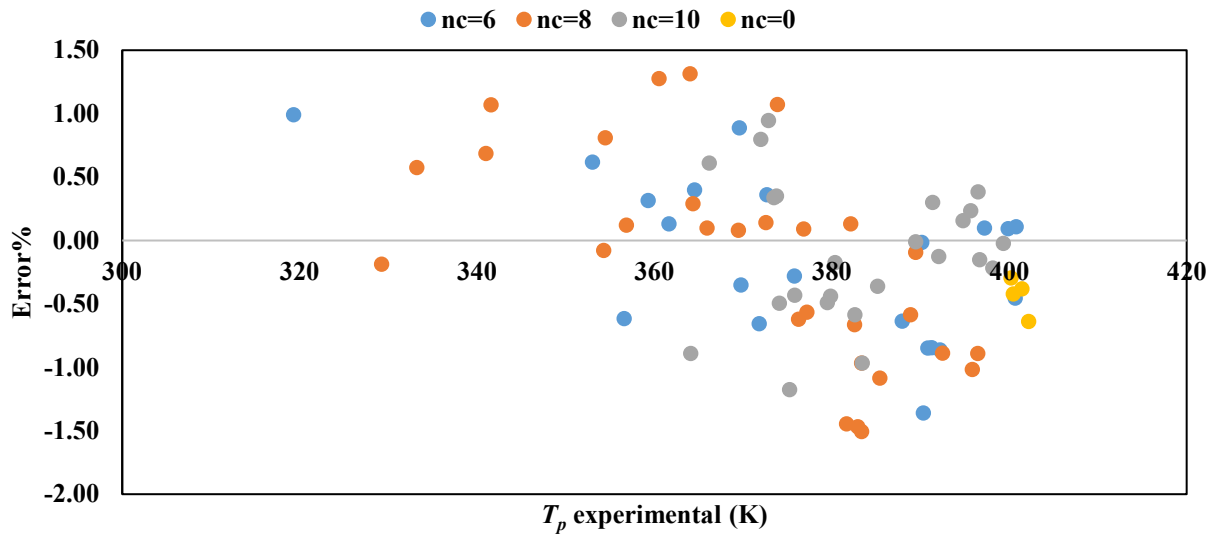
Figure 4-13. Error distribution for all copolymers.

Chapter 5. General Calibration Curve for a HT-TGIC Column Packed with a Novel Non-Porous Packing

5.1. Introduction

This chapter investigates the behaviour of a novel non-porous packing material for HT-TGIC analysis. The new material had to fulfill three criteria: *i*) have the same as, or better resolution than, conventional HT-TGIC packings, *ii*) fractionate polyolefins only by physical adsorption, and *iii*) have dimensions similar to those of conventional packings to avoid channelling in the HT-TGIC column.

The new packing was made of spherical SiO_2 particles coated with graphene (GNPSi). The nonporous spherical silica was purchased from Glantreo (Cork, Ireland). Their density was 2.2 g/cm^3 and average particle size was 9.5 μm. Figure 5-1 shows that the diameter of the SiO_2 particles varied from 9 to 11 μm. The Glantreo silica was sent to Graphene-XT (Bologna, Italy) to be coated with graphene. Figure 5-2 shows SEM images of the SiO_2 support after graphene deposition. The available surface area after coating was 0.3 m^2/g, which agrees well with the theoretical values calculated with the equations,

$$A_s = 4\pi r^2 \tag{5-1}$$

$$m_s = \rho_s V_s = \rho_s \frac{4}{3}\pi r^3 \tag{5-2}$$

$$\frac{A_s}{m_s} = \frac{3}{\rho_s r} = \frac{3}{2.2 \times 10^6 \; \frac{g}{m^3} \times \frac{9.5 \times 10^{-6}}{2} m} = 0.287 \frac{m^2}{g}$$

where A_s is the area of a sphere, V_s is the volume of a sphere, m_s is the mass of a SiO_2 particle, and ρ_s is the density of the SiO_2 particles.

63

The HT-TGIC column was filled with about 2 g of the new packing material with help of Dr. S. Mehdiabadi. The new column was carefully tested to make sure channelling did not take place during the analyses.

The HT-TGIC column packed with GNPSi was run under the same conditions described in Chapter 4 to compare it with the Hypercarb support. The same ethylene/α-olefin copolymers investigate in Chapter 4 were used to determine the calibration curves for the non-porous support.
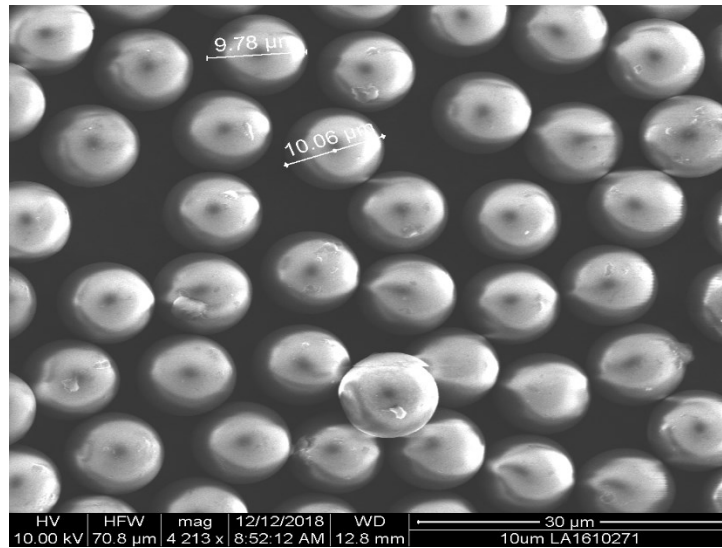
Figure 5-1. SEM images of non-porous SiO₂ particles.
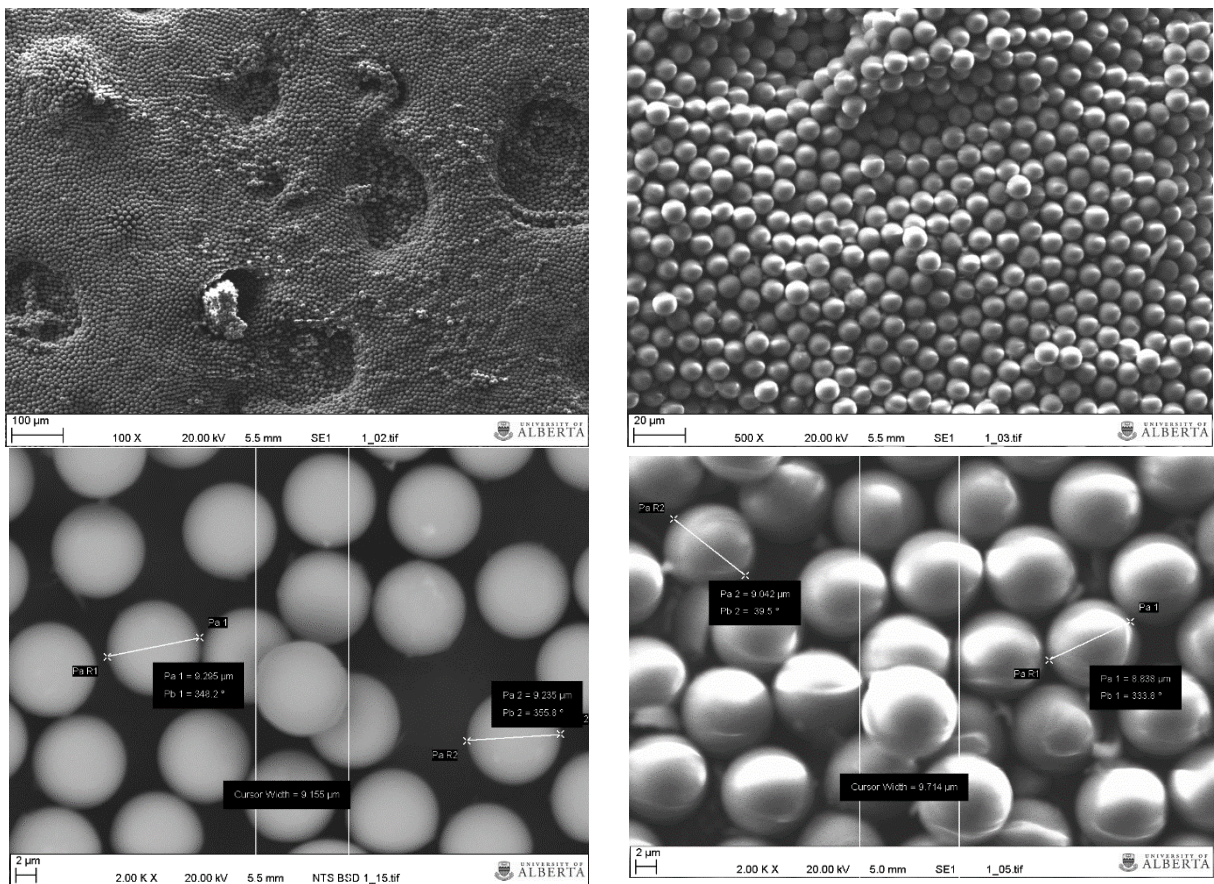
Figure 5-2. SEM images of non-porous SiO₂ particles coated with graphene (GNPSi).

65

5.2. Ethylene/1-Hexene Calibration Curve

Figure 5-3 compares the HT-TGIC profiles of all ethylene/1-hexene copolymers, while

Figure 5-4 shows the HT-TGIC profile of the ethylene homopolymers.
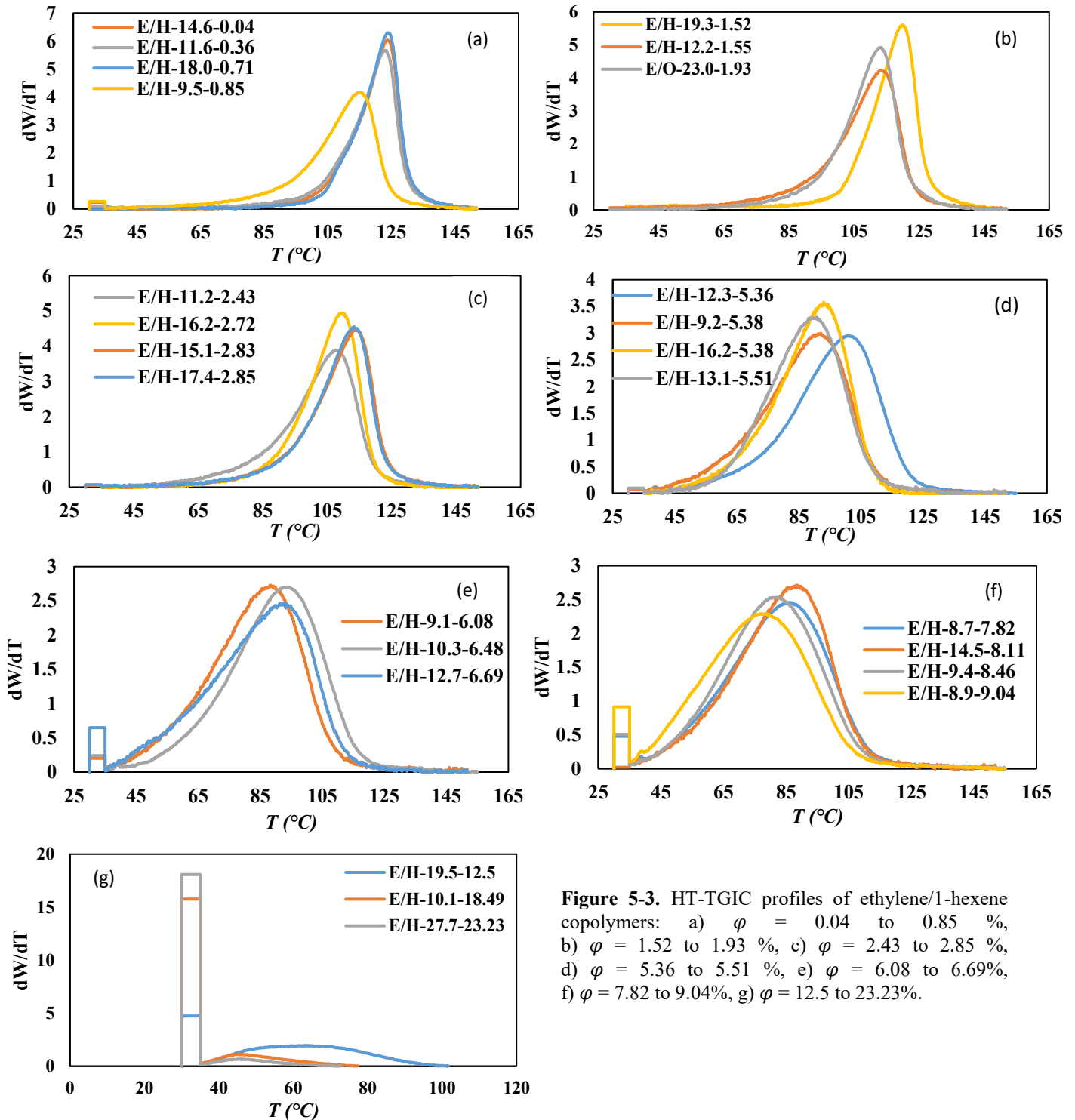
Figure 5-3. HT-TGIC profiles of ethylene/1-hexene copolymers: a) φ = 0.04 to 0.85 %, b) φ = 1.52 to 1.93 %, c) φ = 2.43 to 2.85 %, d) φ = 5.36 to 5.51 %, e) φ = 6.08 to 6.69%, f) φ = 7.82 to 9.04%, g) φ = 12.5 to 23.23%.
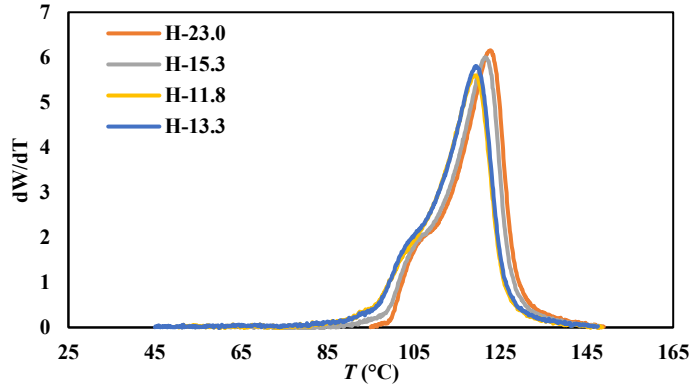
Figure 5-4. HT-TGIC profile of ethylene homopolymers.

The subroutine fitlnm (MATLAB) was used to estimate the coefficients of Equation (4.11) for the ethylene/1-hexene copolymers (Table 5-1).

$$\frac{1}{Tp} = (a_1 e^{a_2 \varphi}) \frac{1}{M_w} + (b_1 \varphi + b_2) \tag{4.11}$$

Table 5-1. Calibration curve coefficients for ethylene/1-hexene copolymers.

	a_1	a_2	b_1	b_2	R^2	RMSD
Coefficients	0.39	0.031	3.1556×10^{-5}	0.002500	0.984	2.02×10^{-5}

The calibration curve for ethylene/1-hexene copolymers is given by,

$$\frac{1}{T_p} = (0.39 e^{0.031\varphi}) \frac{1}{M_w} + (3.1556 \times 10^{-5} \varphi + 0.0025) \tag{5.3}$$

When $M_n \to \infty$ and $\varphi = 0$, Equation (5.3) becomes $1/T_p = 0.0025$ or $T_p = 400K = 127\ °C$, which is 8 °C lower than the temperature for the Hypercarb column.

Figure 5-5 compares T_p predicted by Equation (5.3) with experimental values. The prediction errors are randomly distributed around zero for all ethylene/1-hexene copolymers.
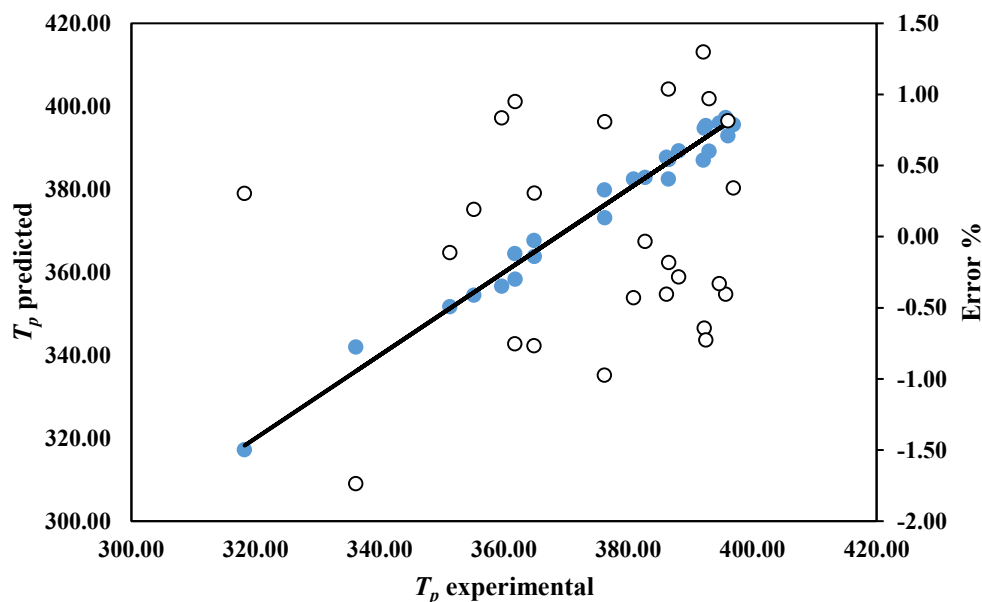
Figure 5-5. Predicted versus experimental HT-TGIC peak temperatures and prediction errors for ethylene/1-hexene copolymers.

5.3. Ethylene/1-Octene Calibration Curve

In addition to the samples described in Section 4.4, Table 5-2 lists three more ethylene/1-octene copolymers used to determine the calibration curve for the non-porous support.

Table 5-2. Characterization data for ethylene/1-octene copolymers.

Sample ID	SCB/1000C	M_w	M_n	PDI	1-octene%	$T_p(°C)$
E/O-15.0-1.40	6.7	15 000	6 400	2.37	1.40	115.2
E/O-9.0-9.35	36.5	9 000	3 900	2.32	9.35	75.0
E/O-6.9-16.96	56.2	6 900	3 300	2.06	16.96	44.2

Figure 5-6 compares the HT-TGIC profiles of all ethylene/1-octene copolymers, including those listed in Table 5-2.
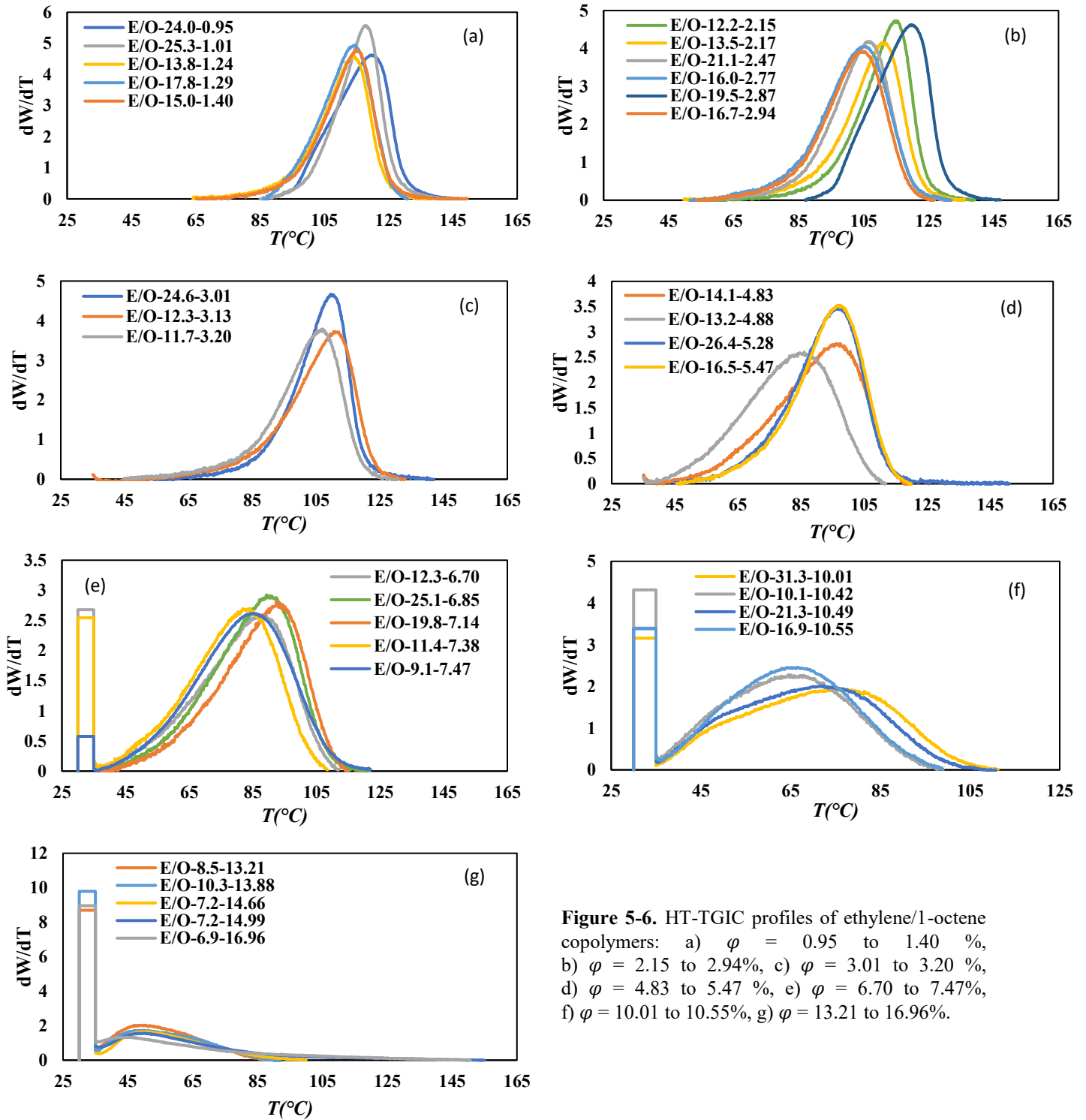
Figure 5-6. HT-TGIC profiles of ethylene/1-octene copolymers: a) φ = 0.95 to 1.40 %, b) φ = 2.15 to 2.94%, c) φ = 3.01 to 3.20 %, d) φ = 4.83 to 5.47 %, e) φ = 6.70 to 7.47%, f) φ = 10.01 to 10.55%, g) φ = 13.21 to 16.96%.

The model parameters for the ethylene/1-octene copolymers were estimated using the same MATLAB algorithm used for the ethylene/1-hexene samples. Table 5-3 lists these values.

Table 5-3. Calibration curve coefficients for ethylene/1-octene copolymers.

	a_1	a_2	b_1	b_2	R^2	RMSD
Coefficients	0.39	0.021	3.5366×10^{-5}	0.002500	0.990	1.73×10^{-5}

$$\frac{1}{T_p} = 0.39e^{0.021\varphi}\frac{1}{M_w} + 3.5366 \times 10^{-5}\varphi + 0.0025 \qquad (5.4)$$

The coefficients b_1 in Equation (5.4) is larger than the equivalent one in Equation (5.3) for ethylene/1-hexene copolymers, implying that the longer SCBs made by 1-octene copolymerization affect more the value of T_p than the shorter 1-hexene SCBS, as also seen in the calibration curve for the Hypercarb column. Figure 5-7 compares predicted versus experimental T_p values and show the prediction errors.
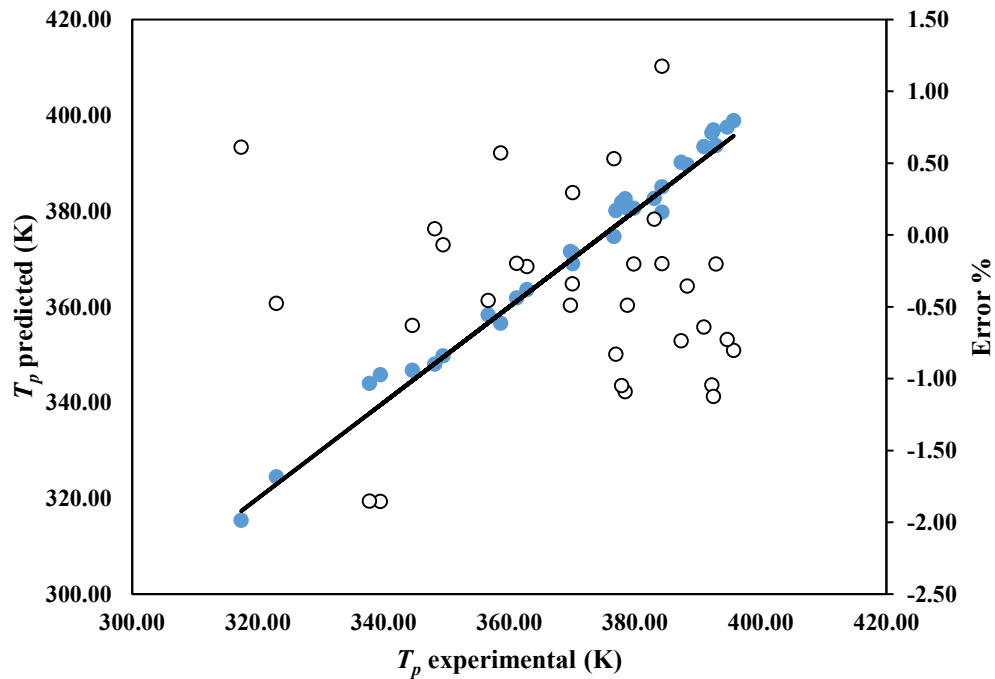
Figure 5-7. Predicted versus experimental HT-TGIC peak temperatures and prediction errors for ethylene/1-octene copolymers.

5.4. Ethylene/1-Decene Calibration Curve

Figure 5-8 compares the HT-TGIC profiles of all ethylene/1-decene copolymers, subdivided according to their φ ranges.
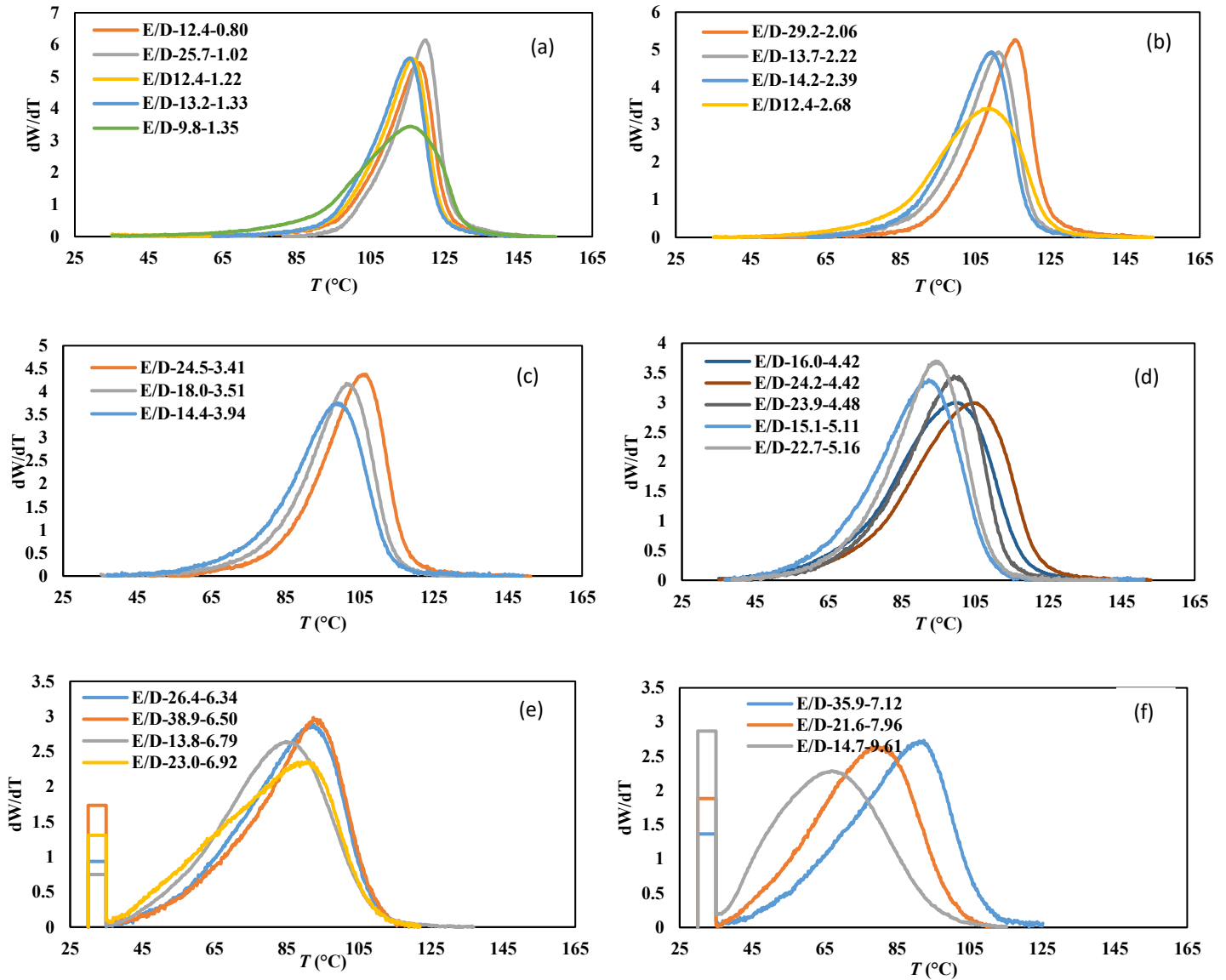
Figure 5-8. HT-TGIC profile of ethylene/1-decene copolymers: a) φ = 0.80 to 1.35 %, b) φ = 2.06 to 2.68 %, c) φ = 3.41 to 3.94 %, d) φ = 4.42 to 5.16 %, e) φ = 6.34 to 6.92 %, f) φ = 7.12 to 9.61 %.

The model parameters for the ethylene/1-decene copolymers were estimated using the same MATLAB algorithm used for the ethylene/1-hexene and ethylene/1-octene samples. Table 5-4 lists these values.

Table 5-4. Calibration curve coefficients for ethylene/1-decene copolymers.

	a_1	a_2	b_1	b_2	R^2	RMSD
Coefficients	0.39	0.018	3.7668×10^{-5}	0.002500	0.963	1.69×10^{-5}

The calibration curve for these copolymers is,

$$\frac{1}{T_p} = 0.39 e^{0.018\varphi} \frac{1}{M_w} + 3.7668 \times 10^{-5} \varphi + 0.0025 \tag{5.5}$$

The estimated values for Equation (5.5) are smaller than the one in Equation (4.14). Moreover, the coefficient is larger than the one for ethylene/1-octene and ethylene/1-hexene calibration curves. This implies that the presence of 1-decene in the copolymer (longer SCBs) affects the value of T_p more than 1-hexene and 1-octene, as expected.

Figure 5-9 shows that the prediction errors are randomly distributed around zero for ethylene/1-decene.
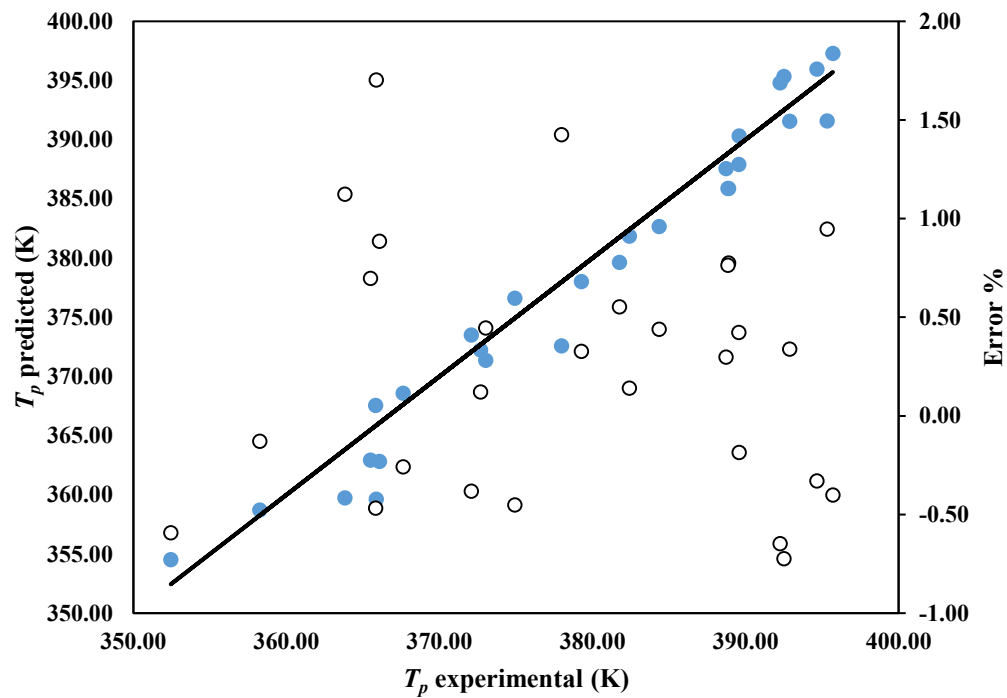
Figure 5-9. Predicted versus experimental HT-TGIC peak temperatures and prediction errors for ethylene/1-decene copolymers.

5.5. General Calibration Curve: Simultaneous Effect of Molecular Weight, Comonomer Fraction, and Comonomer Type

In the preceding sections, individual calibration curves were derived for ethylene/1-hexene, ethylene/1-octene, and ethylene/1-decene copolymers. All calibration curves had the same form,

$$\frac{1}{T_p} = a_1 e^{a_2 \varphi} \frac{1}{M_w} + b_1 \varphi + b_2 \tag{4.11}$$

Table 5-5 summarizes the estimated coefficients, R^2, and root mean squared deviation for each copolymer.

Table 5-5. Parameters of all calibration curves for the non-porous support.

	a_1	a_2	b_1	b_2	R^2	RMSD
1-Hexene	0.39	0.031	3.1556×10^{-5}	0.002500	0.984	2.02×10^{-5}
1-Octene	0.39	0.021	3.5366×10^{-5}	0.002500	0.990	1.73×10^{-5}
1-Decene	0.39	0.018	3.7668×10^{-5}	0.002500	0.963	1.69×10^{-5}

As discussed in Chapter 4, Equation (4.17) can be used as the general form for all calibration curves,

$$\frac{1}{T_p} = \left[a_1 \exp(a_{21} e^{a_{22} n_C} \varphi) \right] \frac{1}{M_w} + (b_{11} n_C + b_{12}) \varphi + b_2 \tag{4.17}$$

Figure 5-10 and Figure 5-11 illustrate these empirical correlations.
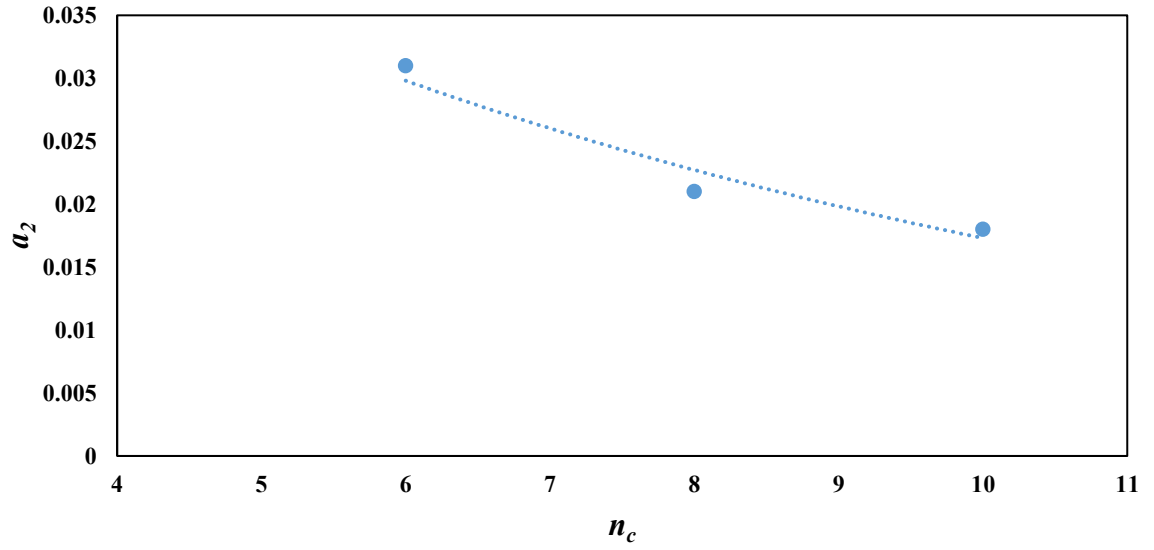
Figure 5-10. Correlation for a_2 as a function of n_c.
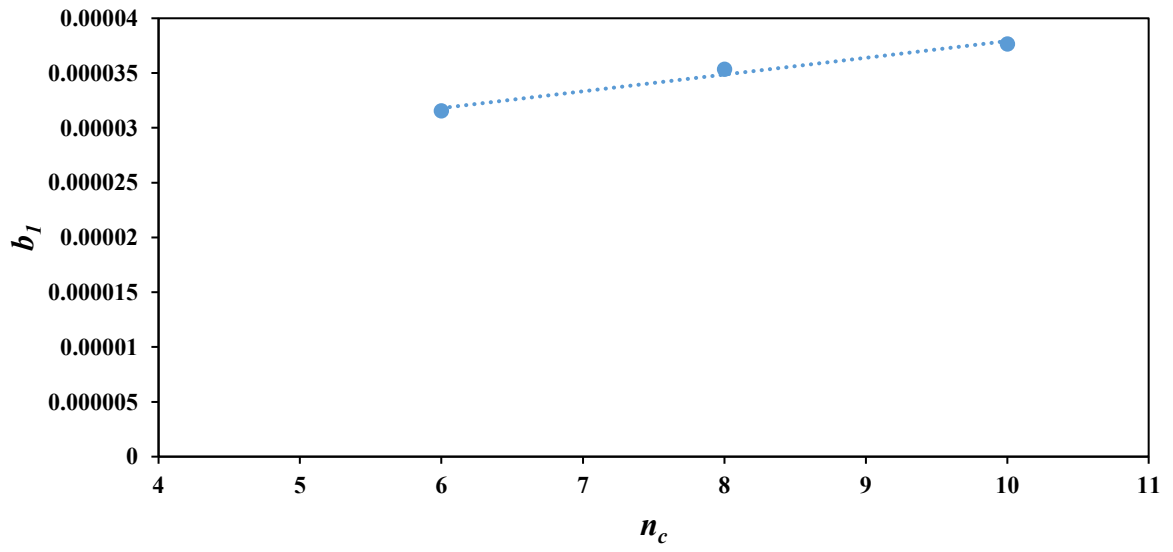
Figure 5-11. Correlation for b_1 as a function of n_c.

Table 5-6. Predicted constants for Equation.

a_{21}	a_{22}	b_{11}	b_{12}
0.0674	-0.136	2.1×10^{-5}	1.7×10^{-5}

Using these results, the general calibration curve becomes,

$$\frac{1}{T_p} = 0.39 \frac{e^{\left(0.0674e^{-0.136n_c}\right)\varphi}}{M_w} + (2.1 \times 10^{-6}n_c + 1.7 \times 10^{-5})\varphi + 0.0025 \qquad (5.6)$$

Figure 5-12 and 5-13 show the comparison between predicted and experimental peak temperature and the error distribution. The detailed information on the errors calculated between experimental and predicted peak temperature was presented in Appendix E.
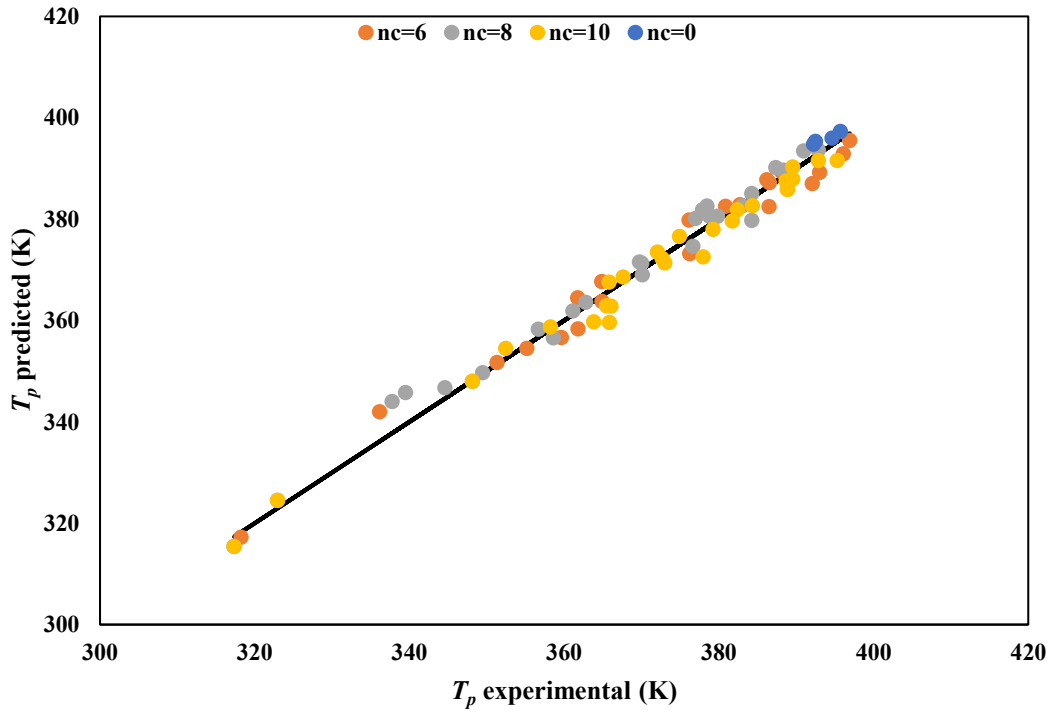
Figure 5-12. Predicted versus experimental HT-TGIC peak temperatures for all copolymers with the novel non-porous support.
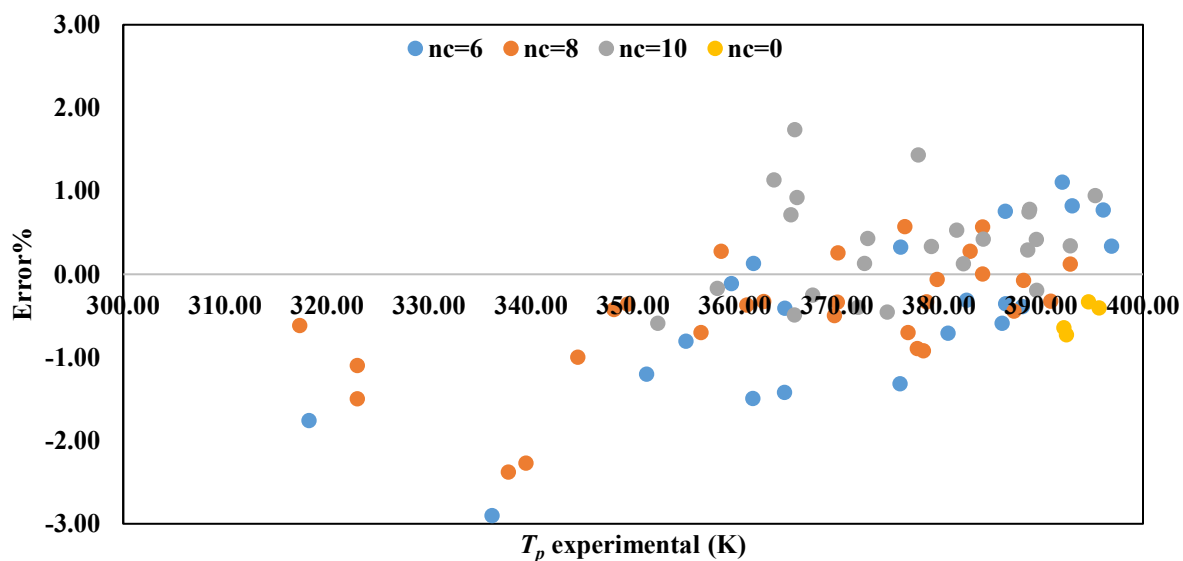
Figure 5-13. Error distribution of all copolymers analyzed with novel non-porous support (Comparison between theoretical and experimental peak temperature).

5.6. Comparison of HT-TGIC profiles in the Conventional and New Column

Our results showed that better separation (higher resolution) was achieved when HT-TGIC column packing was replaced with non-porous materials (graphene). Figure 5-15 shows the HT-TGIC profiles for a group of ethylene/1-hexane copolymers analyzed by the two different columns, one filled with Hypercarb (dotted lines), and the other filled with GNPSi (solid lines).

The peak temperatures with GNPSi were lower than those measured with Hypercarbs, regardless of the α-olefin fractiom in the copolymer. In addition, the novel support promoted a broader temperature distribution than the conventional support. Broader distributions are an indication of higher resolution.
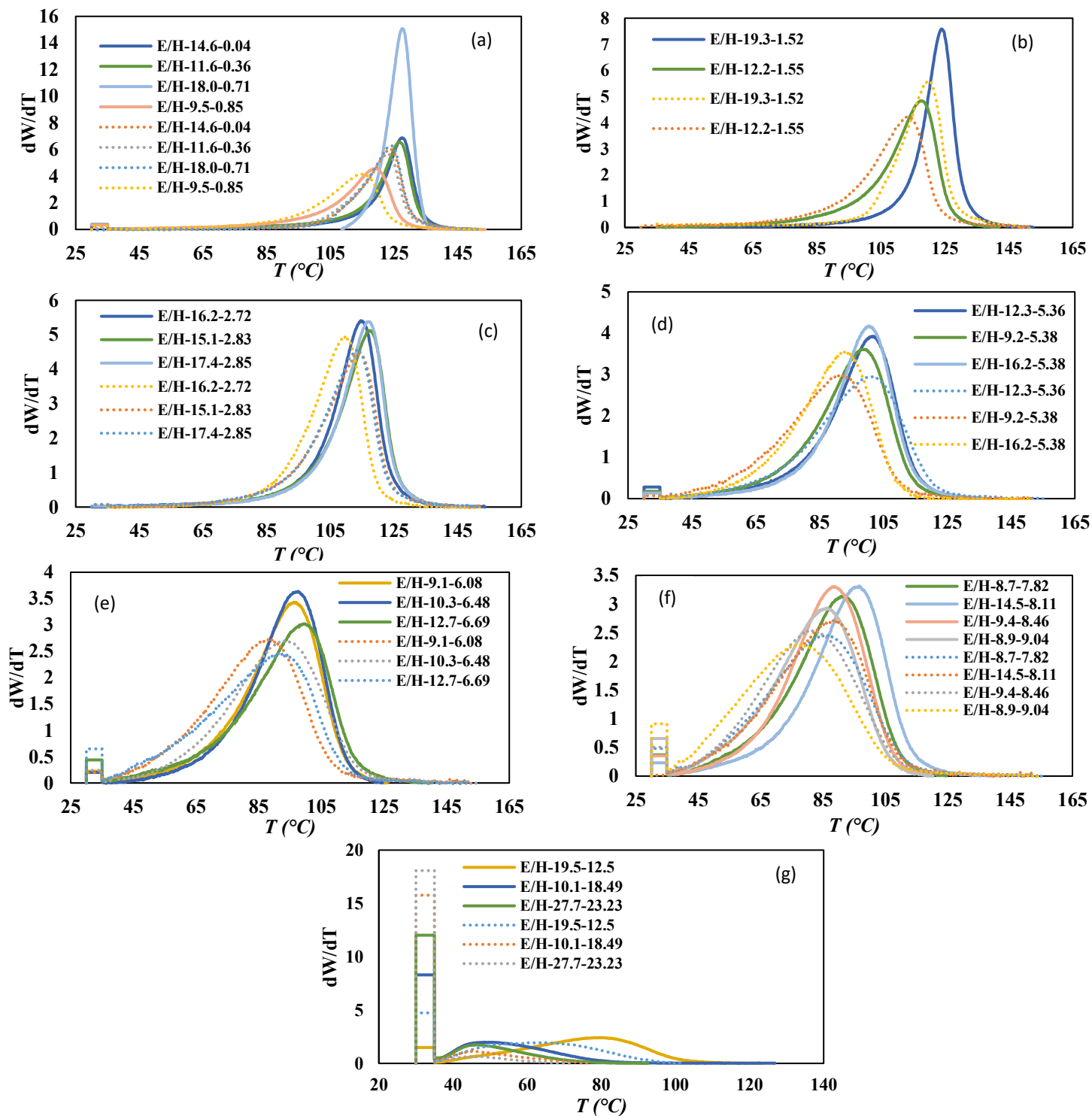
Figure 5-14. Comparison between HT-TGIC profile of ethylene/1-hexene in Hypercarb (solid lines) and GNPSi supports (dotted lines): a) φ = 0.04 to 0.85 %,b) φ = 1.52 to 1.55 %, c) φ = 2.72 to 2.85 %, d) φ = 5.36 to 5.38 %, e) φ = 6.08 to 6.69%,f) φ = 7.82 to 9.04%, g) φ = 12.5 to 23.23%.

An easier way to visualize how the GNPSi support had better resolution than the Hypercarb support is to compare the slope of their calibration curves. Higher slopes indicate better resolution. Figure 5-16 plots the calibration curves for 1-hexene, 1-octene, and 1-decene for when polymer molecular weight effects could be ignored ($M_n \rightarrow \infty$). Table 5-7 compares the slopes and intercepts of all calibration curves.
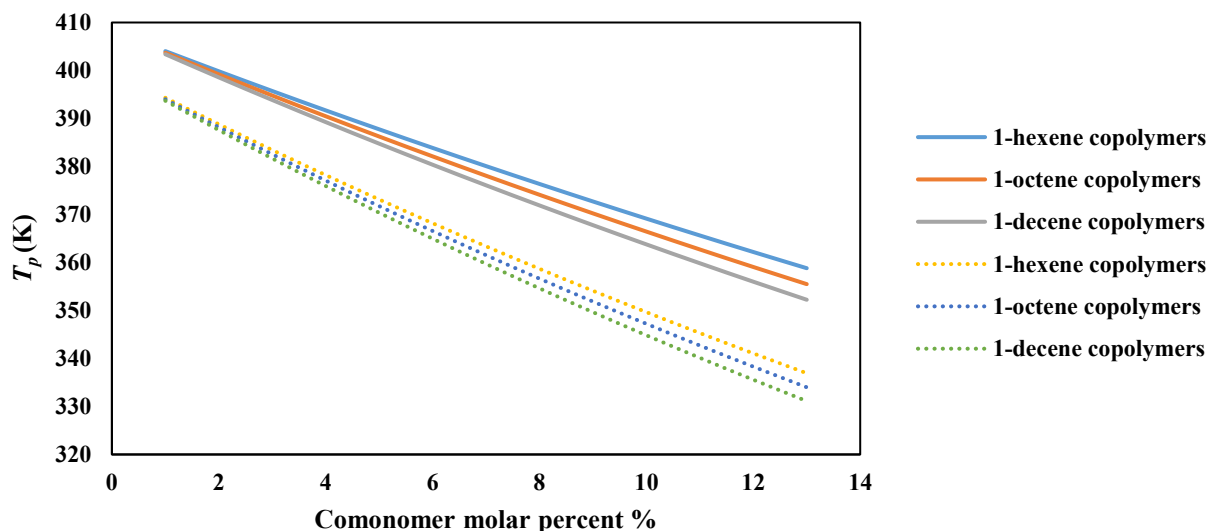
Figure 5-15. Calibration curves for different type of comonomer types: Solid lines = Hypercarb, Dotted lines = novel GNPSi support.

Table 5-7. Slopes and intercepts of the calibration curves.

		Slope	Intercept
	1-Hexene	-4.06	406.7
Hypercarb	1-Octene	-4.40	406.4
	1-Decene	-4.73	406.1
	1-Hexene	-4.11	398.4
GNPSi	1-Octene	-4.53	397.9
	1-Decene	-.4.99	397.4

Table 5-7 shows that the slopes of the calibration curves for the three comonomers are higher when the proposed GNPSi support is used. Therefore, small changes in comonomer fraction results in larger changes in peak temperature, which means that the HT-TGIC profiles of copolymers with different comonomer contents are more widely separated (higher resolution) when the novel non-porous support is used.

Figure 5-17 shows that the difference between the peak temperatures, ΔT_p, of the conventional and new support increases as the comonomer content of the copolymer increases. For all comonomers, the ΔT_p value increases from approximately 4 °C to about 16 °C when the comonomer percentage increases from under 4 % to about 15 %. For copolymers with comonomer contents higher than 15 %, the ΔT_p values appear to decline, but this is an artifact of the HT-TGIC analysis. Figure 5-3 shows that when the comonomer content of ethylene/1-hexene copolymers increases over 15 mol %, most of the fractions do not adsorb on the support and elute from the HT-TGIC column at room temperature. Consequently, the actual T_p for these copolymers is lower than the values reported in Figure 5-17. We expect that the ΔT_p values would keep increasing for higher comonomer mol % if we could run HT-TGIC experiments under sub-ambient temperatures.

Similar figures for ethylene/1-octene and ethylene/1-decene copolymers are presented in Appendix D.
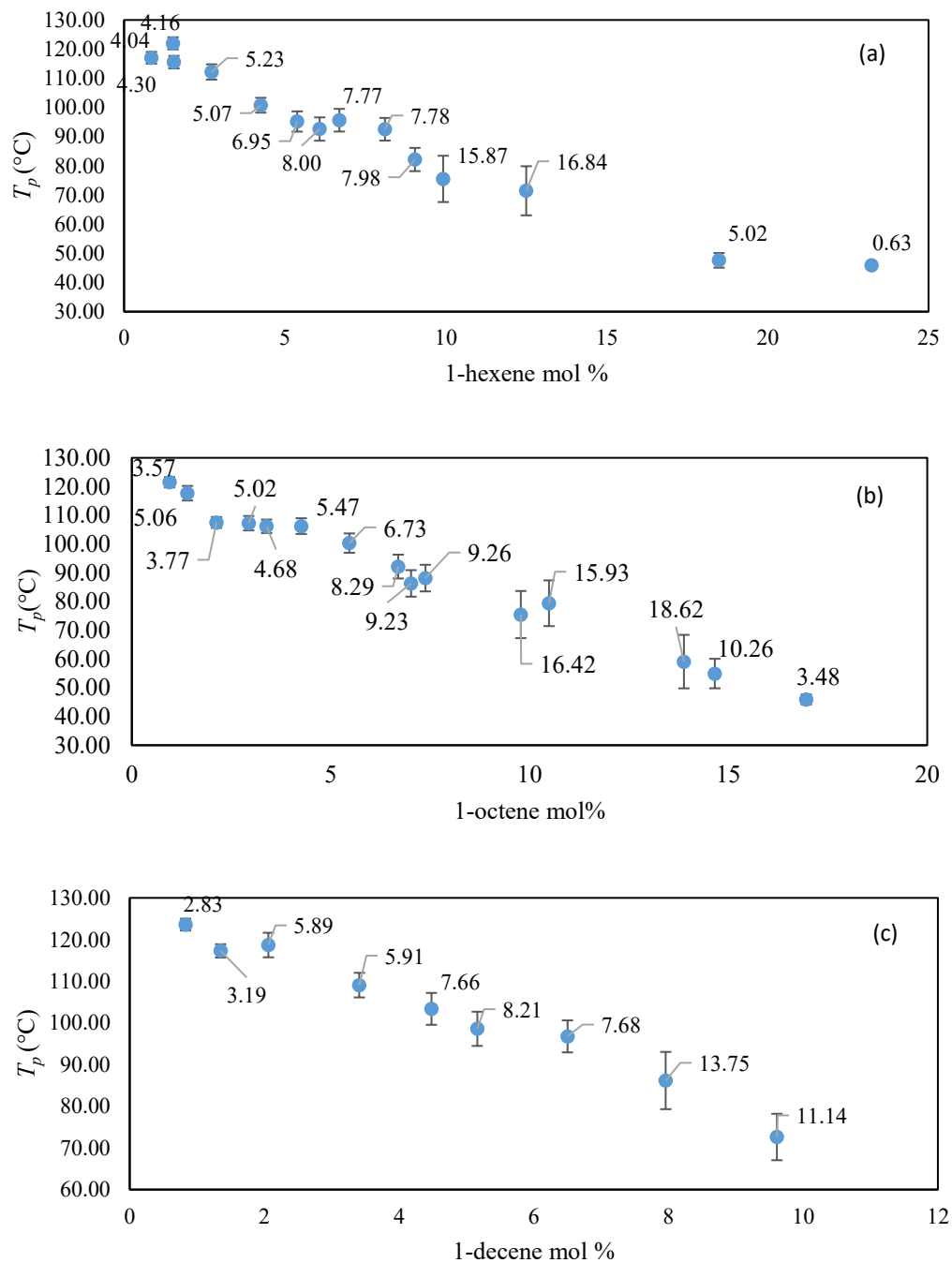
Figure 5-16. Differences in peak temperatures between Hypercarb and GNPSi supports: a) ethylene/1-hexene copolymers, b) ethylene/1-octene copolymers, c) ethylene/1-decene copolymers.

Chapter 6. Conclusions and Future Work

6.1. Conclusion

This dissertation determined general calibration curves for HT-TGIC fractionation of ethylene/α-olefin copolymers with two different columns. One of the columns was filled with conventional Hypercarb non-porous graphite particles. The other column was filled with newly designed graphene-coated non-porous SiO_2 (GNPSi) support.

Ethylene/α-olefin copolymers for HT-TGIC analysis were made with a single site catalyst. They had $M_w < 25\ 000$, a wide range of α-olefin fractions, and three different comonomer types: 1-hexene, 1-octene, and 1-decene. The two calibration curves quantified the effects of weight average molecular weight (M_w), comonomer molar percent (φ), and comonomer type (n_c) on HT-TGIC peak temperature (T_p). The medians of the HT-TGIC profiles were considered as an alternative to T_p, but they did not lead to more precise calibration curves. Consequently, T_p was chosen since it is more practical to determine T_p than to calculate the median temperature.

The newly developed non-porous support had higher resolution than the conventional Hypercarb support. The novel GNPSi support provided: 1) Broader HT-TGIC profiles, indicating better separation of the polymer chains, 2) More widely spread peaks as a function of α-olefin molar percent, and 3) Steeper calibration curves.

6.2. Recommendations for Future work

The results in this thesis demonstrated that it is possible to derive general calibrations curves for the HT-TGIC analysis of ethylene/α-olefin copolymers. Our findings also show that the current resolution of HT-TGIC can be increased by substituting conventional porous supports with non-porous supports. Even though these findings are important advancements, many other topics of research remain open for future HT-TGIC investigations.

The calibration curves developed in this thesis were based on experimental data only for ethylene copolymers with 1-hexene, 1-octene, and 1-decene. It would be interesting to run additional experiments to find out whether the calibration curves could be extended to ethylene/1-butene copolymers, which have significant industrial importance. On the higher end of the α-olefin range, it would be interesting to find out whether the same curves apply to α-olefins longer than 1-decene. These copolymers are not commercially relevant, but from a theoretical point of view it would be enlightening to know when (or whether) the length of the SCBs stop affecting HT-TGIC fractionation.

One of the assumptions of the novel GNPSi support was that it could eliminate size exclusion effects that take place in porous supports. Even though the increased resolution of GNPSi indicates that size exclusion effects were at least minimized, the work in this thesis did not fully test this assumption. A set of HT-TGIC analyses using ethylene/α-olefin copolymers with the same α-olefin molar percent but different M_w values would test this hypothesis. If size exclusion effects are absent, polyolefins with the same α-olefin molar percent should elute from the column at the same temperature, independently of their molecular weights, provided that chain end effects were accounted for.

From a fundamental point of view, a quartz crystal microbalance with dissipation/damping (QCM-D) could be used to study polyolefin adsorption and desorption from graphene-coated sensors. These results could be used to develop a first-principle model for the fractionation of polyolefins with HT-TGIC and, perhaps, lead to the development of a universal calibration curve for this method, instead of the empirical equations discovered in this thesis.

Chapter 7. References

(1)   Soares, J. B. P. An Overview of Important Microstructural Distributions for Polyolefin Analysis. *Macromol. Symp.* **2007**, *257* (3), 1–12. https://doi.org/10.1002/masy.200751101.

(2)   Monrabal, B. Crystaf: Crystallization Analysis Fractionation. A New Approach to the Composition Analysis of Semicrystalline Polymers. *Macromol. Symp.* **1996**, *110* (1), 81–86.

(3)   Garside, M. Production of Plastics Worldwide from 1950 to 2018 https://www.statista.com/statistics/282732/global-production-of-plastics-since-1950/.

(4)   Garside, M. Distribution of Polymer Demand Worldwide in 2016 by Major Polymer https://www.statista.com/statistics/756728/worldwide-distribution-of-polymer-demand-by-type/.

(5)   McKenna, T. F.; Soares, J. B. P. *Encyclopedia of Polymer Blends Macromolecular Engineering Encyclopedia of Polymer Blends Handbook of Polymer Reaction Engineering Functional Fillers for Plastics Tailor-Made Polymers Macromolecules, P. 1-13*; Wiley-VCH Verlag GmbH & Co. KGaA: Weinheim, 2012.

(6)   Mortimer, G. A.; Hammer, W. F. Density of Polyethylene. *Polym. Sci.* **1964**, *2* (3), 1301–1309.

(7)   Patel, R. *"Types and Basics of Polyethylene," in Handbook of Industrial Polyethylene and Technology,*; Scrivener Publishing, 2017.

(8)   Peacock, A. *Handbook of Polyethylene: Structure, Properties, and Applications*; Marcel Dekker: New York, 2000.

(9)   Carraher, C. *Carraher's Polymer Chemistry*; 2011.

(10)   B. Malpass, D. *Introduction to Industrial Polyethylene: Properties, Catalysts, Processes*; Scrivener Publishing LLC, 2010.

(11)   Ziegler, K. Folgen Und Werdegang Einer Erfindung Nobel-Vortrag Am 12. Dezember 1963. *Angew. chemie* **1964**, *76* (13), 545–553.

(12)   Nakayama, Y.; Bando, H.; Sonobe, Y.; Fujita, T. Olefin Polymerization Behavior of Bis (Phenoxy-Imine) Zr , Ti , and V Complexes with MgCl 2 -Based Cocatalysts. *Mol. Catal.* **2004**, *213* (1), 141–150.

(13)   Kojoh, S.; Matsugi, T.; Kashiwa, N.; Kaneko, H.; Kawahara, N.; Matsuo, S.; Nobori, T.; Imuta, J.-I. Functionalization of Polyethylene Based on Metallocene Catalysis and Its Application to Syntheses of New Graft Copolymers Possessing Polar Polymer Segments. *Polym. Sci.* **2003**, *41* (22), 3657–3666.

(14)   Stevens, J. C. Constrained Geometry and Other Single Site Metallocene Polyolefin Catalysts: A Revolution In Olefin Polymerization. *Stud. Surf. Sci. Catal.* **1996**, *101*, 11–20.

(15)   Kaminsky, W. Highly Active Metallocene Catalysts for Olefin Polymerization. *R. Soc.*

Chem. **1998**, No. 9, 1413–1418.

(16) Guo, S.; Fan, H.; Bu, Z.; Li, B.-G.; Zhu, S. Tandem Action of SNS–Cr and CGC–Ti in Preparation of Ethylene–1-Hexene Copolymers from Ethylene Feedstock. *Macromol. Chem. Phys.* **2014**, *215* (17), 1661–1667.

(17) Cano, J.; Kunz, K. How to Synthesize a Constrained Geometry Catalyst (CGC) – A Survey. *Organomet. Chem.* **2007**, *692* (21), 4411–4423. https://doi.org/10.1016/j.jorganchem.2007.05.015.

(18) Rieger, B.; Baugh, L. S.; Kacker, S.; Strielger, S. *Late Transition Metal Polymerization Catalysis*; 2006.

(19) Cong, R.; degoort, W.; Parrott, A.; Yau, W.; Hazlitt, L.; Brown, R.; Miller, M.; Zhou, Z. A New Technique for Characterizing Comonomer Distribution in Polyolefins: High-Temperature Thermal Gradient Interaction Chromatography (HT-TGIC). *Macromolecules* **2011**, *44* (8), 3062–3072.

(20) Lochm, C. H.; Moebus, M. A.; Liu, Q.; Jiang, C.; Elomaa, M. Temperature Effect on Retention and Separation of Poly(Ethylene Glycol)s in Reversed-Phase Liquid Chromatography. *Chromatogr. Sci.* **1996**, *34* (2), 69–76.

(21) Lee, H. C.; Chang, T. Polymer Molecular Weight Characterization by Temperature Gradient High Performance Liquid Chromatography. *Polymer (Guildf).* **1996**, *37* (25), 5747–5749.

(22) Wild, L.; Glöckner, G. Temperature Rising Elution Fractionation. *Adv. Polym. Sci.* **1990**, *98*, 1–47. https://doi.org/10.1007/3-540-53135-1_4.

(23) Haward, R. N.; Wright, B.; Williamson, G. R.; Thackery, G. Effect of Blending on the Molecular Weight Distribution of Polymers. *Polym. Sci.* **1964**, *2* (7), 2977–3007.

(24) Yu, Y.; Hildebrand, M. Development of an Integrated On-Line 2D Analytical TREF-High Throughput SEC Technique for Polyolefins Characterization. *Macromol. Symp.* **2020**, *390* (1), 1900015. https://doi.org/10.1002/masy.201900015.

(25) Xu, J.; Feng, L. Application of Temperature Rising Elution Fractionation in Polyolefins. *Eur. Polym. J.* **2000**, *36* (5), 867–878.

(26) Flory, P. J. Thermodynamics of Crystallization in High Polymers. IV. A Theory of Crystalline States and Fusion in Polymers, Copolymers, and Their Mixtures with Diluents. *Chem. Phys.* **1949**, *17* (3), 223.

(27) Alghyamah, A. Comparison Between CEF and HT-TGIC of Polyolefins Made by Ziegler-Natta and Metallocene Catalysts, Ph.D. Thesis, University of Waterloo, 2012.

(28) Soares, J. B. P.; Hamielec, A. E. Temperature Rising Elution Fractionation of Linear Polyolefins. *Elsevier* **1995**, *36* (8), 1639–1654.

(29) Wild., L.; Ryle, T. R.; Peat, I. R. Determination of Branching Distributions in Polyethylene and Ethylene Copolymers. *Polym. Sci.* **1982**, *20* (3), 441–445.

(30) Anantawaraskul, S.; Soares, J. B. P.; Wood-Adams, P. M. Fractionation of Semicrystalline

Polymers by Crystallization Analysis Fractionationand Temperature Rising Elution Fractionation. *Polym. Anal. Polym. Theory* **2005**, *182*, 1–54.

(31) Anantawaraskul, S.; Soares, J. B. P.; Wood-Adams, P. M. Effect of Operation Parameters on Temperature Rising Elution Fractionation and Crystallization Analysis Fractionation. *Polym. Phys.* **2003**, *41* (14), 1762–1778.

(32) De Rosa, C.; Ruiz de Ballesteros, O.; Auriemma, F.; Talarico, G.; Scoti, M.; Di Girolamo, R.; Malafronte, A.; Piemontesi, F.; Liguori, D.; Camurati, I.; Morini, G. Crystallization Behavior of Copolymers of Isotactic Poly(1-Butene) with Ethylene from Ziegler–Natta Catalyst: Evidence of the Blocky Molecular Structure. *Macromolecules* **2019**, *52* (23), 9114–9127.

(33) Soares, J. B. P.; Anantawaraskul, S. Crystallization Analysis Fractionation. *Polym. Phys.* **2005**, *43* (13), 1557–1570.

(34) Monrabal, B. Crystallization Analysis Fractionization. 5,222,390, 1991.

(35) Monrabal, B. Crystallization Analysis Fractionation: A New Technique for the Analysis of Branching Distribution in Polyolefins. *Appl. Polym. Sci.* **1994**, *52* (4), 491–499.

(36) Monrabal, B. Crystaf: Crystallization Analysis Fractionation. A New Approach to the Composition Analysis of Semicrystalline Polymers. *Macromol. Symp.* **1996**, *110* (1), 81–86.

(37) Nieto, J.; Oswald, T.; Blanco, F.; Soares, J. B. P.; Monrabal, B. Crystallizability of Ethylene Homopolymers by Crystallization Analysis Fractionation. *Polym. Phys.* **2001**, *39* (14), 1616–1628.

(38) Anantawaraskul, S.; Soares, J. B. P.; Wood-Adams, P. M.; Monrabal, B. Effect of Molecular Weight and Average Comonomer Content on the Crystallization Analysis Fractionation (Crystaf) of Ethylene α-Olefin Copolymers. *Polymer (Guildf).* **2003**, *44* (8), 2393–2401.

(39) McKenna, T. F.; Soares, J. B. P. Polyolefin Microstructural Characterization. In *Polyolefin Reaction Engineering*; Wiley- VCH Verlag GmbH & Co. KGaA: Weinheim, 2012; pp 15–52.

(40) Monrabal, B.; Sancho-Tello, J.; Mayo, N.; Romero, L. Crystallization Elution Fractionation. A New Separation Process for Polyolefin Resins. *Macromol. Symp.* **2007**, *257* (1), 71–79.

(41) Monrabal, B. Advances in Crystallization Elution Fractionation. *Macromol. Symp.* **2009**, *282* (1), 14–24.

(42) Monrabal, B.; Blanco, J.; Nieto, J.; Soares, J. B. P. Characterization of Homogeneous Ethylene/1-Octene Copolymers Made with a Single-Site Catalyst. CRYSTAF Analysis and Calibration. *Polym. Sci.* **1999**, *37* (1), 89–93.

(43) Sarzotti, D. M.; Soares, J. B. P.; Penlidis, A. Ethylene/1-Hexene Copolymers Synthesized with a Single-Site Catalyst: Crystallization Analysis Fractionation, Modeling, and Reactivity Ratio Estimation. *Polym. Phys.* **2002**, *40* (23), 2595–2611.

(44)   Alkhazaal, A. Characterization of Ethylene / 1-Octene Copolymers with High-Temperature Thermal Gradient Interaction Chromatography, Ph.D. Thesis, University of Waterloo, 2016.

(45)   Cong, R.; Degroot, W.; Parrott, A.; Yau, W.; Hazlitt, L.; Brown, R.; Cheatham, M.; Miller, M.; Zhou, Z. High Temperature Thermal Gradient Interaction Chromatography (HT-TGIC) for Microstructure Analysis of Polyolefins. *Macromol. Symp.* **2012**, *312* (1), 108–114.

(46)   Trathnigg, B.; Kollroser, M. Liquid Chromatography of Polyethers Using Universal Detectors V. Quantitative Aspects in the Analysis of Low-Molecular-Mass Poly(Ethylene Glycol)s and Their Derivatives by Reversed-Phase High-Performance Liquid Chromatography with an Evaporative Light Sca. *Chromatogr. A* **1997**, *768* (2), 223–238.

(47)   Chen, S. S. Encyclopedia of Chromatography; 2010; pp 818–820.

(48)   Chitta, R.; Macko, T.; Brüll, R.; Kalies, G. Elution Behavior of Polyethylene and Polypropylene Standards on Carbon Sorbents. *Chromatogr. A* **2010**, *1217* (49), 7717–7722.

(49)   Macko, T.; Brüll, R.; Alamo, R. G.; Thomann, Y.; Grumel, V. Separation of Propene/1-Alkene and Ethylene/1-Alkene Copolymers by High-Temperature Adsorption Liquid Chromatography. *Polymer (Guildf).* **2009**, *50* (23), 5443–5448.

(50)   Macko, T.; Brüll, R.; Alamo, R. G.; Stadler, F. J.; Losio, S. Separation of Short-Chain Branched Polyolefins by High-Temperature Gradient Adsorption Liquid Chromatography. *Anal. Bioanal. Chem.* **2011**, *399*, 1547–1556.

(51)   Macko, T.; Brüll, R.; Wang, Y.; Coto, B.; Suarez, I. Characterization of Ethylene-Propylene Copolymers with High-Temperature Gradient Adsorption Liquid Chromatography and CRYSTAF. *Appl. Polym. Sci.* **2011**, *122* (5), 3211–3217.

(52)   Macko, T.; Brüll, R.; Zhu, Y.; Wang, Y. A Review on the Development of Liquid Chromatography Systems for Polyolefins. *Sep. Sci.* **2010**, *33* (22), 3446–3454.

(53)   Cheruthazhekatt, S.; Pasch, H. Improved Chemical Composition Separation of Ethylene–Propylene Random Copolymers by High-Temperature Solvent Gradient Interaction Chromatography. *Anal. Bioanal. Chem.* **2013**, *405*, 8607–8614.

(54)   Ndiripo, A.; Pasch, H. Retention of Polypropylene Stereoisomers in Solvent Gradient Interaction Chromatography on Porous Graphitic Carbon as Influenced by Temperature and Mobile Phase Composition. *J. Chromatogr. A* **2020**, *1618*, 460865.

(55)   Monrabal, B.; Mayo, N.; Cong, R. Crystallization Elution Fractionation and Thermal Gradient Interaction Chromatography. Techniques Comparison. *Macromol. Symp.* **2012**, *312* (1), 115–129.

(56)   Alghyamah, A.; Soares, J. B. P. Effect of Solvent Type on High-Temperature Thermal Gradient Interaction Chromatography of Polyethylene and Ethylene–1-Octene Copolymers. *Macromol. Chem. Phys.* **2015**, *216* (1), 38–48.

(57)   Alghyamah, A.; Soares, J. B. P. Fractionation of Ethylene/1-Octene Copolymers by High-Temperature Thermal Gradient Interaction Chromatography. *Ind. Eng. Chem. Res.* **2014**, *53* (22), 9228–9235.

(58) A. Alkhazaal. Characterization of Ethylene/α-Olefin Copolymers Made with a Single-Site Catalyst Using Crystallization Elution Fractionation, University of Waterloo, 2011.

(59) Al-khazaal, A. Z.; Soares, J. B. P. Effect of Column Type on Polyolefin Fractionation by High-Temperature Thermal Gradient Interaction Chromatography. *Macromol. Symp.* **2015**, *356* (1), 10–18.

(60) Al-khazaal, A. Z.; Soares, J. B. P. Joint Effect of Poly (Ethyhlene- Co -1-Octene) Chain Length and 1-Octene Fraction on High-Temperature Thermal Gradient Interaction Chromatography. *Macromol. Chem. Phys.* **2017**, *218* (1), 1–20. https://doi.org/10.1002/macp.201600332.

(61) Al-khazaal, A. Z.; Soares, J. B. P. Characterization of Ethylene/α-Olefin Copolymers Using High-Temperature Thermal Gradient Interaction Chromatography. *Mol. Chem. Phys.* **2014**, *215* (5), 465–475.

(62) Monrabal, B.; Lopez, E.; Romero, L. Advances in Thermal Gradient Interaction Chromatography and Crystallization Techniques for Composition Analysis in Polyolefins. *Macromol. Symp.* **2013**, *330* (1), 9–21.

(63) DOW GLOBAL TECHNOLOGIES LLC. Chromatography of Polymers Using Particles Coated with Graphene-Based Compositions. WO 2019/090092 Al, 2019.

(64) Monrabal, B. Polyolefin Characterization: Recent Advances in Separation Techniques. In *Kaminsky W. (eds) Polyolefins: 50 years after Ziegler and Natta I. Advances in Polymer Science*; 2013; pp 203–251. https://doi.org/10.1007/12_2013_216.

(65) Anantawaraskul, S.; Inwong, N.; Soares, J. B. P.; Al-khazaal, A. Z. High Temperature Thermal Gradient Interaction Chromatography (HT-TGIC) for Blends of Ethylene/1-Octene Copolymers: A Mathematical Model. *Macromol. Symp.* **2015**, *354* (1), 361–366.

(66) Caldera Palacios, A. A. Polymerization Kinetics and Structure-Property Relationships of Ethylene/1-Hexene Copolymers, Master thesis, University of Alberta, 2018.

(67) Zurek, E.; Ziegler, T. Theoretical Studies of the Structure and Function of MAO (Methylaluminoxane). *Prog. Polym. Sci.* **2004**, *29* (2), 107–148. https://doi.org/10.1016/j.progpolymsci.2003.10.003.

Appendix A: Previous HT-TGIC Results from Alkhazaal et al.[60]

Table A-1. HT-GPC and HT-TGIC results for ethylene homopolymers.[60]

Sample ID	HT-GPC			HT-TGIC		
	M_n (g mol^{-1})	PDI	r_n	T_p (°C)	σ	T_μ (°C)
H-1.0	970	1.79	35	122.3	21.4	96.5
H-1.2	1200	1.82	44	126.5	20.8	104.5
H-1.7	1700	2.33	62	129.9	19.6	113.7
H-2.7	2700	2.09	97	132.4	12.9	123.5
H-3.6	3600	2.24	131	134.0	10.4	129.4
H-9.2	9200	2.01	329	135.9	8.4	130.8
H-12.2	12200	2.01	436	136.2	4.6	134.4
H-21.0	21000	2.16	748	136.7	4.9	135.9
H-25.3	25300	2.13	904	137.8	3.8	136.4
H-56.6	56600	2.11	2021	137.2	3.3	136.4
H-75.0	75000	2.23	2680	137.2	2.9	137.3
H-97.0	97000	2.12	3464	137.1	2.8	137.5

Table A-2. HT-GPC and HT-TGIC results for ethylene/1-octene copolymers with 1 mol % of comonomer.[60]

Sample ID	HT-GPC					HT-TGIC		
	M_n (g mol^{-1})	PDI	r_n	AES	LES	T_p (°C)	σ	T_μ (°C)
C1-1.4	1400	1.79	50	33	35	114.8	19.3	100.0
C1-1.7	1700	1.82	61	37	40	119.1	16.8	104.5
C1-2.4	2400	2.33	84	45	52	125.5	14.6	112.8
C1-4.6	4600	2.09	162	61	70	129.6	12.6	122.2
C1-8.2	8200	2.24	286	74	100	131.6	9.6	127.5
C1-15.6	15600	2.01	540	84	156	132.3	6.3	130.6
C1-19.5	19500	2.01	678	87	178	132.5	5.7	131.2
C1-27.1	27100	2.16	943	90	210	132.7	3.9	132.1
C1-36.3	36300	2.13	1260	92	240	132.9	3.4	132.6
C1-68.1	68100	2.23	2360	95	305	132.9	2.9	132.7
C1-129.4	129400	2.12	4485	96	371	132.7	2.7	132.7

Table A-3. HT-GPC and HT-TGIC results for ethylene/1-octene copolymers with 2.6 mol % of comonomer.[60]

Sample ID	HT-GPC					HT-TGIC		
	M_n (g mol^{-1})	PDI	r_n	AES	LES	T_p (°C)	σ	T_μ (°C)
C2.6-1.5	1500	1.66	51	21	22	93.1	19.5	84.7
C2.6-1.7	1700	1.78	58	23	25	99.7	18.1	92.7
C2.6-2.0	2000	1.79	69	24	31	104.4	17.5	96.1
C2.6-3.4	3400	2.01	113	28	39	114.8	15.4	105.3
C2.6-4.8	4800	1.97	159	30	50	119.5	13.3	111.9
C2.6-7.0	7000	2.18	235	32	64	121.3	10.1	116.3
C2.6-14.1	14100	2.06	469	34	90	123.1	7.1	120.4
C2.6-23.6	23600	2.15	785	35	111	124.3	6.2	122.6
C2.6-36.0	36000	2.24	1193	36	127	124.5	5.3	123.5
C2.6-61.1	61100	2.22	2025	37	148	124.5	4.1	124.6
C2.6-115.7	115700	2.23	3833	37	173	124.6	3.8	124.6

Table A-4. HT-GPC and HT-TGIC results for ethylene/1-octene copolymers with 3.7 mol % of comonomer.[60]

Sample ID	HT-GPC					HT-TGIC		
	M_n (g mol^{-1})	PDI	r_n	AES	LES	T_p (°C)	σ	T_μ (°C)
C3.7-2.3	2300	1.88	73	19	28	96.8	16.1	88.4
C3.7-5.4	5400	2.06	172	22	46	111.4	13.3	105.3
C3.7-7.2	7200	2.04	233	23	53	113.3	11.1	108.5
C3.7-10.6	10600	2.07	340	24	63	114.5	11.0	110.5
C3.7-16.8	16800	1.97	539	24	76	115.8	8.4	113.6
C3.7-29.2	29200	2.12	938	25	91	117.0	7.6	115.4
C3.7-34.8	34800	2.23	1118	25	95	117.7	6.7	117.3
C3.7-52.2	52200	2.11	1672	25	106	117.8	5.6	117.4
C3.7-85.2	85200	2.11	2736	25	120	117.8	4.7	117.5

Table A-5. HT-GPC and HT-TGIC results for ethylene/1-octene copolymers with 7.8 mol % of comonomer.[60]

Sample ID	HT-GPC					HT-TGIC		
	M_n (g mol^{-1})	PDI	r_n	AES	LES	T_p (°C)	σ	T_μ (°C)
C7.8-1.9	1900	1.54	56	10	16	55.3	12.2	50.0
C7.8-2.9	2900	1.83	83	10	23	76.1	16.0	73.2
C7.8-4.6	4600	2.01	132	11	27	82.6	14.0	79.4
C7.8-9.7	9700	2.13	279	11	37	90.6	13.4	84.8
C7.8-18.5	18500	2.12	534	11	45	96.0	10.3	93.1
C7.8-40.1	40100	2.10	1160	12	55	98.2	9.4	98.8
C7.8-55.7	55700	2.15	1611	12	59	98.2	7.9	98.0
C7.8-117.0	117000	2.09	3384	12	68	98.3	7.0	98.2

Table A-6. HT-GPC and HT-TGIC results for ethylene/1-octene copolymers with 12.9 mol % of comonomer.[60]

Sample ID	HT-GPC					HT-TGIC		
	M_n (g mol^{-1})	PDI	r_n	AES	LES	T_p (°C)	σ	T_μ °C)
C13-2.5	2500	1.51	64	6	14	23.5	2.3	25.8
C13-4.5	4500	1.99	116	6	18	53.9	10.6	59.5
C13-9.4	9400	1.93	242	6	24	63.5	10.2	62.9
C13-15.4	15400	1.92	397	7	28	68.9	10.9	67.7
C13-28.0	28000	2.19	729	7	32	71.5	11.7	69.6
C13-48.8	48800	2.10	1256	7	36	73.5	11.4	72.0
C13-57.3	57300	2.17	1476	7	38	73.7	10.5	73.2
C13-127.0	127000	2.06	3266	7	43	73.7	9.0	73.5
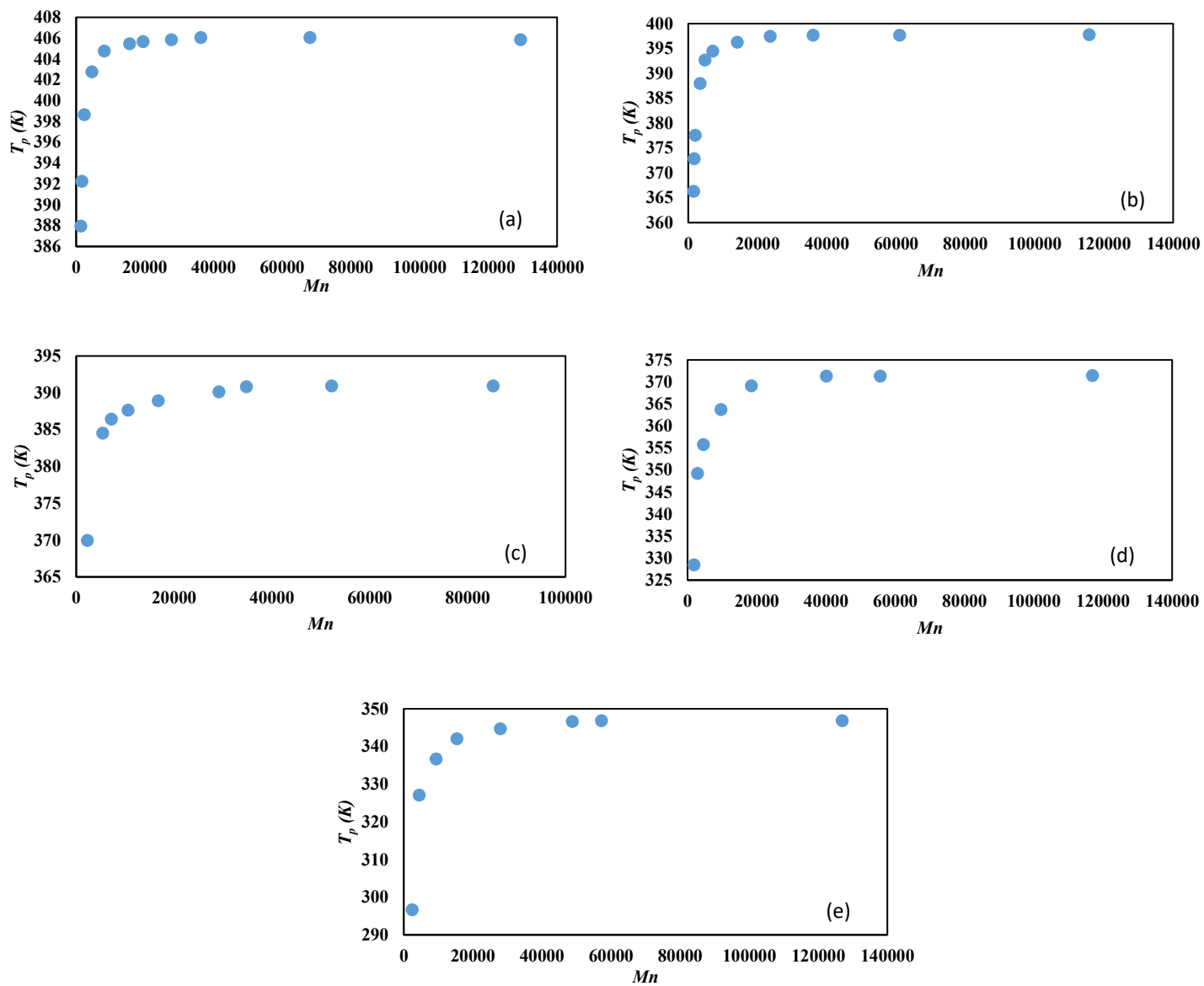
Figure A-1. Relation between T_p(K) and M_n for ethylene/1-octene copolymers, a) φ =1%, b) φ =2.6%, c) φ =3.7%, d) φ =7.8%, e) φ =12.9%.
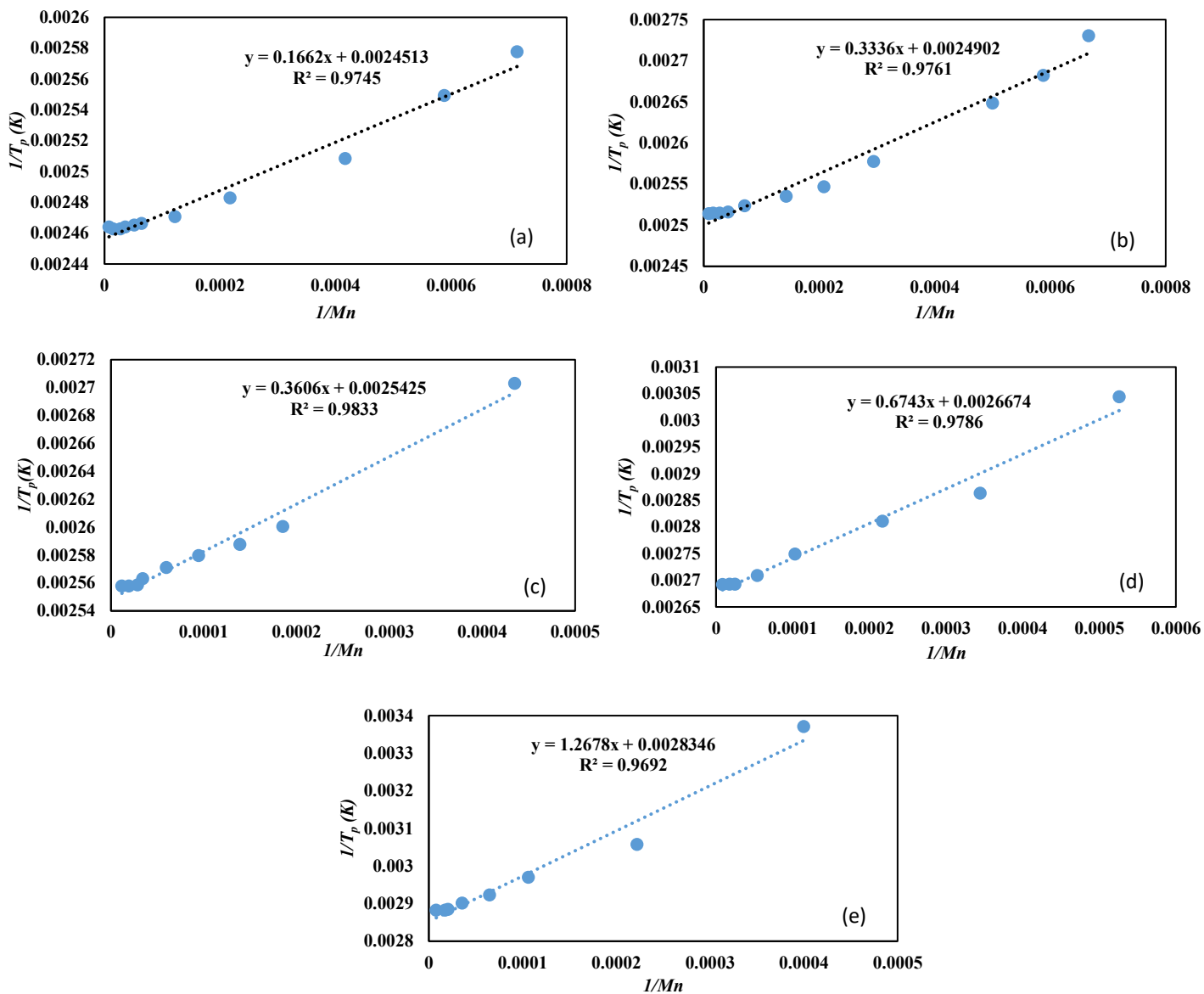
Figure A-2. Relation between $1/T_p(K)$ and $1/M_n$ for ethylene/1-octene copolymers, a) φ =1%, b) φ =2.6%, c) φ =3.7%, d) φ =7.8%, e) φ =12.9%.

Appendix B: Comparison between Predicted and Experimental Data for Conventional Column

Table B-1. Peak temperature deviations for conventional column.

Sample	M_w	φ(%)	Tp(K)-Experimental	n_c	Tp(K)-Calculated	%
E/H-18.0-0.71	18 000	0.71	400.8	6	400.3	0.11
E/H-17.5-1.91	17 500	1.91	391.2	6	394.6	-0.85
E/H-16.2-2.72	16 200	2.72	388.0	6	390.4	-0.64
E/H-17.4-2.85	17 400	2.85	390.1	6	390.2	-0.02
E/H-14.6-0.04	14 600	0.04	400.7	6	402.5	-0.46
E/H-14.5-8.11	14 500	8.11	369.6	6	366.3	0.89
E/H-14.2-9.92	14 200	9.92	356.6	6	358.8	-0.62
E/H-11.6-0.36	11 600	0.36	399.9	6	399.5	0.09
E/H-12.2-1.55	12 200	1.55	390.8	6	394.2	-0.85
E/H-12.3-5.36	12 300	5.36	375.8	6	376.8	-0.28
E/H-12.7-6.69	12 700	6.69	372.7	6	371.3	0.36
E/H-9.5-0.85	9 500	0.85	392.2	6	395.6	-0.86
E/H-9.2-5.38	9 200	5.38	371.8	6	374.3	-0.66
E/H-9.1-6.08	9 100	6.08	369.8	6	371.1	-0.35
E/H-8.7-7.82	8 700	7.82	364.5	6	363.1	0.40
E/H-9.4-8.46	9 400	8.46	361.6	6	361.2	0.13
E/H-8.9-9.04	8 900	9.04	359.3	6	358.2	0.32
E/H-23.0-1.93	23 000	1.93	390.3	6	395.6	-1.36
E/H-27.7-23.23	27 700	23.23	319.3	6	316.2	0.99
E/H-19.3-1.52	19 300	1.52	397.2	6	396.8	0.10
E/H-19.5-12.50	19 500	12.50	353.0	6	350.8	0.62

Table B-1. Peak temperature deviations for conventional column (continued).

Sample	M_w	$\varphi(\%)$	Tp(K)-Experimental	n_c	Tp(K)-Calculated	%
E/O -31.3-10.01	31 300	10.01	364.0	8	359.2	1.31
E/O-24.0-0.95	24 000	0.95	396.4	8	400.0	-0.89
E/O-25.3-1.01	25 300	1.01	395.8	8	399.8	-1.02
E/O-24.6-3.01	24 600	3.01	389.4	8	389.8	-0.09
E/O-26.4-5.28	26 400	5.28	377.2	8	379.3	-0.57
E/O-25.1-6.85	25 100	6.85	372.6	8	372.0	0.14
E/O-19.5-2.87	19 500	2.87	385.4	8	389.6	-1.09
E/O-20.0-3.39	20 000	3.39	381.7	8	387.2	-1.45
E/O-19.8-7.14	19 800	7.14	373.8	8	369.8	1.07
E/O-21.3-10.49	21 300	10.49	360.5	8	355.9	1.28
E/O-16.0-2.77	16 000	2.77	383.4	8	389.2	-1.51
E/O-16.7-2.94	16 700	2.94	382.9	8	388.5	-1.47
E/O-15.0-4.26	15 000	4.26	382.1	8	381.6	0.13
E/O-16.5-5.47	16 500	5.47	376.8	8	376.5	0.09
E/O-16.9-10.55	16 900	10.55	354.3	8	354.6	-0.08
E/O-13.8-1.24	13 800	1.24	392.5	8	396.0	-0.89
E/O-13.5-2.17	13 500	2.17	388.9	8	391.2	-0.58
E/O-14.2-3.06	14 200	3.06	383.4	8	387.1	-0.97
E/O-14.1-4.83	14 100	4.83	376.2	8	378.6	-0.62
E/O-13.4-9.78	13 400	9.78	356.8	8	356.4	0.12
E/O-12.3-6.70	12 300	6.70	369.4	8	369.2	0.08
E/O-11.4-7.38	11 400	7.38	365.9	8	365.6	0.10
E/O-10.1-10.42	10 100	10.42	354.4	8	351.6	0.81
E/O-10.3-13.88	10 300	13.88	341.6	8	337.9	1.07
E/O-6.6-2.13	6 600	2.13	382.6	8	385.1	-0.66

Table B-1. Peak temperature deviations for conventional column (continued).

Sample	M_w	$\varphi(\%)$	Tp(K)-Experimental	n_c	Tp(K)-Calculated	%
E/O-9.1-7.47	9 100	7.47	364.3	8	363.3	0.29
E/O-8.5-13.21	8 500	13.21	341.0	8	338.7	0.69
E/O-7.3-14.66	7 300	14.66	333.2	8	331.3	0.58
E/O-7.2-14.99	7 200	14.99	329.2	8	329.9	-0.19
E/D -38.9-6.50	38 900	6.50	373.8	10	372.4	0.35
E/D-35.9-7.12	35 900	7.12	372.9	10	369.3	0.95
E/D-29.2-2.06	29 200	2.06	394.8	10	394.2	0.16
E/D-25.7-1.02	25 700	1.02	399.3	10	399.4	-0.02
E/D-24.5-3.41	24 500	3.41	385.2	10	386.5	-0.36
E/D-24.2-4.42	24 200	4.42	379.5	10	381.4	-0.49
E/D-23.9-4.48	23 900	4.48	380.4	10	381.0	-0.17
E/D-22.7-5.16	22 700	5.16	375.8	10	377.4	-0.43
E/D-26.4-6.34	26 400	6.34	373.5	10	372.2	0.34
E/D-23.0-6.92	23 000	6.92	372.0	10	369.0	0.80
E/D-21.6-7.96	21 600	7.96	366.2	10	364.0	0.61
E/D-17.6-0.83	17 600	0.83	398.2	10	399.0	-0.22
E/D-18.0-3.51	18 000	3.51	382.6	10	384.8	-0.59
E/D-14.2-2.39	14 200	2.39	389.4	10	389.5	-0.01
E/D-14.4-3.94	14 400	3.94	379.8	10	381.5	-0.44
E/D-16.0-4.42	16 000	4.42	375.2	10	379.6	-1.18
E/D-15.1-5.11	15 100	5.11	374.1	10	375.9	-0.50
E/D-12.4-0.80	12 400	0.80	396.6	10	397.2	-0.15
E/D-12.4-1.22	12 400	1.22	396.5	10	395.0	0.38
E/D-13.2-1.33	13 200	1.33	395.7	10	394.7	0.24
E/D-13.7-2.22	13 700	2.22	391.4	10	390.2	0.30

Table B-1. Peak temperature deviations for conventional column (continued).

Sample	M_w	$\varphi(\%)$	Tp(K)-Experimental	n_c	Tp(K)-Calculated	%
E/D-12.4-2.68	12 400	2.68	383.4	10	387.1	-0.97
E/D-13.8-6.79	13 800	6.79	364.1	10	367.3	-0.89
E/D-9.8-1.35	9 800	1.35	392.0	10	392.5	-0.13
H-23.0	23 000	0	402.2	0	404.7	-0.64
H-15.3	15 300	0	401.4	0	403.0	-0.38
H-11.8	11 800	0	400.2	0	401.4	-0.30
H-13.3	13 300	0	400.5	0	402.2	-0.42

Appendix C: ^{13}C-NMR Results

Table C-1. Integration limits of ^{13}C NMR spectra of the ethylene/1-decene samples.

Area	Region (ppm)	E/H-191.0	E/H-147.0	E/H-178.0	E/H-137.0	E/H-210.0
A	40.5 to 41.5	0.000	0.000	0.000	0.000	0.000
B	39.5 to 40.5	0.000	0.000	0.000	0.000	0.000
C	37.0 to 39.5	0.011	0.035	0.012	0.054	0.006
D	Peak at 35.8	0.000	0.000	0.000	0.000	0.000
D+E	33.2 to 36.8	0.076	0.144	0.060	0.212	0.027
F+G+H	25.5 to 33.2	1.231	1.434	1.140	1.753	1.177
H	26.5 to 28.5	0.044	0.111	0.055	0.166	0.027
I	24.0 to 25.0	0.000	0.000	0.000	0.000	0.000
P	22.0 to 24.0	0.019	0.057	0.020	0.095	0.009
O_1		0.011	0.035	0.012	0.054	0.006
O_2		0.025	0.048	0.020	0.106	0.009
O'		0.018	0.042	0.016	0.080	0.008
E'		0.602	0.675	0.548	0.826	0.578
φ		2.90	5.86	2.84	8.83	0.14

Appendix D: HT-TGIC Profiles of Ethylene/1-Octene and Ethylene/1-Decene Copolymers
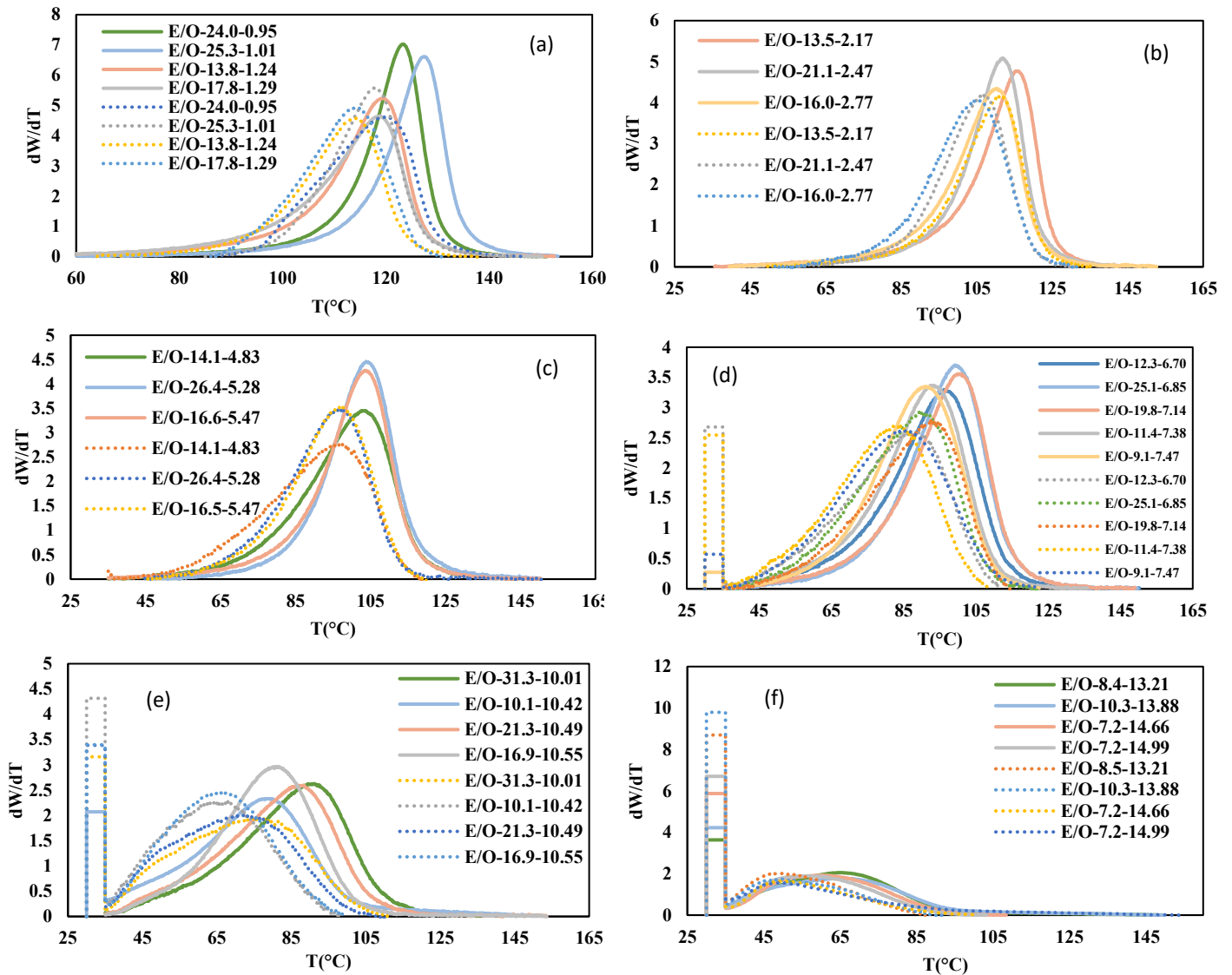
Figure D-1. Comparison between HT-TGIC profile of ethylene/1-octene in Hypercarb (solid lines) and GNPSi supports (dotted lines): a) $\varphi = 0.95$ to 1.29 %, b) $\varphi = 2.17$ to 2.77%, c) $\varphi = 4.83$ to 5.47 %, d) $\varphi = 6.70$ to 7.47%, e) $\varphi = 10.01$ to 10.55%, f) $\varphi = 13.21$ to 14.99%.
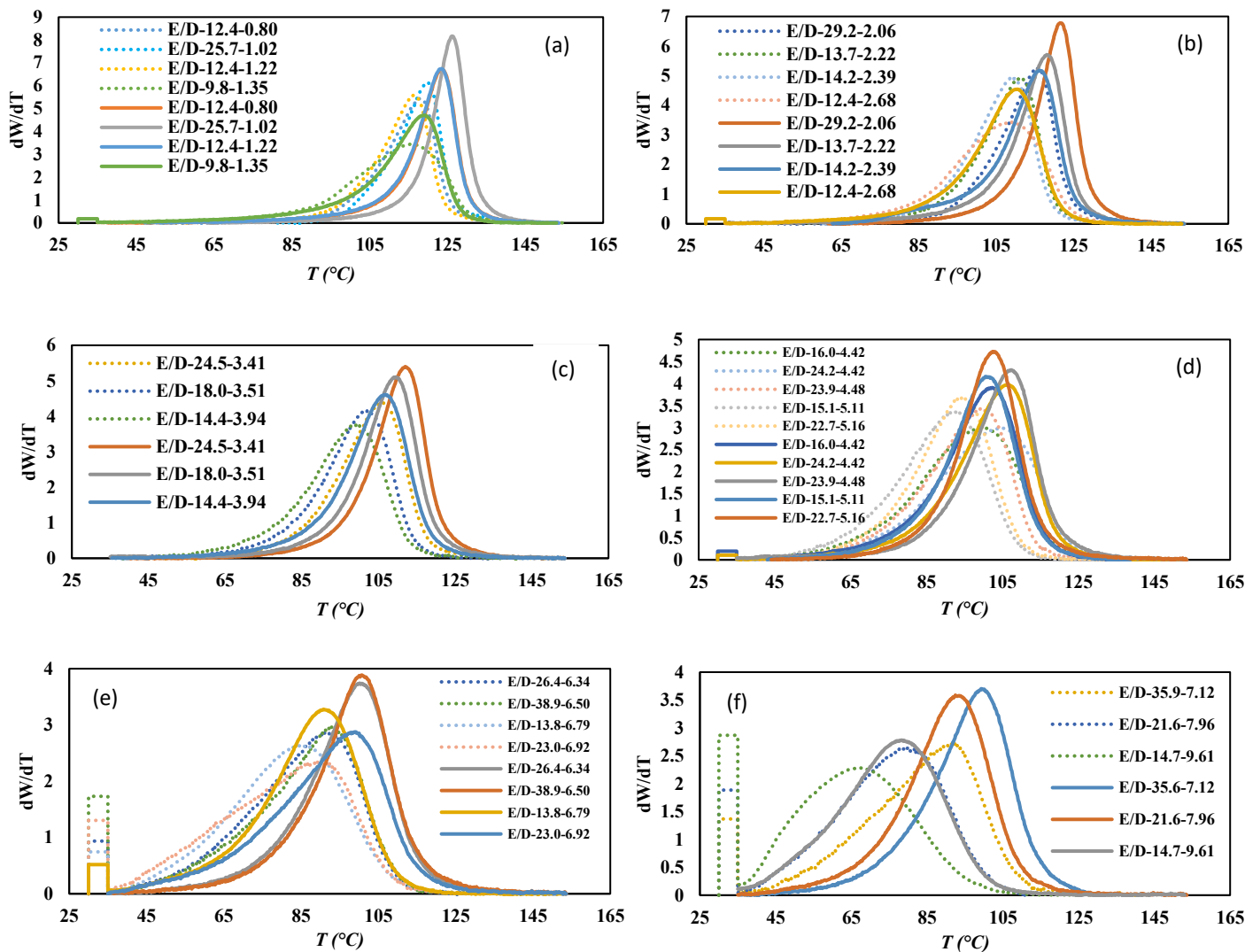
Figure D-2. Comparison between HT-TGIC profile of ethylene/1-decene in Hypercarb (solid lines) and GNPSi supports (dotted lines): a) φ = 0.80 to 1.35 %, b) φ = 2.06 to 2.68 %, c) φ =3.41 to 3.94 %, d) φ = 4.42 to 5.16 %, e) φ = 6.34 to 6.92 %, f) φ = 7.12 to 9.61 %.

Appendix E: Comparison Between Predicted and Experimental Data for Graphene-Coated Non-Porous SiO$_2$ Support (GNPSi)

Table E-1. Peak temperature deviations for proposed column.

Sample	M_w	φ(%)	n_c	Tp(K)-Experimental	Tp(K)-Calculated	%
E/H-17.5-1.91	17 500	1.91	6	392.1	387.8	1.11
E/H-16.2-2.72	16 200	2.72	6	382.7	383.9	-0.31
E/H-17.4-2.85	17 400	2.85	6	386.5	383.6	0.76
E/H-14.6-0.04	14 600	0.04	6	396.9	395.6	0.34
E/H-15.2-4.75	15 200	4.75	6	376.2	375.0	0.33
E/H-14.5-8.11	14 500	8.11	6	361.8	361.3	0.13
E/H-11.6-0.36	11 600	0.36	6	396.1	393.0	0.77
E/H-12.2-1.55	12 200	1.55	6	386.5	387.9	-0.35
E/H-11.2-2.43	11 200	2.43	6	380.9	383.6	-0.71
E/H-12.7-6.69	12 700	6.69	6	364.9	366.4	-0.41
E/H-9.5-0.85	9 500	0.85	6	388.2	389.7	-0.39
E/H-9.2-5.38	9 200	5.38	6	364.9	370.0	-1.42
E/H-9.1-6.08	9 100	6.08	6	361.8	367.2	-1.49
E/H-8.7-7.82	8 700	7.82	6	359.6	360.0	-0.11
E/H-9.4-8.46	9 400	8.46	6	355.2	358.0	-0.81
E/H-8.9-9.04	8 900	9.04	6	351.3	355.5	-1.20
E/H-10.1-18.49	10 100	18.49	6	318.2	323.8	-1.76
E/H-23.0-1.93	23 000	1.93	6	386.2	388.5	-0.59
E/H-19.3-1.52	19 300	1.52	6	393.0	389.8	0.82
E/H-19.2-3.49	19 200	3.49	6	376.2	381.1	-1.32
E/H-19.5-12.50	19 500	12.50	6	336.2	345.9	-2.90
E/O-31.3-10.01	31 300	10.01	8	349.5	350.7	-0.36
E/O-24.0-0.95	24 000	0.95	8	392.9	392.4	0.12

Table E-1. Peak temperature deviations for proposed column (continued).

Sample	M_w	$\varphi(\%)$	n_c	Tp(K)-Experimental	Tp(K)-Calculated	%
E/O-25.3-1.01	25 300	1.01	8	391.0	392.2	-0.32
E/O-24.6-3.01	24 600	3.01	8	383.1	382.0	0.28
E/O-26.4-5.28	26 400	5.28	8	370.0	371.3	-0.33
E/O-25.1-6.85	25 100	6.85	8	362.8	364.0	-0.33
E/O-19.5-2.87	19 500	2.87	8	384.3	382.1	0.57
E/O-20.0-3.39	20 000	3.39	8	377.0	379.6	-0.70
E/O-21.3-10.49	21 300	10.49	8	344.6	348.0	-1.00
E/O-15.0-1.40	15 000	1.40	8	388.3	388.6	-0.07
E/O-16.0-2.77	16 000	2.77	8	378.5	382.0	-0.92
E/O-16.7-2.94	16 700	2.94	8	377.9	381.3	-0.89
E/O-15.0-4.26	15 000	4.26	8	376.7	374.5	0.57
E/O-16.5-5.47	16 500	5.47	8	370.1	369.2	0.26
E/O-16.9-10.55	16 900	10.55	8	339.5	347.2	-2.27
E/O-13.8-1.24	13 800	1.24	8	387.4	389.1	-0.44
E/O-13.5-2.17	13 500	2.17	8	384.3	384.3	0.00
E/O-14.2-3.06	14 200	3.06	8	379.8	380.1	-0.06
E/O-14.1-4.83	14 100	4.83	8	369.7	371.6	-0.50
E/O-12.3-6.70	12 300	6.70	8	361.2	362.5	-0.37
E/O-11.4-7.38	11 400	7.38	8	356.7	359.2	-0.70
E/O-10.1-10.42	10 100	10.42	8	337.8	345.8	-2.38
E/O-6.6-2.13	6 600	2.13	8	378.8	380.0	-0.33
E/O-9.1-7.47	9 100	7.47	8	358.6	357.6	0.27
E/O-9.0-9.35	9 000	9.35	8	348.1	349.6	-0.42
E/O-7.3-14.66	7 300	14.66	8	323.0	327.8	-1.50
E/O-7.2-14.99	7 200	14.99	8	323.0	326.5	-1.10

Table E-1. Peak temperature deviations for proposed column (continued).

Sample	M_w	$\varphi(\%)$	n_c	Tp(K)-Experimental	Tp(K)-Calculated	%
E/O-6.9-16.96	6 900	16.96	8	317.3	319.3	-0.62
E/D-38.9-6.50	38 900	6.50	10	366.1	362.7	0.92
E/D-35.9-7.12	35 900	7.12	10	365.9	359.5	1.74
E/D-29.2-2.06	29 200	2.06	10	388.9	385.8	0.78
E/D-25.7-1.02	25 700	1.02	10	392.9	391.6	0.34
E/D-24.5-3.41	24 500	3.41	10	379.3	378.0	0.34
E/D-24.2-4.42	24 200	4.42	10	378.0	372.6	1.44
E/D-23.9-4.48	23 900	4.48	10	372.7	372.2	0.13
E/D-22.7-5.16	22 700	5.16	10	367.6	368.5	-0.25
E/D-26.4-6.34	26 400	6.34	10	365.5	362.9	0.72
E/D-23.0-6.92	23 000	6.92	10	363.8	359.7	1.13
E/D-21.6-7.96	21 600	7.96	10	352.4	354.5	-0.59
E/D-17.6-0.83	17 600	0.83	10	395.3	391.6	0.95
E/D-18.0-3.51	18 000	3.51	10	374.9	376.6	-0.45
E/D-14.2-2.39	14 200	2.39	10	382.4	381.9	0.13
E/D-14.4-3.94	14 400	3.94	10	372.1	373.6	-0.40
E/D-16.0-4.42	16 000	4.42	10	373.0	371.4	0.43
E/D-15.1-5.11	15 100	5.11	10	365.8	367.6	-0.49
E/D-12.4-0.80	12 400	0.80	10	389.6	390.3	-0.19
E/D-12.4-1.22	12 400	1.22	10	389.6	387.9	0.42
E/D-13.2-1.33	13 200	1.33	10	388.7	387.5	0.29
E/D-13.7-2.22	13 700	2.22	10	384.3	382.7	0.42
E/D-12.4-2.68	12 400	2.68	10	381.8	379.7	0.53
E/D-13.8-6.79	13 800	6.79	10	358.2	358.9	-0.17
E/D-9.8-1.35	9 800	1.35	10	388.8	385.9	0.75

Table E-1. Peak temperature deviations for proposed column (continued).

Sample	M_w	$\varphi(\%)$	n_c	Tp(K)-Experimental	Tp(K)-Calculated	%
H-23.0	23 000	0	0	395.7	397.3	-0.40
H-15.3	15 300	0	0	394.7	396.0	-0.33
H-11.8	11 800	0	0	392.3	394.8	-0.64
H-13.3	13 300	0	0	392.5	395.4	-0.73